

A Chemical Switch for Transforming a Purine Agonist for Toll-like Receptor 7 to a Clinically Relevant Antagonist

Ayan Mukherjee,^{||} Deblina Raychaudhuri,^{||} Bishnu Prasad Sinha,^{||} Biswajit Kundu, Mousumi Mitra, Barnali Paul, Purbita Bandopadhyay, Dipyaman Ganguly,^{*} and Arindam Talukdar^{*}Cite This: *J. Med. Chem.* 2020, 63, 4776–4789

Read Online

ACCESS |



Metrics & More

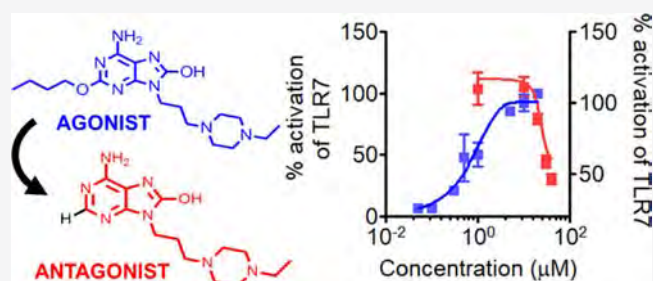


Article Recommendations



Supporting Information

ABSTRACT: Toll-like receptor 7 (TLR7) is an established therapeutic target in myriad autoimmune disorders, but no TLR7 antagonist is available for clinical use to date. Herein, we report a purine scaffold TLR7 antagonist, first-of-its-kind to our knowledge, which was developed by rationally dissecting the structural requirements for TLR7-targeted activity for a purine scaffold. Specifically, we identified a singular chemical switch at C-2 that could make a potent purine scaffold TLR7 agonist to lose agonism and acquire antagonist activity, which could further be potentiated by the introduction of an additional basic center at C-6. We ended up developing a clinically relevant TLR7 antagonist with favorable pharmacokinetics and 70.8% oral bioavailability in mice. Moreover, the TLR7 antagonists depicted excellent selectivity against TLR8. To further validate the *in vivo* applicability of this novel TLR7 antagonist, we demonstrated its excellent efficacy in preventing TLR7-induced pathology in a preclinical murine model of psoriasis.



INTRODUCTION

Toll-like receptors (TLRs) are the critical first line of immune defense that are mostly expressed on antigen presenting cells, for example, dendritic cells and recognize molecular signature patterns associated with pathogens.^{1–3} The members of the TLR family of receptors that can recognize nucleic acid molecules, both of self and nonself origins, *viz.* TLR7, TLR8, and TLR9, are located inside the acidic endosomal compartments of the immune cells.^{2,4–6} Among them, TLR7, which recognizes single-stranded RNA, is expressed in humans selectively in plasmacytoid dendritic cells (pDCs) and B lymphocytes and when activated in pDCs drives type I interferon production from pDCs.⁴ pDC-derived type I interferons (IFNs) are critical innate immune events in a number of autoimmune diseases, *viz.* systemic lupus erythematosus (SLE), psoriasis, Sjögren's syndrome, systemic sclerosis, and so forth.^{7–11} Thus, the endosomal TLRs in pDCs, for example, TLR7, are important therapeutic targets for these clinical contexts.^{12–14} Application of the TLR7 agonist imiquimod on the skin leads to cutaneous autoimmunity in mice, which mimics the human skin autoimmunity in psoriasis, and consequently is an established preclinical model for psoriasis.¹⁵ However, a suitable TLR7 antagonist is yet to be available for clinical use.¹⁶

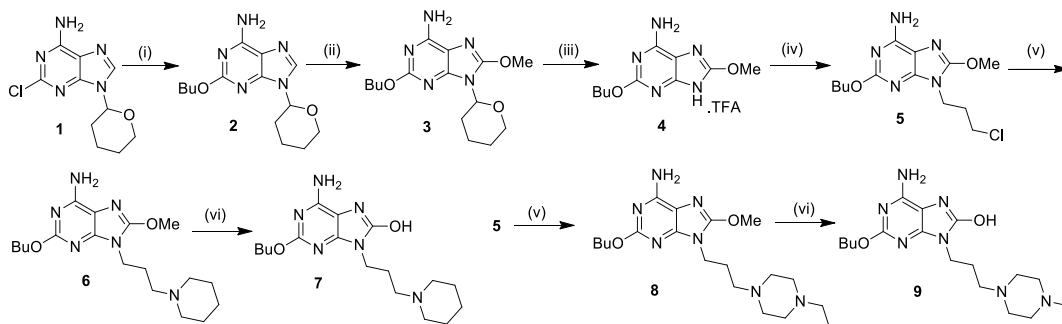
Both receptor agonists and antagonists are important therapeutic molecules in different clinical contexts and in many cases agonists and antagonists share overlapping binding region in their target molecules. Thus, agonistic chemical

scaffolds are often used as a template for designing antagonists with shared region-specificities for the receptors,^{17–19} for example, development of β -adrenergic receptor antagonists from the endogenous agonist adrenalin,²⁰ histamine receptor 2 antagonists from histamine,²¹ and opioid receptor antagonists from opioids.²² TLR7-mediated immune activation has implication in autoimmune diseases like SLE, psoriasis. In SLE autoreactivity against RNA and RNA binding proteins are very prevalent and these immune complexes activate TLR7 in both pDCs and B cells, thereby perpetuating the inflammatory cascade.¹⁰ In psoriasis self-RNA molecules released by dying keratinocytes form complexes with cationic antimicrobial peptides. These complexes have been shown to activate both plasmacytoid and conventional dendritic cells thus fuelling the cutaneous inflammation.^{8,10} Hence, blocking TLR7 activation with suitable antagonist is sought for, which may intercept one of the key pathogenic nodes in these diseases. Purine scaffold is extensively studied for its potent TLR7 agonist activity.^{23–26} Interestingly, guanosine, an endogenous purine class molecule, is also an agonist for TLR7.²⁷ The mechanism of TLR7 activation by guanosine has been shown through crystallo-

Received: January 3, 2020

Published: April 17, 2020



Scheme 1^a

^aReagents and conditions: (i) sodium *t*-butoxide (4.0 equiv), *n*-BuOH, 100 °C, 12 h, 77%; (ii) a. *N*-bromosuccinimide (1.05 equiv), CHCl₃, 3 h, rt, b. sodium methoxide (2.7 equiv), CH₃OH, reflux, 4 h, 80%; (iii) 10% TFA in methanol, rt, 72 h, 73%; (iv) 1-bromo-3-chloropropane (2.0 equiv), potassium carbonate (2.6 equiv), rt, 16 h, 67%; (v) piperidine for compound 11 or ethylpiperazine for compound 12 (3.0 equiv), potassium carbonate (1.5 equiv), rt, 6 h, 67–73%; (vi) 4 M HCl in 1,4-dioxane, 3 h, 87–91%.

graphic study which is of great value in design and development of TLR7 ligands.²⁸ Previous efforts directed toward the purine scaffold have led to potent agonists' thorough understanding about the region-specificities of critical substituents. From crystallographic evidence and structural development of TLR7 agonist, it is understandable that the –NH₂ group at C-6 position is crucial for scaffold recognition by TLR7.²⁸ Thus, logically, we did not change the –NH₂ group at C-6 position in our initial SAR development. Development of 2-substituted-8-hydroxyadenine as IFN α inducer via TLR7 pathway revealed the profound effect of four carbon long alkoxy chain at C-2 position on the agonistic activity.^{25,29} Among various substituents, O-alkyl groups at C-2 position have been found to have superior ability to modulate the agonistic activity in combination with *N*-benzyl or *N*-alkylamine at N-9 position.^{30–32} Previous study on pteridinone core-based TLR7 agonist showed that C-2 position butoxy linker bind to the conserved hydrophobic pocket of TLR7.³³ The N-9 substitutions modulate both activity and pharmacokinetic profile of purine,^{23,24} perhaps because the weak base gets protonated and trapped in the acidic endosomal compartment,^{34,35} harboring TLR7. Throughout the literature, the C-2 position was substituted, and subsequently modification was done in N-9 position but not the other way round. Keeping this in mind, we intended to evaluate the fate of the agonist where the C-2 substituent is absent keeping the known relevant N-9 substituents and –NH₂ group at C-6 position. Although extensive focus has been devoted toward the development of TLR7 agonist, there is no reported TLR7 antagonist of purine scaffold, to our knowledge. Imiquimod belongs to imidazoquinoline class of molecules, which also includes other well-known TLR7 agonists like gardiquimod and resiquimod.³⁶ TLR7 agonist gardiquimod was successfully transformed into TLR7 antagonist by converting to its 3*H* regioisomer.¹⁸

We have initiated our study from a representative purine agonist 7 containing essential TLR7 agonistic features at C-2, C-6, C-8, and N-9. We have explored the minimal structural features that impart antagonism in compound 7, for mapping the synthetic path to a novel purine scaffold antagonist. We have depicted that a small structural modification in the ligand can lead to major changes in their functional activity. For assessing the TLR7-targeted activity (both agonism and antagonism) of the molecules, we used engineered HEK293 cells that expressed exogenous human TLR7 and reported

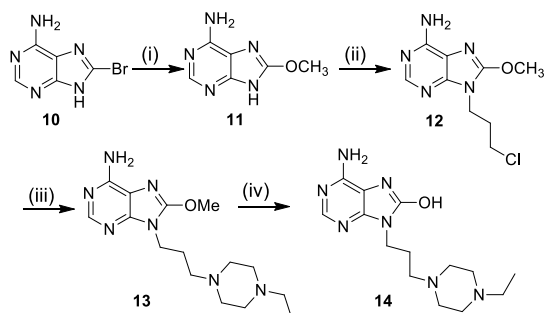
TLR7-induced NF- κ B activation in a secreted alkaline phosphatase (SEAP)-driven colorimetric assay. We have used a nonselective TLR7 antagonist hydroxychloroquine as a positive control. Through SAR development, we identified clinically relevant TLR7 antagonist 23 that has favorable pharmacokinetic properties with 70.8% oral bioavailability in mice. The nature of antagonism was determined by subjecting these antagonists to agonism assay. The TLR7 antagonists reported herewith showed excellent selectivity against TLR8. *In vivo* efficacy of 23 was demonstrated by its ability to prevent TLR7-induced pathology in a preclinical murine model of psoriasis.

CHEMISTRY

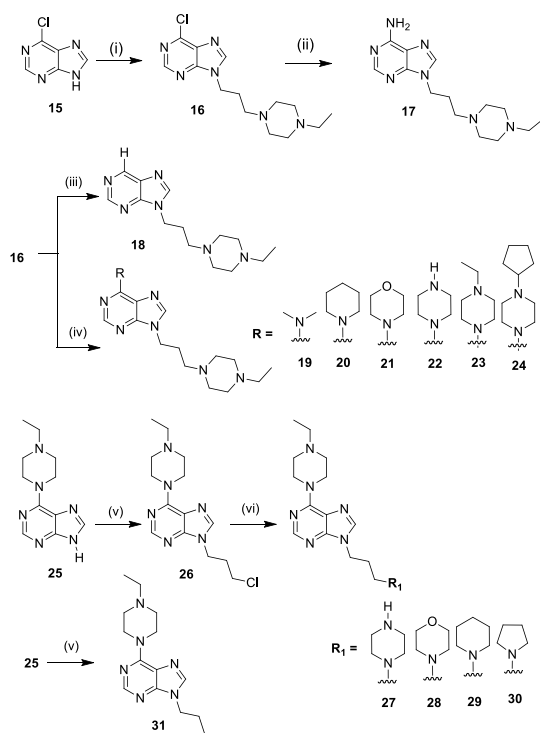
Chemical Synthesis of TLR7 Agonist 7 and 9. C-6 position of compound 1³⁰ was substituted with *n*-butoxy linkage via sodium *t*-butoxide treatment to obtain compound 2. The methoxy group at C-8 was introduced by bromination of 2 using *N*-bromosuccinimide followed by refluxing with a 5 M solution of sodium methoxide in methanol to provide compound 3 (Scheme 1). Deprotection of pyran ring from compound 3 using 10% trifluoroacetic acid (TFA) followed by 3-chloropropyl substitution in compound 4 using 1-bromo-3-chloropropane yielded compound 5. The chlorine group in compound 5 was then substituted with either piperidine or ethylpiperazine to give compounds 6 and 8. Finally, C-8 position methoxy group was deprotected using 4 M HCl in 1,4-dioxane to get compounds 7 and 9.

Chemical Synthesis of Weak TLR7 Antagonist 14. In the present Scheme 2, we successfully standardized a protocol for the synthesis of compound 14 by avoiding protection–deprotection chemistry at N-9 position in purine scaffold. Bromo group of 8-bromo adenine 10³⁷ was substituted with methoxy group by refluxing with a 5 M solution of sodium methoxide in methanol to obtain compound 11, which on treatment with 1-bromo-3-chloropropane provided compound 12. Chlorine group was substituted by ethylpiperazine to yield compound 13 and that followed by deprotection of methoxy group gave compound 14.

Chemical Synthesis of Potent TLR7 Antagonist. Substitution of 3-carbon linker with ethylpiperazine group at N-9 position of 6-chloropurine (15) resulted in the intermediate compound 16 (Scheme 3). In the formation of compound 16, there is a mechanistic possibility of getting two structural isomers, namely, N-9 isomer and N-7 isomer. Here,

Scheme 2^a

^aReagents and conditions: (i) 5 M solution of sodium methoxide in methanol (10 equiv), reflux, 12 h, 72%; (ii) 1-bromo-3-chloropropane (2.0 equiv), potassium carbonate (2.6 equiv), rt, 16 h, 78%; (iii) ethylpiperazine (3.0 equiv), potassium carbonate (1.5 equiv), rt, 6 h, 63%; (iv) 4 M HCl in 1,4-dioxane 3 h, 86%.

Scheme 3^a

^aReagents and conditions: (i) 1-(3-chloropropyl)-4-ethylpiperazine (2.0 equiv), potassium carbonate (2.0 equiv), DMF, 60 °C, 12 h, 84%; (ii) ammonia in ethanol (7.0 equiv), 60 °C, 12 h, 67%; (iii) H₂, Pd/C, THF, rt, 2 h, 91%; (iv) respective amine, potassium carbonate (2.0 equiv), CH₃CN, reflux, 12 h, 73–95%; (v) 1-bromo-3-chloropropane for (26) and 3-bromopropane for (31) potassium carbonate (2.0 equiv), DMF, rt, 12 h, 71–78%; (vi) respective amine, potassium carbonate (2.0 equiv), DMF, 60 °C, 12 h, 78–93%.

we obtained exclusively N-9 isomer, and the structure was confirmed by the X-ray crystallographic structure of hydrochloride salt of intermediate compound 16 (Supporting Information, Figure S6). Thereafter, the chloride group at C-6 position was replaced by free –NH₂ group by treating with ammonia in ethanol at 60 °C to derive compound 17. Reduction of the C-6 chloro group using palladium-carbon in 16 gave compound 18. The chloro group at C-6 of intermediate 16 was substituted with different organic amines

such as dimethylamine, piperidine, morpholine, piperazine, ethylpiperazine, and cyclopentylpiperazine to yield compounds 19, 20, 21, 22, 23, and 24, respectively. The N-9 position of 25 was treated with 1-bromo-3-chloropropane to get chloro intermediate 26, which was subsequently reacted with various azacyclic bases such as piperazine, morpholine, piperidine, and pyrrolidine to yield compounds 27, 28, 29, and 30 respectively. Compound 31 with propyl substitution at N-9 position was made from 25 using the same protocol used for the preparation of 26. Structural conformation of compound 23 was made by the analysis of NOESY, HMBC spectra, the detail is in the Supporting Information.

RESULTS AND DISCUSSION

The importance of butoxy at C-2, –NH₂ at C-6 and hydroxyl at C-8 in TLR7-agonism by purine chemotypes is established.^{38,39} We selected compound 7 as a starting point as it contains all the essential features of a TLR7 agonist. The synthetic strategy (Scheme 1) for compound 7 allowed us to readily introduce an additional basic center at N-9. Replacing piperidine with ethylpiperazine led to the enhancement in agonism in 9 (Scheme 1), which had an EC₅₀ of 0.9 μM as opposed to 2.6 μM for 7 (Figure 1a,b, Table 1). Based on the previous SAR studies, it has been established that substituents such as butoxy at C-2 position are a key feature for TLR7 agonism.^{23,25} As discussed before, we hypothesized that C-2 butoxy may be targeted to transform the potent TLR7 agonist 9 into a TLR7 antagonist. Indeed, the removal of C-2 butoxy in 14 (Scheme 2), led to the disappearance of TLR7 agonism and acquisition of considerable antagonism (Figure 1c,d, Table 1). Thus, we were able to identify a “chemical switch” at C-2 that could make a potent purine scaffold TLR7 agonist to loose agonistic properties and acquire antagonistic properties toward TLR7.

This novel purine scaffold molecule 14, despite showing significant antagonism to human TLR7, had an IC₅₀ (43.1 μM) too high for a therapeutically relevant antagonist. Therefore, we explored if omission of other essential agonist-specific molecular features from 14 can help to develop more potent antagonists with translational potential. We found that removal of the hydroxyl group at C-8 led to rather a loss of all activity against TLR7 in compound 17 at 50 μM. The importance of the –NH₂ group was evident from the crystal structure of guanosine as well as the chemical ligands from imidazoquinoline class too.²⁷ Also, the SAR study at C-6 position of purines has depicted the significance of –NH₂ group.⁴⁰ Accordingly, we focused on the modification at C-6 position. Neither complete deletion of the –NH₂ group from C-6 in compound 18 nor converting the –NH₂ at C-6 to dimethylamino in compound 19 brought antagonistic activity toward TLR7 (Table 1) at 50 μM. Next, we extended the dimethylamino group of compound 19 with different azacyclic moieties like piperidine, morpholine, and piperazine. Interestingly, piperidine substitution at C-6 position in compound 20 regained the TLR7 antagonistic effect, and the compound shows moderate TLR7 antagonism with an IC₅₀ value of 23.9 μM. Replacement of piperidine with morpholine in compound 21 showed comparable TLR7 antagonism with an IC₅₀ of 25 μM. Because morpholine cannot be further extended at 4' position, we introduced piperazine in compound 22 with an aim for further derivatization, but the TLR7 antagonistic potency decreased to 39.3 μM. However, ethyl substitution on the piperazine NH group in compound 23 regained the TLR7

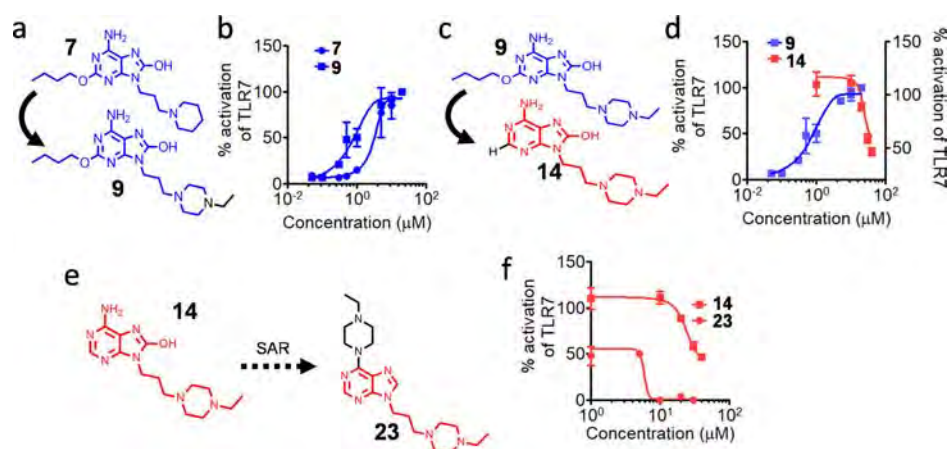
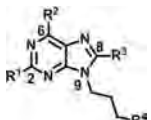


Figure 1. Discovery of TLR7 antagonist from known TLR7 agonist. (a,c,e) Conversion of TLR7 agonist 7 ($EC_{50} = 2.6 \mu M$) to a more potent TLR7 agonist 9 ($EC_{50} = 0.9 \mu M$) by the addition of ethylpiperazine group (a) compound 9 to weak TLR7 antagonist 14 ($IC_{50} = 43.1 \mu M$) by the elimination of butoxyl group (c) 3 to potent TLR7 antagonist 23 ($IC_{50} = 4.7 \mu M$) by systematic SAR study (e). (b,d,f) HEK-Blue TLR7 reporter cells were incubated overnight in the presence of indicated concentrations of given compounds and on the following day the culture supernatants were subjected to a colorimetric assay to measure the degree of TLR activation/inhibition. Data are represented as mean \pm SEM.

Table 1. SAR Depicting the Conversion of Agonist to Antagonist



Comp. No.	R ¹	R ²	R ³	R ⁴	TLR7 Agonism (μM) EC_{50}	TLR7 Antagonism (μM) IC_{50}
7	-OBu	-NH ₂	-OH		2.6 \pm 0.05	a
9	-OBu	-NH ₂	-OH		0.9 \pm 0.01	a
14	H	-NH ₂	-OH		b	43.1 \pm 4.1
17	H	-NH ₂	H		b	a
18	H	H	H		b	a
19	H	NMe ₂	H		b	a
20	H		H		b	23.9 \pm 3.1
21	H		H		b	25.0 \pm 3.5
22	H		H		b	39.3 \pm 3.7
23	H		H		b	4.7 \pm 0.4
24	H		H		b	6.2 \pm 1.5
27	H		H		b	37% ^c
28	H		H		b	40.0 \pm 4.2
29	H		H		b	15.8 \pm 1.8
30	H		H		b	48.3 \pm 4.9
31	H		H	H	b	a
Hydroxychloroquine					NT	8.6 \pm 1.2

^aNo significant inhibition at 50 μM . ^bNo significant activation at 50 μM . ^c% inhibition at 50 μM . NT-not tested. Hydroxychloroquine is a positive control.

antagonistic effect in single digit micromolar level with an IC_{50} value of 4.7 μM . Of note here, an ethylpiperazine group at N-9 led to enhancement of TLR7 agonism, while introducing the same group at C-6 potentiated TLR7 antagonism. Further logical extension of the ethyl group in compound 23 with more hydrophobic cyclopentane group in compound 24 led to slight decrease in the TLR7 antagonist activity (IC_{50} value of 6.2 μM , Table 1). Figure 1 is a snapshot of our SAR development depicting minimal structural requirements and a singular chemical switch that could transform a TLR7 agonist into a

TLR7 antagonist in the same purine scaffold, which is represented in a TLR7 reporter assay done in parallel using an established TLR7 agonist (CL264), the purine agonists 7 and 9 as well as the TLR7 antagonist 23 which has been shown to inhibit CL264-induced TLR7 activation (Figure 1g).

Initially, in compound 9 it was observed that the introduction of weak base at N-9 can modulate TLR7 activity. Thus in our next development, we further explored the role of weak base at N-9 position with different groups such as morpholine, pyrrolidine, and piperidine. Replacing ethyl-

piperazine group in compound **23** with piperazine in **27** led to drastic fall in TLR7 antagonist activity (37% inhibition at 50 μM). The result suggests that the hydrophobic ethyl group is essential for TLR7 antagonistic activity. The result correlates well with our first set of SAR results where unsubstituted piperazine at C-6 in compound **22** showed 8 fold less potency than ethyl substituted piperazine group in **23**. Further substitution with morpholine, piperidine, and pyrrolidine yielded less potent TLR7 antagonist compound **28**, **29**, and **30** with IC_{50} 40.0, 15.8, 48.27 μM , respectively. Expectedly, elimination of weak base at N-9 in compound **31** led to complete loss of TLR7 antagonism at 50 μM (Table 1). To ensure the validity of TLR7 antagonism assay, the ability of different doses of hydroxychloroquine to inhibit TLR7 activation was studied as a positive control. Comparison between compound **17** with **23** suggests that introduction of ethylpiperazine group with an additional basic center and an extended hydrophobic attachment at C-6 had profound potentiating effect on TLR7 antagonism in purine scaffold, whereas additional basic center at N-9 can modulate the TLR7-targeted activity (either agonism as in **7** and **9**, or antagonism as in **23** and **29**).

None of the TLR7 antagonists showed any TLR7 agonism up to 50 μM dose (Supporting Information, Figure S2) which ruled out the possibility of partial agonism. As TLR7 and TLR8 show high degree of structural similarity,¹⁹ next we monitored the efficacy of our TLR7 antagonists in TLR8 antagonistic assay, and we found that none of the TLR7 antagonists showed significant TLR8 inhibition (Supporting Information, Figure S3) up to 50 μM . The result strongly suggests that the TLR7 antagonists reported in the manuscript are selective for TLR7 when compared with TLR8 antagonism.⁴¹ TLR7 antagonistic effect of compound **23** was further assessed by evaluating the ability of our compound to inhibit the production of TLR7-triggered proinflammatory cytokines such as IL-6 and TNF α .^{41,42} Compound **23** showed 42.9% inhibition (Figure 2a) of IL-6 gene transcription at IC_{50} dose (5 μM) in HEK-Blue TLR7 cell line. Inhibition of proinflammatory cytokines was measured by real time polymerase chain reaction (RT-PCR) using selective TLR7 agonist CL264 as positive control. For further validation employing *ex vivo* human blood-derived model, we observed the inhibition of TLR7-driven TNF α induction in primary human peripheral blood mononuclear cells (hPBMCs) by ELISA (Figure 2b). These results led us to conclude that our compound of interest is a potent TLR7 antagonist capable of inhibiting TLR7-mediated immune responses as depicted by the inhibition of IL-6 and TNF α production in response to TLR7 activation. Thus, we have successfully identified hitherto unknown site-specific substitutions that can switch a well-established purine scaffold TLR7 agonist into a TLR7 antagonist, as demonstrated through the TLR7 reporter assay.

TLR7 and TLR8 share almost similar ligand binding domains. Both the TLRs have one small molecule ligand binding site and another ssRNA binding site.²⁷ Zhang *et al.*¹⁹ reported a third binding site for the inhibition of TLR8 in the rest state. The binding model was extrapolated for finding new antagonist binding zone in TLR7. Karroum *et al.* validated this new antagonist binding site in TLR7 through systematic computational analysis of imidazo[1,2-*a*]pyrazines, imidazo[1,5-*a*]quinoxalines, and pyrazolo[1,5-*a*]quinoxalines class TLR7 antagonists.⁴¹ Because of the unavailability of the human TLR7 crystal structure, we have built homology model

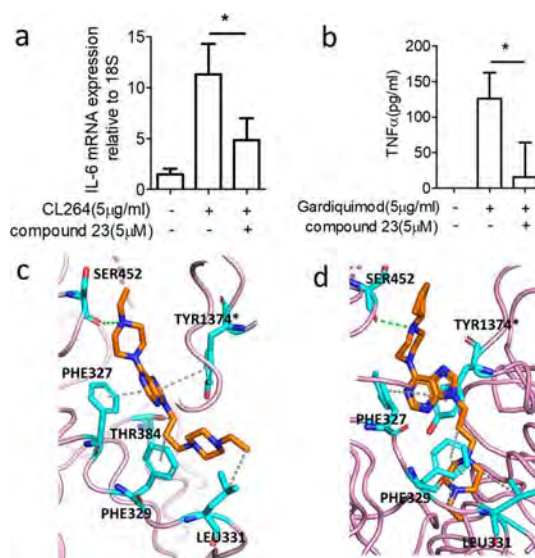


Figure 2. Inhibition of proinflammatory cytokines and docking study of compound **23** with homology modeled hTLR7 (a) HEK-Blue TLR7 reporter cells were treated with 5 μM compound **23**, 1 h prior to stimulation with CL264, 6 h after which, the cells were harvested and subjected to gene expression studies to monitor the mRNA levels of the IL6 gene relative to that of 18S (housekeeping gene) in the presence and absence of compound treatment. Data are represented as mean \pm SEM, $*p < 0.05$, $n = 6$. Unpaired Student's *t*-test was done to measure statistical significance. (b) Primary hPBMCs were treated with 5 μM compound **23**, 1 h prior to stimulation with gardiquimod and incubated overnight. On the following day, the culture supernatants were subjected to ELISA to measure the degree of TLR activation/inhibition in terms of TNF α production. Data are represented as mean \pm SEM, $*p < 0.05$, $n = 4$. Paired Student's *t*-test was done to measure statistical significance. (c) Interaction between TLR7 ectodomain (homology model template PDB ID: 5WYZ) and compound **23**. (d) Interaction between TLR7 ectodomain and compound **24**. Hydrogen bonds and hydrophobic interactions are shown by green dashed line and grey dashed line, respectively. *marks residues are in chain B.

structure of TLR7 (Supporting Information, Figure S7). Molecular docking study and validation was performed using Discovery Studio suite 4.1 (Supporting Information, Figure S8a), which shows that our TLR7 antagonists also bind in the same region, attaining similar pattern of interactions along with newer interactions (Figure 2c,d). The molecular docking indicates that the purine ring of the lead molecule **23** is sandwiched between two hydrophobic residues Phe329 and Tyr1374 forming π - π stacking interactions (Figure 2c). Hydrogen bonding between the hydroxyl group of Ser452 with nitrogen of C-6 position of ethylpiperazine was observed in compound **23** as one of the key important interaction signifying the importance of terminal nitrogen in the piperazine group as observed in the structure-activity relationships between compounds **19**, **20**, and **21** with dimethylamino, piperidine, and morpholine groups, respectively. N-9 position of the alkyl linker with pendent hydrophobic amine was stabilized by the hydrophobic interaction of Leu331 and Phe329. The significance of the ethyl group can be observed by comparing the inhibitory potency of compounds **23** and **27**. Compound **23** showed IC_{50} value of 4.7 μM , whereas compound **27** without the ethyl group showed 37% inhibition at 50 μM . Similar binding interactions were observed for other potent TLR7 antagonist

Table 2. *In Vitro* Pharmacokinetics of Compound 23

aq. sol $\mu\text{g/mL}$	clog P	PSA \AA^2	NRB ^a	Caco-2 permeability P_{app} (10^{-6} cm/s)			plasma stability		microsomal stability			
									human		mice	
				A \rightarrow B ^b	B \rightarrow A ^c	efflux ratio	human ^d	mice ^d	$T_{1/2}$ (min)	QH %	$T_{1/2}$ (min)	QH %
200.3	1.38	52.6	7	3.57	9.28	2.6	95%	99.2%	90.3	26.5	111.8	14.4
^a Number of rotatable bolds. ^b Apical to basal. ^c Basal to apical. ^d Remaining after 2 h.												

^aNumber of rotatable bonds. ^bApical to basal. ^cBasal to apical. ^dRemaining after 2 h.

compound **24** (Figure 2d). From the molecular docking analysis of our other TLR7 antagonists, we can conclude that along with hydrogen bonding with Ser452, hydrophobic interactions play a vital role in determining TLR7 antagonism (Supporting Information, Figure S8).

Selectivity of TLR7 antagonist **23** over TLR8 can be anticipated through docking analysis. TLR8 and TLR7 share similar antagonistic binding sites except for one single residue change.⁴¹ Polar residue Thr384 for TLR7 is replaced by nonpolar bulky Ile403 in TLR8. The molecular modeling of compound **23** in TLR7 indicates that the N-9 flexible linker is 5 \AA away from Thr384 (Figure 2c). It can be anticipated that due to the steric bulk of Ile403 compound **23** is unable to bind to TLR8, which could be the probable reason for selectivity of our antagonists toward TLR7 over TLR8.

We selected compound **23** for further investigation. Initially we aimed at gathering insights about *in vitro* pharmacokinetics of **23** through a series of established assays. The aqueous solubility of **23** was found to be considerable (200 $\mu\text{g/mL}$) at pH 7.4, and calculated clog *P* value was 1.38 (Table 2). The polar surface area (52.6 \AA^2) and seven rotatable bonds were also good indicators that compound **23** would have favorable oral bioavailability (Table 2).⁴³ On Caco-2 permeability assay, the efflux ratio of **23** was found to be 2.6, suggesting that this molecule would have moderate membrane permeability and is not likely to be a substrate for efflux transporters, *viz.* P-glycoprotein. In a nut shell, these results reflect that compound **23** may have good adsorption in the gastrointestinal tract. Compound **23** also showed acceptable plasma stability as well as metabolic stability (liver microsomal assay), assessed in case of both mice and human (Table 2). Moreover, compound **23** showed no cytotoxicity on HEK293 cells *in vitro* up to a concentration of 100 μM (Figure S4).

Finally, to assess *in vivo* applicability of this novel TLR7 antagonist **23**, we checked the *in vivo* pharmacokinetics of the molecule on oral and intravenous administration to C57BL/6 mice in two doses of 10 mg/kg and 15 mg/kg. The maximum plasma concentration (C_{max}) surpassed the *in vitro* IC_{50} against TLR7 in 15 mg/kg oral dose whereas in 10 mg/kg dose C_{max} remained below the IC_{50} . It was found that compound **23** was rapidly absorbed into body (Figure 3a) with a half-life of 4.6 h upon 15 mg/kg oral dose (Figure 3c). As compound **23** is basic in nature, it shows good Vss (4.2 L/kg, Figure 2c) which reflect the high duration of drug in target site.⁴⁴ Finally, all of the favorable range of *in vitro* and *in vivo* pharmacokinetics (Figure 3) of compound **23** adds up to give excellent oral bioavailability ($F = 70.8\%$, Figure 3a,b).

To validate *in vivo* efficacy of **23** for TLR7 antagonism in a clinically relevant context, we utilized an established preclinical model of the cutaneous autoimmune disease psoriasis. Daily application of the TLR7 agonist imiquimod to the skin of C57BL/6 mice leads to a psoriasiform inflammation in 6 days, which closely mimics the human disease in terms of morphology, histopathology, and the underlying immunocel-

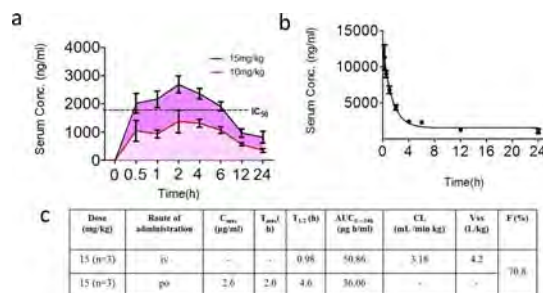


Figure 3. Pharmacokinetics profiling of potent TLR7 antagonist **23**. (a) Doses of 15 mg/kg and 10 mg/kg body weight of compound **23** was orally administered to 3 sets of male C57BL/6 mice. (b) Dose of 15 mg/kg body weight of compound **23** was intravenously administered to 3 male C57BL/6 mice. (c) Calculated pharmacokinetics parameter in tabulated form. 2% ethanol in PBS (0.01 M, pH = 7.4) buffer used as vehicle. The concentration of compound present in serum at indicated time points was quantified by LC–MS/MS (Figure S4).

lular involvements.¹⁵ This preclinical model has not only been the key support for the pathogenetic role of TLR7 in this clinical context but also has been instrumental for discovery of other downstream pathogenetic mechanisms for the disease as well as validation of most of the clinically used targeted biologic therapies used clinically.⁴⁵ We administered 15 mg/kg body weight compound **23** by oral gavage to the mice daily from the first day of application of imiquimod cream and on the 6th day assessed disease development, in comparison with vehicle-administered control mice having developed imiquimod-driven psoriasis (Figure 4a). We found that oral administration of our TLR7 antagonist **23** could totally prevent the cutaneous pathology in terms of macroscopic morphology (Figure 4b). There was also significant retardation in skin thickening in the antagonist-treated mice (Figure 4c).

Histopathologic scoring of the lesional skin in the treated mice revealed nearly complete absence of the pathognomonic features like hyperkeratosis, parakeratosis, acanthosis, spongiosis, papillomatosis, suprapapillary thinning, vascular dilatation, microabscesses and pustule formation (Figure 5a,b). On scoring the histopathology based on the listed features (Figure 5c), there was total amelioration of disease on oral administration **23** (Figure 5d,e).

In a repeat experiment too, the amelioration of cutaneous pathology with compound **23** was evident in terms of reduction in skin fold thickness (Figure S5) as well as in terms of reduction in the tissue expression of the proinflammatory cytokine TNF α (widely implicated in the pathogenesis of psoriasis) and four major type I IFN signature genes (ISGs) MX1, MX2, ISG15, and IFIT1 (surrogate markers for type I IFN induction *in situ*) (Figure 6a–e).

Moreover, histomorphology of lung, liver, and kidney did not show any remarkable pathologic changes following oral administration of compound **23** for 7 consecutive days at a

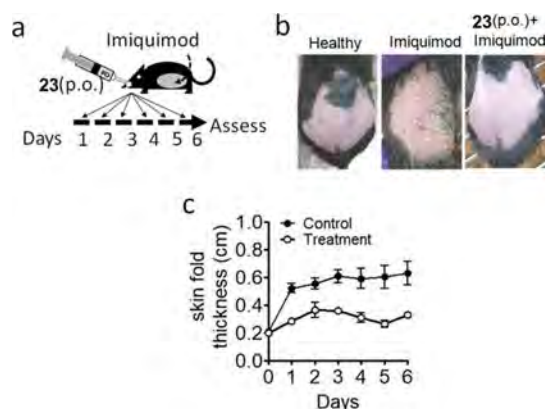


Figure 4. Efficacy of TLR7 antagonist in rodent psoriasis model. (a) Schematic representation of experimental protocol followed—compound 23 or vehicle was orally administered for 7 consecutive days starting one day before (day 0) topical application of imiquimod on the dorsal skin surface, which was done for 6 consecutive days. The following day mice were sacrificed, normal and psoriatic skin harvested and subjected to histopathological evaluation. (b) (Left) Shaved normal dorsal skin before imiquimod application, (middle) shaved imiquimod treated dorsal skin of vehicle treated mouse on day 7 showing significant scale formation on skin, and (right) shaved imiquimod treated dorsal skin of compound 23 treated mouse on day 7 showing markedly lesser scale formation compared to previous group. (c) Thickness of skin fold of vehicle-treated mice ($n = 9$) and compound-treated mice ($n = 9$) were recorded and plotted every day (3 readings each) to monitor the gradual changes taking place upon daily imiquimod application. Data are represented as mean \pm SEM. 2% ethanol in PBS (0.01 M, pH = 7.4) buffer was used as vehicle.

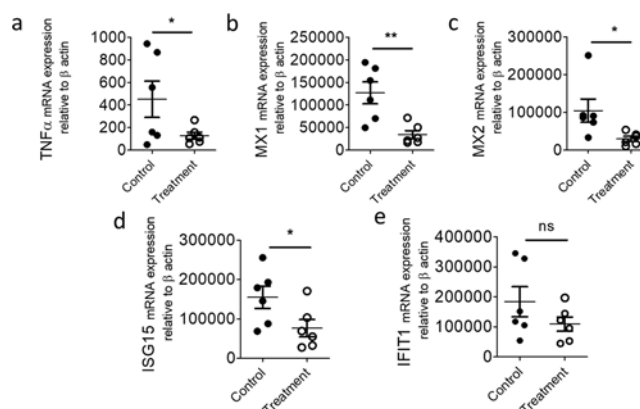


Figure 6. Inhibition of pro-inflammatory TLR7-mediated gene expression in rodent model of psoriasis. (a–e) Dorsal skin sections obtained from C57BL/6 mice treated with vehicle ($n = 6$) or treated with 15 mg/kg compound 23 ($n = 6$) for 7 consecutive days were processed and subjected to gene expression studies to measure expression of indicated genes—TNF α (a), MX1 (b), MX2 (c), ISG15, (d) and IFIT1 (e). (* $p < 0.05$, ** $p < 0.01$, ns = nonsignificant).

dose rate of 15 mg/kg as compared to vehicle administration (Figure 7). No notable toxicity-induced pathology was discernible, viz. changes in parenchymal architecture of the liver, hepatocyte survival, fatty infiltration, or inflammation in compound treated mice as compared to vehicle treated mice (Figure 7a,b). Similarly, no discernible changes were observed in lung microanatomy as well. No evidence of immune

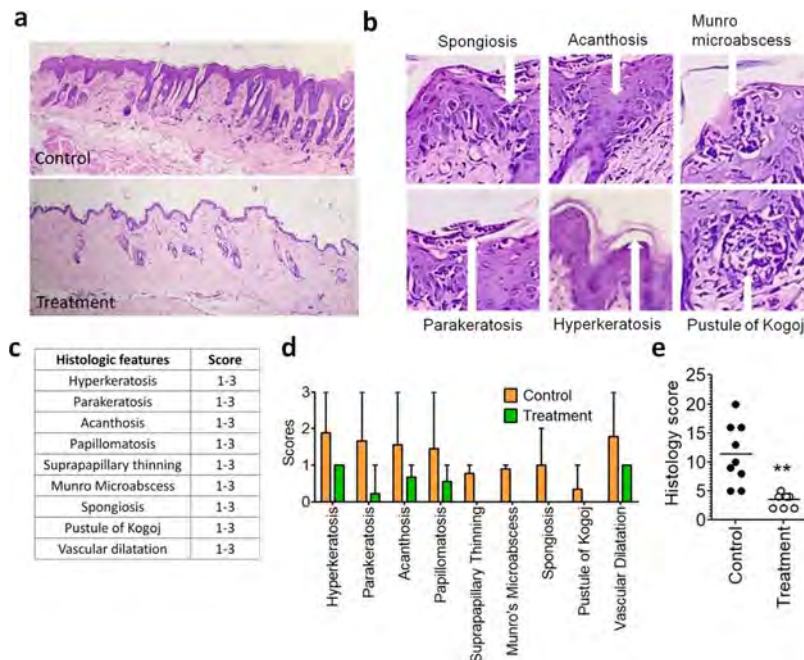


Figure 5. Histopathologic scoring of the H&E-stained skin sections of mice with psoriatic disease. (a) (Upper) H&E stained, imiquimod exposed, dorsal skin section of vehicle-treated mouse showing marked thickening of epidermis and presence of hyperkeratosis, papillomatosis, and acanthosis, (lower) H&E stained, imiquimod exposed, dorsal skin section of compound 23 treated mouse showing appreciably lesser thickening of epidermis. (b) Representative images showing the key pathognomonic histopathologic features used for scoring. (c) All histological features were scored based on their severity and preponderance, 1 being least severe and 3 being most severe. (d) Imiquimod exposed dorsal skin sections from compound-treated or vehicle-treated mice were graded on the basis of different clinically relevant histopathological parameters such as hyperkeratosis, acanthosis, papillomatosis, suprapapillary thinning, Munro's microabscess, spongiosis, pustule of Kogoj, vascular dilatation of control group ($n = 9$), and compound-treated group ($n = 9$), as a measure of disease severity. (e) Data on scores for individual pathognomonic features compared between control and treatment groups. (** $p < 0.01$).

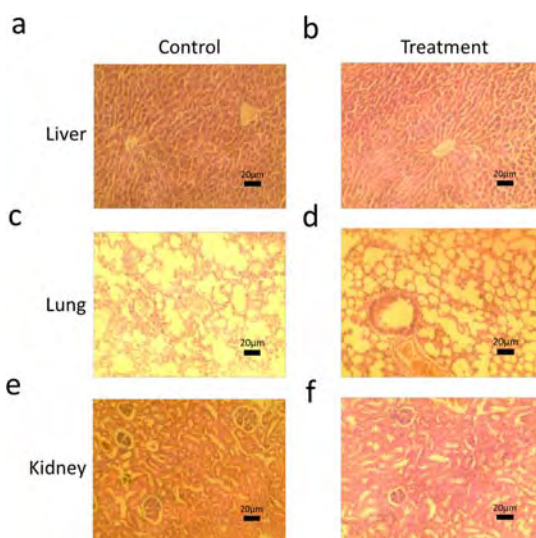


Figure 7. Short-term visceral toxicity assessment. (a–f) Representative images of H&E stained sections of liver specimens (a,b), lung specimens (c,d), and kidney specimens (e,f) obtained from C57BL/6 mice treated with vehicle (a,c,e) or 15 mg/kg compound **23** (b,d,f) for 7 consecutive days.

infiltration or alveolar architecture was observed in the lungs (Figure 7c,d). In kidneys, no glomerular hypertrophy, mesangial proliferation, capsular space obliteration, or inflammation was observed in the compound-treated mice as compared to control mice (Figure 7e,f). We also did not observe any behavioral or physiological abnormalities in experimental animals within the study period, thus indicating that oral administration of compound **23** does not cause any apparent short-term visceral cytotoxicity in C57BL/6 mice. Thus, this novel TLR7 antagonist **23** was very efficient in preventing a TLR7-driven TNF α and type I IFN induction and the autoimmune pathology *in vivo*.

CONCLUSIONS

In summary, we have been able to define minimal structural requirements in a purine scaffold TLR7 agonist **1** and identify a singular “chemical switch” in the scaffold that could transform the molecule to a TLR7 antagonist. We established that a small structural modification in TLR7 ligand can lead to reversal in their functional activity. We further developed on that and could design a potent TLR7 antagonist **23**, which had favorable *in vitro* and *in vivo* pharmacokinetics with excellent oral bioavailability (70.8%) in mice. Interestingly, the ethylpiperazine group at N-9 led to enhancement of TLR7 agonism, while introducing the same at C-6 led to potentiation of TLR7 antagonism. Introduction of an additional basic center at C-6 has a profound potentiating effect on TLR7 antagonism in purine scaffold. Our SAR studies successfully identified site-specific substitutions that can switch a well-established purine scaffold TLR7 agonist into TLR7 antagonist. None of the TLR7 antagonist showed any TLR7 agonism, which signifies that they are pure antagonists. It is worthwhile to mention that all the TLR7 antagonists reported herein showed excellent selectivity against TLR8. The docking analysis of our TLR7 antagonists showed that the purine ring is sandwiched between two hydrophobic residues Phe329 and Tyr1374 forming π – π stacking interactions along with hydrogen bonding with Ser452, which plays a vital role in determining TLR7

antagonism. Finally, we could validate the *in vivo* efficacy of this TLR7 antagonist in a clinically relevant murine model of psoriasis. The histomorphology of lung, liver, and kidney did not show any remarkable pathologic changes following oral administration. The TLR7 antagonist **23** thus appears to be a very promising lead molecule for further development into clinically translatable TLR7 antagonists that can be first-in-class therapeutic agents in the relevant clinical contexts, which include a number of autoimmune diseases accounting for significant morbidity worldwide.

EXPERIMENTAL SECTION

Aqueous Solubility Assay. Dimethyl sulfoxide (DMSO, 6 μ L, 50 mM) stock was added to the deep well plate containing 594 μ L of pH 7.4 0.25 M phosphate buffer (including DMSO control), mixed, and incubated for 18 h at room temperature (rt) with constant mixing at 300 rpm. The plate was sealed well during the incubation process. After incubation, the samples were centrifuged for 20 min at 4000 rpm. The supernatant (400 μ L) was analyzed by high-performance liquid chromatography (HPLC)-UV. The DMSO content in the sample was 1.0%, and the final concentration of the compound in deep-well plate was 500 μ M. The spectrum was read using a Shimadzu UV spectrophotometer at 240 nm (Calculation is in Table S1).

Caco-2 Permeability Assay. Stock (10 mM) of compound in DMSO was diluted with Hank's balanced salt solution (HBSS) buffer pH 7.4 to a final concentration of 10 μ M. For the proliferation of cells, 250 μ L of Dulbecco's modified Eagle medium (DMEM) was added to the basal compartment of 96-well multiscreen Caco-2 plate and seeded 12,000 cells/well (0.16×10^6 cells/mL) in all of the apical wells placed in a CO₂ incubator at 37 °C. On the day of assay, the medium was removed and washed twice with HBSS buffer. HBSS buffer (250 μ L) with 2% bovine serum albumin (BSA) was added to basal wells and 75 μ L of the test compound was added to apical wells. Basal samples (25 μ L) were collected at 120 min and processed as mentioned below. The test compound (250 μ L) and 75 μ L of HBSS buffer with 2% BSA was added to basal wells and apical wells, respectively. At 120 min, 25 μ L of apical samples was collected and processed as stated below. A single-point calibration curve in HBSS buffer with 2% BSA was used. Donor samples and receiver samples were diluted 1:1 with HBSS separately while the former contains 2% BSA. It was precipitated with 200 μ L of acetonitrile containing internal standard and vortexed for 5 min @ 1000 rpm, and centrifuged at 4000 rpm for 10 min. Finally, 100 μ L of the supernatant was diluted with 200 μ L of water and submitted for liquid chromatography–mass spectrometry (LC–MS)/MS analysis. (Calculation is in Table S2).

Plasma Stability Assay. Stock (25 μ M) of test compound was prepared in acetonitrile from the stock solution of 10 mM in DMSO. By diluting acetonitrile/water (50:50) from the previously prepared 10 mM stock, 125 μ M sample of 200 μ L was prepared. For 0 min samples, plasma was heat inactivated at 56 °C for 45 min and to it 3 μ L of 25 μ M test compound was added to make the final volume 75 μ L. In 200 μ L acetonitrile, a 25 μ L aliquot of the mixture was taken and crashed. At 0, 15, 30, 60, and 120 min, a 25 μ L aliquot of the sample was precipitated immediately with 200 μ L of acetonitrile, centrifuged at 4000 \times relative centrifugal force (RCF), 4 °C for 20 min and analyzed on LC–MS/MS (Calculation for human plasma stability in Table S3 and mice plasma stability Table S4).

Microsomal Stability. Stock (10 mM) of test compound in DMSO was diluted with 1:1 water acetonitrile to get 200 μ L 1 mM stock solution. Working concentration (100 μ M) of test compound was prepared by diluting 1 mM stock solution of test compound in DMSO with acetonitrile: water (1:1). Nicotinamide adenine dinucleotide phosphate (NADPH) cofactor solution (2.5 mM) was prepared from 16 mM stock solution and 3.33 mg/mL working stock of liver microsomes was prepared from 20 mg/mL liver microsome master stock solution. Phosphate buffer (85 μ L) of pH 7.4 was mixed

with 2.5 μ L of test compound (100 μ M) and 75 μ L 3.33 mg/mL HLM in a deep well plate for preincubation of 10 min at 37 $^{\circ}$ C. The mixture (32.5 μ L) was added to 17.5 μ L buffer and incubated for 60 min without NADPH cofactor. For 0 min sample, 16.5 μ L of the preincubated mixture was crashed with 200 μ L of acetonitrile and 8.75 μ L of cofactor was added to it. 62 μ L NADPH-cofactor was added to remaining incubation mixture and kept for 60 min at 37 $^{\circ}$ C. For other time point samples, 25 μ L of incubation mixture at 5, 10, 30, 60, and 60 min without cofactor was precipitated immediately with 200 μ L of acetonitrile containing internal standard and vortex for 5 min at 1200 rpm. The samples were centrifuged at 4000 \times RCF, 4 $^{\circ}$ C for 10 min. The supernatant (150 μ L) was diluted with 150 μ L of water and analyzed on LC–MS/MS (calculation for human microsomal stability in Table S5 and mice microsomal stability Table S6).

TLR7 Agonism and Antagonism Assay Using HEK-Blue hTLR7 Reporter Cell Line. The TLR7 agonistic or antagonist activity of synthesized compounds was assayed using a HEK293 cell line engineered to express human TLR7 as well as a NF- κ B induced SEAP. The assay was based on the principle that TLR activation with TLR agonist leads to downstream NF- κ B activation which in turn induces SEAP production and secretion into culture supernatant, causing color change upon interaction with the detection media. 7×10^4 cells/well were seeded in 100 mg/mL Normocin supplemented complete DMEM medium and allowed to adhere to the substrate for 5 h at 37 $^{\circ}$ C and 5% CO₂. For antagonism assays, CL264 (TLR7 agonist, 5 μ g/mL) was added to the cells preincubated for 1 h with indicated doses of compounds, whereas for agonism assays, cells were only treated with indicated doses of compounds. Following overnight incubation, 50 μ L of culture supernatant from each well was added to 200 μ L of QUANTI-Blue detection media and constantly monitored for color change. After 1–2 h of incubation, spectrophotometric reading at 655 nm wavelength was recorded. To ensure the validity of TLR7 antagonism assay, the ability of different doses of hydroxy-chloroquine to inhibit TLR7 activation was studied as a positive control. Two-tailed paired Student's *t*-test was performed using GraphPad Prism software version 5.0. HEK-Blue hTLR7 reporter cell line, Normocin, and CL264 were purchased from Invivogen, USA.

TLR8 Antagonism Assay Using HEK-Blue hTLR8 Reporter Cell Line. To ensure the specificity of the synthesized antagonists for human TLR7 and exclude the possibility of nonspecific antagonism toward human TLR8 which is structurally very similar to human TLR7, we performed reporter assays using HEK-Blue hTLR8 reporter cell line. The protocol used to perform this experiment was exactly same as that for the antagonism assay in HEK-TLR7 cell line, described above. The only difference was the usage of a TLR8 specific agonist CL075 (3 μ g/mL) as the stimulant.

Cytotoxicity Assay in HEK293 Cell Line. 1, 5, 10, 20, 40, 60, 80, and 100 μ M of indicated compounds were added to 6×10^4 HEK293 cells cultured in incomplete DMEM at 37 $^{\circ}$ C and 5% CO₂ overnight, following which cells were harvested in phosphate-buffered saline (PBS) (0.01 M, pH = 7.4), stained with 2.5 mg/mL PI for 1 min, and percentage of cells showing PI uptake in a flow cytometer (BD LSRFortessa) was measured.

IL-6 mRNA Expression Measurement through RT-PCR Analysis. HEK-Blue TLR7 cells were seeded in a 96-well plate at a density of 1×10^5 cells/well and allowed to attach overnight. Next morning, cells were preincubated with 5 μ M of compound 23 for 1 h before being stimulated with 5 μ g/mL of TLR7 agonist-CL264 for 6 h, following which cells were harvested in the TRIzol reagent (Invitrogen). Total RNA was isolated using the manufacturer's protocol followed by cDNA preparation using the Applied Biosystems kit, and RT-PCR was done using Bio-Rad SYBR Green Master Mix to measure the expression levels of IL6 gene relative to that of 18S (housekeeping gene). Primer sequences used, Hu-18S: forward: 5'-GTTGGTTTTCGGAAGCTGAGG-3' reverse: 5'-TCGTTTATGGTCGGAAGTACG-3' and Hu-IL6: forward: 5'-CACAGACAGCCACTCACCTCTTC-3' reverse: 5'-TTTGCTGCTTTCACACATGTTACTC-3'.

TLR7 Antagonism Assay in Primary hPBMCs. Primary hPBMCs were isolated from blood taken from healthy individuals after obtaining their informed consent as well as ethical approval from the Institutional Ethics Committee, in accordance with the guidelines mentioned in the Declaration of Helsinki. PBMCs were obtained by performing density gradient centrifugation and seeded at a density of 2×10^5 cells/well in a 96-well plate. PBMCs were preincubated with 5 μ M of compound 23 for 1 h before being stimulated with 5 μ g/mL of TLR7 agonist-gardiquimod overnight. Next day, the culture supernatant was collected and subjected to TNF α ELISA according to the protocol outlined by the manufacturer (Mabtech).

Homology Modeling and Docking Study. Homology structure of human TLR7 ectodomain was built using sequence Q9NYK1 retrieve from UNIPROT. The homology model structure of hTLR7 was built using TLR8 (PDB SWYZ) as a template in discovery studio modeler suite, according to the reported procedure.⁴¹ The docking experiment was performed using Discover Studio 4.1 C-DOCKER module. The docking method was optimized by analyzing reported TLR7 antagonist binding pose. Random conformers of compounds were searched using dynamics of 1000 steps. Docking simulation was performed using default parameter of C-DOCKER module in Discover Studio 4.1. The docked results were fully minimized using CHARMM force field with conjugate gradient 1.0. Pictorial view of docking pose was made using PyMOL.

In Vivo Pharmacokinetics and Bioavailability Study. Nine 8–10 week old male C57BL/6 mice were recruited for the experiment. They were divided into three groups each having three mice. The compound was reconstituted in 2% ethanol in PBS (0.01 M, pH = 7.4). The mice belonging to the first group were given oral gavage with 15 mg/kg compound, the mice belonging to the second group were given oral gavage with 10 mg/kg compound, and the mice belonging to the third group were given intravenous injections of 15 mg/kg compound. Blood samples were drawn at 0, 0.5, 1, 2, 4, 6, 12, and 24 h after compound administration, and serum was isolated for the mice administered orally with the compound. On the other hand, blood samples were drawn at 0, 0.25, 0.5, 1, 2, 4, 6, 12, and 24 h after compound administration, and serum was isolated from the mice injected intravenously with the compound. 10 μ L of serum from each mouse was extracted with 30 μ L of LC/MS-grade acetonitrile + 0.1% formic acid (J.T. Baker) by alternate vortexing and chilling. Next, the supernatant was collected by centrifugation at 14,000 rpm for 10 min and analyzed by LC–MS/MS to measure the concentration of compound 23 in serum. Standards of compound 23 ranging from 74.688 to 5975 pg was prepared in serum and extracted in acetonitrile + 0.1% formic acid. MS was carried out in LTQ ORBITRAP XL using Hypersil Gold C18 column having a diameter of 100 \times 2.1 mm with particle size being 1.9 μ m. The column formed the stationary phase and a mixture of solution A (acetonitrile + 0.1% formic acid) and solution B (HPLC grade H₂O + 0.1% formic acid) formed the mobile phase. LC (injection volume 2 μ L) was done using an isocratic solution containing 40% acetonitrile and 0.1% formic acid. The intact compound had a retention time of 0.76 min and (*m/z*) of 387.2988, while (*m/z*) of fragmented compound after MS/MS was 273.1852. All data were analyzed using the Thermo Xcalibur software.

In Vivo Efficacy Study. Eighteen wild-type C57BL/6 male mice aged 8–10 weeks, provided by CSIR-IICB animal house facility, were divided into two groups; (1) control group-containing nine mice with induced psoriasis, treated with 2% ethanol in sterile PBS (0.01 M, pH = 7.4) (vehicle) and (2) treatment group-containing nine mice with induced psoriasis treated with compound 23. Psoriasis was induced by daily topical application of 62.5 mg 5% w/w imiquimod cream (Imiquad; Glenmark, India) on a patch of shaved dorsal skin of the mice for 6 consecutive days. Vehicle and compound (15 mg/kg) were administered orally daily for 7 days, beginning 1 day prior to the start of imiquimod application. Skin fold measurement of the affected area was performed by a person blind to the experimental details and outcomes, with a standard Vernier caliper on a daily basis starting prior to imiquimod application and continuing till the end of the experiment. The experimental animals were sacrificed on the 7th day of imiquimod application, and portions of affected skin as well as

normal skin were collected from each animal (in 4% paraformaldehyde) for histopathological evaluation by hematoxylin and eosin (H&E) staining. All animal handling and mouse experiments were conducted in accordance with national and international guidelines and upon approval from the institutional ethics committee. All recommendations enlisted in the ACS Ethical Guidelines were followed while performing the mouse experiments.

RNA Isolation, cDNA Preparation, and Quantitative PCR. Lesional skin tissue derived from six control C57BL/6 mice and six compound **23** (15 mg/kg)-treated mice, following 7 consecutive days of oral administration (according to a protocol identical to that described in *in vivo* efficacy study), was minced into tiny pieces, frozen in liquid nitrogen, crushed using a mortar & pestle in TRIzol reagent (Invitrogen) and RNA was isolated according to the manufacturer's protocol. cDNA was produced using the high-capacity cDNA reverse transcription kit (Applied Biosystems). qPCR was performed to study the expression of the specified genes using SYBR Green Master Mix (Bio-Rad) (normalization was done with respect to the expression of β -actin—housekeeping gene).

Primer Sequences.

Mu- β actin	F: 5'-GAGGTATCCTGACCCTGAAGTA-3'
	R: 5'-GCTCGAAGTCTAGAGCAACATAG-3'
Mu-TNF α	F: 5'-AATGGCCTCCCTCTCATCAGTT-3'
	R: 5'-CCACTTGGTGGTTTGCTACGA-3'
Mu-MX1	F: 5'-TTCAAGGATCACTCATACTTCAGC-3'
	R: 5'-GGGAGGTGAGCTCCTCAGT-3'
Mu-MX2	F: 5'-TTCCAGCATCTGAATGCCTAC-3'
	R: 5'-ACTGGATGATCAAGGGAACG-3'
Mu-ISG15	F: 5'-ACGGTCTTACCCTTTCCAGTC-3'
	R: 5'-CCCCTTTCGTTCCCTCACCAG-3'
Mu-IFIT	F: 5'-AGGCTGGAGTGTGCTGAGAT-3'
	R: 5'-TCTGGATTTAACCGGACAGC-3'

Short-Term *In Vivo* Toxicity Studies. Lung, liver, and kidney specimens of mice, following oral administration of compound **23** and vehicle for 7 consecutive days at a dose rate of 15 mg/kg, were collected and preserved in 10% formalin. H&E staining of tissue sections was performed for histomorphological evaluation. Images were acquired in an Olympus CKX41 brightfield inverted microscope at an objective magnification of 10 \times and monitored to study histomorphological parameters to deduce the visceral toxicity associated with compound **23** administration.

Chemical Synthesis and Methods. General Methods. All starting materials, reagents, and solvents were purchased from commercial suppliers and used without further purification. Air-sensitive reactions were carried out under a dry nitrogen or argon atmosphere. For thin-layer chromatography (TLC) on silica gel plates (Merck silica gel 60, F254) was used. RediSep Rf silica gel columns was used for column chromatographic purification on the Teledyne ISCO CombiFlash Rf system using 230–400 mesh silica gel. ^1H NMR was recorded at 300 MHz (Bruker-DPX), 400 MHz (Jeol), and 600 MHz (Bruker-Avance) frequency and ^{13}C NMR spectra were recorded at 75 MHz (Bruker-DPX), 100 MHz (Jeol), and 150 MHz (Bruker-Avance) using TMS as the internal standard. High-resolution mass spectra, HRMS (m/z), were measured using EI (Jeol-JMS 700 mass spectrometer), ESI (Q-ToF Micro mass spectrometer) techniques, and ESI (LTQ Orbitrap XL mass spectrometer). The purity of all the compounds was determined to be >95%, analyzed by Hitachi HPLC using column Ximate C18 (4.6 mm \times 150 mm, 5.0 μm) using gradient elution of acetonitrile in water 0–90% for 12 min and flow rate 1 mL/min with detection at 254 nm wavelength.

Synthesis of 2-Butoxy-9-(tetrahydro-2H-pyran-2-yl)-9H-purin-6-amine (2).³¹ Sodium *t*-butoxide (0.8 g, 7.8 mmol) was added portion wise to the solution of 6 mL of *n*-BuOH and compound **1** (0.5 g, 2.0 mmol) in rt. The reaction mixture was then stirred for 12 h at 100 $^\circ\text{C}$ and concentrated under vacuum. Reaction mixture was purified by column chromatography to obtain pure compound **2** as yellowish liquid (77%). ^1H NMR (300 MHz, CDCl_3): δ 7.78 (s, 1H), 6.51 (s, 2H), 5.54 (dd, J = 2.4, 9.0 Hz, 1H),

4.23 (t, J = 6.6 Hz, 2H), 4.04 (d, J = 12.6 Hz, 1H), 3.69–3.61 (m, 1H), 1.99–1.88 (m, 3H), 1.72–1.59 (m, 4H), 1.44–1.36 (m, 2H), 1.14–1.09 (m, 1H), 0.87 (t, J = 7.2 Hz, 3H). ^{13}C NMR (100 MHz, CDCl_3): δ 162.3, 156.6, 151.0, 136.6, 115.5, 81.4, 68.6, 67.0, 31.7, 31.1, 24.9, 22.9, 19.3, 13.9. HRMS (ESI) m/z : (M + H) calcd for $\text{C}_{14}\text{H}_{22}\text{N}_5\text{O}_2$, 292.1773; found, 292.1766.

Synthesis of 2-Butoxy-8-methoxy-9-(tetrahydro-2H-pyran-2-yl)-9H-purin-6-amine (3). *N*-Bromosuccinimide (0.06 g, 0.36 mmol) was added to the solution of compound **2** (0.1 g, 0.3 mmol) in 0.6 mL CHCl_3 at 0 $^\circ\text{C}$. Reaction was allowed to warm rt and stirred for 4 h at rt. The reaction mixture was diluted with CHCl_3 and washed with sodium thiosulfate. Evaporation of the CHCl_3 layer gave TLC wise pure bromo-substituted compound, and the next step was forwarded without further purification. This bromo derivative was refluxed with a 5 M solution of sodium methoxide in methanol (2.7 equiv) for 4 h, and the reaction mixture was concentrated under vacuum. The reaction mixture was then purified by column chromatography to give pure compound **3** as brownish semisolid (80%). ^1H NMR (300 MHz, CDCl_3): δ 5.54 (dd, J = 1.8, 11.1 Hz, 1H), 5.28 (s, 2H), 4.28 (t, J = 6.6 Hz, 2H), 4.17–4.12 (m, 4H), 3.73–3.65 (m, 1H), 2.84–2.72 (m, 1H), 2.06–2.02 (m, 1H), 1.79–1.63 (m, 6H), 1.58–1.46 (m, 3H), 0.97 (t, J = 7.5 Hz, 3H). ^{13}C NMR (100 MHz, CDCl_3): δ 160.7, 154.3, 153.9, 151.5, 110.9, 81.3, 68.9, 66.9, 56.9, 31.2, 28.6, 24.9, 23.5, 19.3, 13.9. HRMS (ESI) m/z : (M + H) calcd for $\text{C}_{15}\text{H}_{24}\text{N}_5\text{O}_3$, 322.1879; found, 322.1884.

Synthesis of 2-Butoxy-8-methoxy-9H-purin-6-amine (4). Compound **3** (0.2 g, 0.5 mmol) was added to 1 mL solution of 10% TFA in methanol and stirred for 72 h. Completion of reaction was monitored by TLC and white precipitation was obtained after dilution of reaction mixture with ethyl acetate. Precipitation was filtered to obtain pure compound **4** as TFA salt (73%). ^1H NMR (300 MHz, CDCl_3 + 1 drop CD_3OD): δ 4.34 (t, J = 6.6 Hz, 2H), 4.05 (s, 3H), 1.74–1.64 (m, 2H), 1.41–1.33 (m, 2H), 0.88 (t, J = 7.5 Hz, 3H). HRMS (ESI) m/z : (M + H) calcd for $\text{C}_{10}\text{H}_{26}\text{N}_5\text{O}_2$, 238.1304; found, 238.1311.

General Procedure A for Synthesis of 2-Butoxy-9-(3-chloropropyl)-8-methoxy-9H-purin-6-amine (5). Compound **4** (0.1 g, 0.5 mmol) and potassium carbonate (0.2 g, 1.5 mmol) were dissolved in 1 mL of dimethylformamide (DMF), and the reaction mixture was heated at 50 $^\circ\text{C}$ for 2 h. 1-Bromo-3-chloropropane was added to the reaction mixture at rt and stirred for 16 h. The solvent was then removed, and the reaction was partitioned between CHCl_3 and water. Organic layer was then dried, and column chromatography was performed to get pure compound **5** as white solid (67%, mp 115 $^\circ\text{C}$). ^1H NMR (300 MHz, CDCl_3): δ 5.32 (s, 2H), 4.26 (t, J = 6.6 Hz, 2H), 4.11–4.06 (m, 5H), 3.52 (t, J = 6.6 Hz, 2H), 2.28–2.20 (m, 2H), 1.77–1.70 (m, 2H), 1.51–1.44 (m, 2H), 0.95 (t, J = 7.2 Hz, 3H). ^{13}C NMR (100 MHz, CDCl_3): δ 160.8, 154.6, 153.8, 151.9, 110.9, 67.0, 56.8, 41.8, 38.7, 32.0, 31.2, 19.3, 13.9. HRMS (ESI) m/z : (M + H) calcd for $\text{C}_{13}\text{H}_{21}\text{N}_5\text{O}_2\text{Cl}$, 314.1384; found, 314.1387.

General Procedure B for Synthesis of 2-Butoxy-8-methoxy-9-(3-(piperidin-1-yl)propyl)-9H-purin-6-amine (6). Compound **5** (0.1 g, 0.3 mmol), potassium carbonate (0.1 g, 0.7 mmol), and piperidine (0.1 mL, 1.0 mmol) were dissolved in 0.5 mL of DMF. The reaction mixture was then stirred for 6 h at rt. Completion of reaction was confirmed by TLC, and column chromatography was performed to obtain pure compound **6** as semisolid (73%). ^1H NMR (400 MHz, CDCl_3): δ 5.22 (s, 2H), 4.24 (t, J = 6.8 Hz, 2H), 4.07 (s, 3H), 3.94 (t, J = 7.2 Hz, 2H), 2.37–2.34 (m, 6H), 2.00–1.92 (m, 2H), 1.77–1.70 (m, 2H), 1.59–1.53 (m, 4H), 1.49–1.43 (m, 2H), 1.41–1.35 (m, 2H), 0.93 (t, J = 7.2 Hz, 3H). ^{13}C NMR (100 MHz, CDCl_3): δ 160.8, 154.8, 153.7, 152.0, 110.9, 66.9, 56.7, 56.2, 54.5, 39.6, 31.2, 26.1, 25.7, 24.2, 19.3, 14.0. HRMS (ESI) m/z : (M + H) calcd for $\text{C}_{18}\text{H}_{31}\text{N}_6\text{O}_2$, 363.2508; found, 363.2512.

General Procedure C for Synthesis of 6-Amino-2-butoxy-9-(3-(piperidin-1-yl)propyl)-9H-purin-8-ol (7). Compound **6** (0.1 g, 0.03 mmol) was dissolved in 0.5 mL of 4 M HCl in dioxane at rt for 3 h. The reaction mixture was then neutralized with ammonia and concentrated in vacuum. Column chromatography was performed using 5% ammonia in methanol and CHCl_3 as a mobile phase to

obtain pure compound **7** as white solid (87%, mp > 250 °C). ¹H NMR (600 MHz, CDCl₃): δ 5.84 (s, 1H), 4.22 (t, *J* = 6.6 Hz, 2H), 3.87 (t, *J* = 6.6 Hz, 2H), 2.61–2.59 (m, 6H), 2.07–2.04 (m, 2H), 1.74–1.70 (m, 2H), 1.67–1.65 (m, 4H), 1.46–1.43 (m, 4H), 0.94 (t, *J* = 7.2 Hz, 3H). ¹³C NMR (125 MHz, CDCl₃ + 1 drop CD₃OD): δ 160.7, 153.7, 149.7, 147.9, 99.0, 67.0, 55.8, 54.1, 38.0, 31.0, 25.0, 24.8, 23.5, 19.2, 13.8. HRMS (ESI) *m/z*: (M + H) calcd for C₁₇H₂₉N₆O₂, 349.2352; found, 349.2351. HPLC purity 97.9%.

Synthesis of 2-Butoxy-9-(3-(4-ethylpiperazin-1-yl)propyl)-8-methoxy-9H-purin-6-amine (8). Compound **6** (0.1 g, 0.3 mmol), potassium carbonate (0.1 g, 0.7 mmol), and ethylpiperazine (0.13 mL, 1.0 mmol) were dissolved in 0.5 mL of DMF. The reaction was then performed according to general procedure B to obtain pure compound **8** as semisolid (67%). ¹H NMR (400 MHz, CDCl₃): δ 5.31 (s, 2H), 4.22 (t, *J* = 6.4 Hz, 2H), 4.05 (s, 3H), 3.93 (t, *J* = 6.8 Hz, 2H), 2.48–2.32 (m, 12H), 1.93–1.88 (m, 2H), 1.74–1.67 (m, 2H), 1.49–1.41 (m, 2H), 1.03 (t, *J* = 7.2 Hz, 3H), 0.91 (t, *J* = 7.2 Hz, 3H). ¹³C NMR (100 MHz, CDCl₃): δ 160.8, 154.8, 153.7, 151.9, 110.8, 66.9, 56.7, 55.5, 53.0, 52.7, 52.3, 39.6, 31.2, 26.2, 19.3, 13.9, 11.9. HRMS (ESI) *m/z*: (M + H) calcd for C₁₉H₃₄N₇O₂, 392.2774; found, 349.2773.

Synthesis of 6-Amino-2-butoxy-9-(3-(4-ethylpiperazin-1-yl)propyl)-9H-purin-8-ol (9). Compound **8** (0.1 g, 0.3 mmol) was dissolved in 0.5 mL of 4 M HCl in dioxane at rt for 3 h. The reaction was then performed according to general procedure C to obtain pure compound **9** as white solid (91%, mp > 250 °C). ¹H NMR (400 MHz, CD₃OD): δ 4.25 (t, *J* = 6.8 Hz, 2H), 3.85 (t, *J* = 6.8 Hz, 2H), 2.76–2.04 (m, 12H), 1.95–1.88 (m, 2H), 1.74–1.66 (m, 2H), 1.51–1.43 (m, 2H), 1.04 (t, *J* = 7.2 Hz, 3H), 0.94 (t, *J* = 7.2 Hz, 3H). ¹³C NMR (100 MHz, CD₃OD): δ 160.8, 153.8, 149.9, 148.4, 98.5, 66.6, 55.5, 52.2, 52.0, 51.9, 38.2, 30.9, 24.8, 18.9, 12.8, 10.3. HRMS (ESI) *m/z*: (M + H) calcd for C₁₈H₃₂N₇O₂, 378.2617; found, 378.2617. HPLC purity 99.2%.

Synthesis of 8-Methoxy-9H-purin-6-amine (11). Compound **10** (0.2 g, 6.3 mmol) was refluxed with a 5 M solution of sodium methoxide in methanol (63 mmol, 10 mL) for 12 h. The reaction mixture was then concentrated in vacuum and diluted with 2 mL of water. The reaction mixture was neutralized, and the precipitation was filtered to obtain pure compound **11** as brown solid (72%, mp > 250 °C). ¹H NMR (400 MHz, DMSO-*d*₆): δ 8.06 (s, 1H), 7.38 (s, 2H), 6.81 (s, 1H), 3.98 (s, 3H). ¹³C NMR (100 MHz, CD₃OD): δ 154.5, 151.4, 150.5, 148.5, 106.3, 57.2. HRMS (ESI) *m/z*: (M + H) calcd for C₆H₈N₅O, 166.0729; found, 166.0732.

Synthesis of 9-(3-Chloropropyl)-8-methoxy-9H-purin-6-amine (12). The reaction was performed according to general procedure A using compound **11** (0.2 g, 1.2 mmol), potassium carbonate (0.5 g, 3.6 mmol), and 1-bromo-3-chloropropane in 3 mL DMF to obtain compound **12** as white semisolid (78%). ¹H NMR (400 MHz, CDCl₃): δ 8.22 (s, 1H), 5.38 (s, 2H), 4.17–4.14 (m, 5H), 3.54–3.49 (m, 2H), 2.30–2.23 (m, 2H). ¹³C NMR (100 MHz, CDCl₃): δ 155.6, 152.9, 151.3, 150.2, 115.7, 57.2, 41.7, 39.0, 31.9. HRMS (ESI) *m/z*: (M + H) calcd for C₆H₁₃N₅OCl, 242.0809; found, 242.0809.

Synthesis of 9-(3-(4-Ethylpiperazin-1-yl)propyl)-8-methoxy-9H-purin-6-amine (13). Compound **12** (0.1 g, 0.4 mmol), potassium carbonate (0.1 g, 0.7 mmol), and ethylpiperazine (0.2 mL, 1.1 mmol) were dissolved in 0.5 mL of DMF. The reaction was then performed according to general procedure B to obtain pure compound **13** as semisolid (63%). ¹H NMR (300 MHz, CDCl₃): δ 8.21 (s, 1H), 5.49 (s, 2H), 4.12 (s, 3H), 4.04 (t, *J* = 6.9 Hz, 2H), 2.45–2.36 (m, 12H), 1.97–1.92 (m, 2H), 1.07 (t, *J* = 7.2 Hz, 3H). ¹³C NMR (100 MHz, CDCl₃): δ 155.8, 152.8, 151.1, 150.3, 115.7, 56.9, 55.5, 52.9, 52.8, 52.3, 39.9, 26.2, 11.8. HRMS (ESI) *m/z*: (M + H) calcd for C₁₅H₂₆N₇O, 320.2199; found, 320.2195.

Synthesis of 6-Amino-9-(3-(4-ethylpiperazin-1-yl)propyl)-9H-purin-8-ol (14). Compound **13** (0.1 g, 0.3 mmol) was dissolved in 0.5 mL of 4 M HCl in dioxane at rt for 3 h. The reaction was then performed according to general procedure C to obtain pure compound **14** as white semisolid (86%). ¹H NMR (300 MHz, CD₃OD): δ 8.09 (s, 1H), 3.95 (t, *J* = 6.6 Hz, 2H), 2.49–2.40 (m,

12H), 2.02–1.93 (m, 2H), 1.04 (t, *J* = 7.2 Hz, 3H). ¹³C NMR (100 MHz, CD₃OD): δ 153.5, 150.9, 147.9, 147.1, 100.0, 55.5, 52.2, 51.9, 51.8, 38.3, 24.7, 10.3. HRMS (ESI) *m/z*: (M + H) calcd for C₁₄H₂₄N₇O, 306.2042; found, 306.2038. HPLC purity 97.7%.

6-Chloro-9-(3-(4-ethylpiperazin-1-yl)propyl)-9H-purine (16). Compound **15** (0.1 g, 0.7 mmol) and 1-(3-chloropropyl)-4-ethylpiperazine (0.3 g, 1.2 mmol) were taken in dry 0.5 mL of DMF and potassium carbonate (0.2 g, 1.2 mmol) was added to it. The reaction mixture was heated at 60 °C for 12 h. Water was added to the reaction mixture. The aqueous solution was extracted with chloroform and the organic layer was dried over Na₂SO₄ and evaporated under vacuum. The residue was purified by silica gel column chromatography eluting with 4% methanol in chloroform to provide compound **16** as semisolid (84%). ¹H NMR (300 MHz, CDCl₃): δ 8.74 (s, 1H), 8.17 (s, 1H), 4.38 (t, *J* = 6.6 Hz, 2H), 2.51–2.37 (m, 8H), 2.30 (t, *J* = 6.6 Hz, 2H), 2.10–2.07 (m, 2H), 1.75–1.69 (m, 2H), 1.08 (t, *J* = 7.2 Hz, 3H). ¹³C NMR (75 MHz, CDCl₃): δ 151.9, 151.8, 150.9, 145.9, 131.7, 54.2, 52.4, 52.3, 42.4, 29.7, 26.0, 11.5. HRMS (ESI) *m/z*: (M + H) calcd for C₁₄H₂₂ClN₆, 309.1594; found, 309.1588.

9-(3-(4-Ethylpiperazin-1-yl)propyl)-9H-purin-6-amine (17). Compound **16** (0.1 g, 0.3 mmol) and 2 mL of ammonia in ethanol (7 equiv) were taken in a pressure tube. The reaction mixture was heated at 60 °C for 12 h. Ethanol was evaporated, and residue was purified by column chromatography to obtain compound **17** as semisolid (67%). ¹H NMR (400 MHz, CDCl₃ + CD₃OD): δ 8.10 (s, 1H), 7.79 (s, 1H), 4.14 (t, *J* = 6.8 Hz, 2H), 3.01–2.81 (m, 6H), 2.70–2.53 (m, 4H), 2.36 (t, *J* = 6.8 Hz, 2H), 1.97–1.90 (m, 2H), 1.20 (t, *J* = 7.2 Hz, 3H). ¹³C NMR (100 MHz, CDCl₃ + CD₃OD): δ 156.6, 153.5, 145.0, 123.0, 100.0, 57.0, 56.0, 55.2, 53.8, 53.7, 45.8, 30.3, 13.2, 4.8. HRMS (ESI) *m/z*: (M + H) calcd for C₁₄H₂₄N₇, 290.2093; found, 290.2084. HPLC purity 99.6%.

9-(3-(4-Ethylpiperazin-1-yl)propyl)-9H-purin-6-amine (18). Compound **16** (0.1 g, 0.3 mmol) was dissolved in 10 mL of tetrahydrofuran (THF), and solution was degassed using argon. 10% palladium on carbon (10 mol %) was added to the reaction mixture and then the reaction mixture was stirred at rt under a hydrogen atmosphere for 1 h. Completion of the reaction was confirmed by monitoring TLC, and the catalyst was separated using Celite filtration. The filtrate was evaporated, and the residue was purified by column chromatography to obtain compound **18** as semisolid (91%). ¹H NMR (400 MHz, CDCl₃): δ 9.13 (s, 1H), 8.98 (s, 1H), 8.13 (s, 1H), 4.38 (t, *J* = 6.6 Hz, 2H), 2.58–2.38 (m, 10H), 2.32 (t, *J* = 6.6 Hz, 2H), 2.13–2.05 (m, 2H), 1.08 (t, *J* = 7.2 Hz, 3H). ¹³C NMR (150 MHz, CDCl₃): δ 152.5, 151.4, 148.5, 145.9, 134.1, 54.4, 52.6, 52.3, 41.7, 26.2, 11.7. HRMS (ESI) *m/z*: (M + H) calcd for C₁₄H₂₃N₆, 275.1984; found, 275.1973. HPLC purity 96.4%.

9-(3-(4-Ethylpiperazin-1-yl)propyl)-N,N-dimethyl-9H-purin-6-amine (19). Compound **16** (0.1 g, 0.3 mmol) and 2 mL of dimethylamine in THF (2 M) were added to 3 mL of acetonitrile in presence of base potassium carbonate (0.06 g, 0.62 mmol). The reaction mixture was refluxed for 12 h and then solvent was evaporated and column chromatography was performed to obtain pure compound **19** as semisolid (89%). ¹H NMR (400 MHz, CDCl₃): δ 8.31 (s, 1H), 7.71 (s, 1H), 4.22 (t, *J* = 6.8 Hz, 2H), 3.50 (s, 6H), 2.44–2.37 (m, 10H), 2.28 (t, *J* = 6.8 Hz, 2H), 2.04–1.99 (m, 2H), 1.07 (t, *J* = 7.2 Hz, 3H). ¹³C NMR (100 MHz, CDCl₃): δ 155.0, 152.4, 150.6, 138.8, 120.3, 54.5, 52.9, 52.8, 52.4, 41.6, 26.6, 11.9. HRMS (ESI) *m/z*: (M + H) calcd for C₁₆H₂₆N₇, 318.2406; found, 318.2404. HPLC purity 98.6%.

General Procedure C 9-(3-(4-Ethylpiperazin-1-yl)propyl)-6-(piperidin-1-yl)-9H-purine (20). Compound **16** (0.1 g, 0.2 mmol) was dissolved in acetonitrile (1 mL), and potassium carbonate (0.04 g, 0.28 mmol) and piperidine (0.02 g, 1.2 mmol) were added. The reaction was refluxed under the N₂ atmospheric condition for 12 h. The organic layer was extracted with a CHCl₃ system, and column chromatography was done by using CH₃OH and CHCl₃ systems to give compound **20** (73%) as a semisolid. ¹H NMR (400 MHz, CDCl₃): δ 8.29 (s, 1H), 7.72 (s, 1H), 4.24–4.20 (m, 6H), 2.51–2.41 (m, 8H), 2.31 (t, *J* = 6.8 Hz, 2H), 2.05–1.98 (m, 4H), 1.70–1.65 (m, 6H), 1.08 (t, *J* = 7.2 Hz, 3H). ¹³C NMR (100 MHz, CDCl₃): δ 154.0,

152.4, 150.8, 138.6, 119.9, 54.5, 52.8, 52.7, 52.4, 41.6, 26.6, 26.2, 24.9, 11.8. HRMS (ESI) m/z : (M + H) calcd for $C_{19}H_{32}N_7$, 358.2719; found, 358.2721. HPLC purity 95.6%.

4-(9-(3-(4-Ethylpiperazin-1-yl)propyl)-9H-purin-6-yl)-morpholine (21). Compound 16 (0.1 g, 0.2 mmol) was dissolved in acetonitrile (1 mL), and potassium carbonate (0.04 g, 0.28 mmol) and morpholine (0.03 g, 1.2 mmol) were added. The reaction then proceeds according to general procedure C to get compound 21 (82%) as a semisolid. 1H NMR (600 MHz, $CDCl_3$): δ 8.35 (s, 1H), 7.76 (s, 1H), 4.33–4.30 (m, 4H), 4.26 (t, J = 6.6 Hz, 2H), 3.83 (t, J = 4.8 Hz, 4H), 2.49–2.40 (m, 8H), 2.31 (t, J = 6.6 Hz, 2H), 2.06–2.02 (m, 2H), 1.97–1.91 (m, 2H), 1.08 (t, J = 7.2 Hz, 3H). ^{13}C NMR (150 MHz, $CDCl_3$): δ 156.4, 154.7, 153.4, 141.6, 122.5, 69.5, 56.8, 55.3, 55.2, 54.7, 43.9, 28.8, 14.3. HRMS (ESI) m/z : (M + H) calcd for $C_{18}H_{30}N_7O$, 360.2512; found, 360.2523. HPLC purity 95.1%.

9-(3-(4-Ethylpiperazin-1-yl)propyl)-6-(piperazin-1-yl)-9H-purine (22). Compound 16 (0.1 g, 0.2 mmol) was dissolved in acetonitrile (1 mL), and potassium carbonate (0.04 g, 0.28 mmol) and piperazine (0.1 g, 1.2 mmol) were added. The reaction then proceeds according to general procedure C to get compound 22 (86%) as a semisolid. 1H NMR (600 MHz, $CDCl_3$): δ 8.30 (s, 1H), 7.72 (s, 1H), 4.27–4.21 (m, 6H), 3.00–2.95 (m, 4H), 2.49–2.33 (m, 10H), 2.27 (t, J = 6.6 Hz, 2H), 2.04–1.98 (m, 2H), 1.05 (t, J = 7.2 Hz, 3H). ^{13}C NMR (150 MHz, $CDCl_3$): δ 156.4, 154.7, 153.3, 141.3, 122.4, 56.8, 55.4, 55.2, 54.7, 48.7, 43.7, 28.8, 14.4. HRMS (ESI) m/z : (M + H) calcd for $C_{18}H_{31}N_8$, 359.2672; found, 35.92675. HPLC purity 99.4%.

6-(4-Ethylpiperazin-1-yl)-9-(3-(4-ethylpiperazin-1-yl)propyl)-9H-purine (23). Compound 16 (0.5 g, 0.7 mmol) was dissolved in acetonitrile (8 mL), and potassium carbonate (0.2 g, 1.5 mmol) and ethylpiperazine (0.13 mL, 1.2 mmol) were added. The reaction then proceeds according to general procedure C to get compound 23 (95%) as a semisolid. 1H NMR (300 MHz, $CDCl_3$): δ 8.34 (s, 1H), 7.76 (s, 1H), 4.43–4.29 (m, 4H), 4.25 (t, J = 6.6 Hz, 2H), 2.60–2.57 (m, 4H), 2.51–2.39 (m, 12H), 2.31 (t, J = 6.6 Hz, 2H), 2.08–2.01 (m, 2H), 1.16–1.06 (m, 6H). ^{13}C NMR (150 MHz, $CDCl_3$): δ 153.9, 152.3, 150.9, 138.9, 120.0, 54.4, 53.0, 52.8, 52.7, 52.5, 52.3, 41.5, 26.5, 12.0. HRMS (ESI) m/z : (M + H) calcd for $C_{20}H_{35}N_8$, 387.2985; found, 387.2979. HPLC purity 99.2%.

6-(4-Cyclopentylpiperazin-1-yl)-9-(3-(4-ethylpiperazin-1-yl)propyl)-9H-purine (24). Compound 16 (0.1 g, 0.4 mmol) was dissolved in acetonitrile (1 mL), and potassium carbonate (0.05 g, 0.4 mmol) and piperazine (0.03 g, 0.34 mmol) were added. The reaction then proceeds according to general procedure C to get compound 24 (86%) as a semisolid. 1H NMR (300 MHz, $CDCl_3$): δ 8.33 (s, 1H), 7.74 (s, 1H), 4.46–4.30 (m, 4H), 4.25 (t, J = 6.6 Hz, 2H), 2.71–2.55 (m, 13H), 2.36 (t, J = 6.9 Hz, 2H), 2.09–2.00 (m, 2H), 1.91–1.87 (m, 4H), 1.78–1.68 (m, 2H), 1.62–1.49 (m, 4H), 1.19 (t, J = 7.2 Hz, 3H). ^{13}C NMR (150 MHz, $CDCl_3$): δ 153.7, 152.3, 150.9, 138.8, 119.9, 67.6, 54.2, 52.3, 52.2, 51.6, 41.5, 30.1, 26.4, 23.9, 24.0, 10.9. HRMS (ESI) m/z : (M + H) calcd for $C_{23}H_{39}N_8$, 427.3298; found, 427.3297. HPLC purity 97.3%.

9-(3-Chloropropyl)-6-(4-ethylpiperazin-1-yl)-9H-purine (26). Compound 25 (1.6 g, 6.7 mmol) and potassium carbonate (1.9 g, 14 mmol) were dissolved in 1 mL of DMF, and the reaction mixture was heated at 50 °C for 2 h. 1-Bromo-3-chloropropane was added to the reaction mixture at rt and stirred for 12 h. The solvent was then removed and the reaction was partitioned between $CHCl_3$ and water. The organic layer was then dried, and column chromatography was performed to get pure compound 5 as semisolid (71%). 1H NMR (300 MHz, $CDCl_3$): δ 8.17 (s, 1H), 7.63 (s, 1H), 4.25–4.12 (m, 6H), 3.35 (t, J = 6.0 Hz, 2H), 3.43 (t, J = 5.1 Hz, 4H), 2.35–2.28 (m, 2H), 2.25–2.16 (m, 2H), 0.98 (t, J = 7.2 Hz, 3H). ^{13}C NMR (100 MHz, $CDCl_3$): δ 153.8, 152.4, 150.7, 138.5, 120.1, 52.8, 52.4, 41.4, 40.8, 31.8, 11.9. HRMS (ESI) m/z : (M + H) calcd for $C_{14}H_{22}N_6Cl$, 309.1594; found, 309.1599.

6-(4-Ethylpiperazin-1-yl)-9-(3-(piperazin-1-yl)propyl)-9H-purine (27). Compound 26 (0.1 g, 0.3 mmol), potassium carbonate (0.1 g, 0.7 mmol), and piperidine (0.11 mL, 1.0 mmol) were dissolved in 0.5 mL of DMF. The reaction was then performed according to

general procedure B to obtain pure compound 8 as semisolid (78%). 1H NMR (400 MHz, $CDCl_3$): δ 8.29 (s, 1H), 8.10 (s, 1H), 4.56–4.41 (m, 4H), 4.31 (t, J = 6.8 Hz, 2H), 3.12 (t, J = 5.2 Hz, 8H), 2.99–2.95 (m, 2H), 2.60–2.58 (m, 4H), 2.41 (t, J = 6.8 Hz, 2H), 2.08–2.01 (m, 2H), 1.19 (t, J = 7.2 Hz, 3H). ^{13}C NMR (150 MHz, $CDCl_3$): δ 155.8, 154.0, 153.3, 143.2, 122.2, 56.7, 54.4, 53.9, 51.7, 45.9, 43.9, 28.4, 11.4. HRMS (ESI) m/z : (M + H) calcd for $C_{18}H_{31}N_8$, 359.2672; found, 359.2675. HPLC purity 95.4%.

4-(3-(6-(4-Ethylpiperazin-1-yl)-9H-purin-9-yl)propyl)-morpholine (28). Compound 26 (0.1 g, 0.3 mmol), potassium carbonate (0.1 g, 0.7 mmol), and morpholine (0.09 mL, 1.0 mmol) were dissolved in 0.5 mL of DMF. The reaction was then performed according to general procedure B to obtain pure compound 8 as semisolid (85%). 1H NMR (300 MHz, $CDCl_3$): δ 8.31 (s, 1H), 7.72 (s, 1H), 4.34–4.31 (m, 4H), 4.24 (t, J = 6.8 Hz, 2H), 3.68–3.66 (m, 4H), 2.59–2.57 (m, 4H), 2.50–2.45 (m, 2H), 2.38–2.36 (m, 4H), 2.27 (t, J = 6.8 Hz, 2H), 2.05–1.98 (m, 2H), 1.12 (t, J = 7.2 Hz, 3H). ^{13}C NMR (150 MHz, $CDCl_3$): δ 153.8, 152.3, 150.9, 138.8, 120.0, 66.9, 54.9, 53.5, 52.8, 52.4, 41.5, 29.6, 26.1, 11.8. HRMS (ESI) m/z : (M + H) calcd for $C_{18}H_{30}N_7O$, 360.2512; found, 360.2523. HPLC purity 96.0%.

6-(4-Ethylpiperazin-1-yl)-9-(3-(piperidin-1-yl)propyl)-9H-purine (29). Compound 26 (0.1 g, 0.3 mmol), potassium carbonate (0.1 g, 0.7 mmol), and piperidine (0.11 mL, 1.0 mmol) were dissolved in 0.5 mL of DMF. The reaction was then performed according to general procedure B to obtain pure compound 8 as semisolid (93%). 1H NMR (600 MHz, $CDCl_3$): δ 8.33 (s, 1H), 7.75 (s, 1H), 4.41–4.39 (m, 4H), 4.24 (t, J = 6.6 Hz, 2H), 2.59–2.57 (m, 4H), 2.49–2.45 (m, 2H), 2.42–2.35 (m, 4H), 2.31 (t, J = 6.6 Hz, 2H), 2.07–2.03 (m, 2H), 1.60–1.55 (m, 4H), 1.47–1.41 (m, 2H), 1.13 (t, J = 7.2 Hz, 3H). ^{13}C NMR (150 MHz, $CDCl_3$): δ 153.8, 152.2, 150.8, 138.9, 119.9, 55.0, 54.3, 52.9, 52.4, 41.5, 26.4, 25.6, 24.1, 11.8. HRMS (ESI) m/z : (M + H) calcd for $C_{19}H_{32}N_7$, 358.2719; found, 358.2713. HPLC purity 96.8%.

6-(4-Ethylpiperazin-1-yl)-9-(3-(pyrrolidin-1-yl)propyl)-9H-purine (30). Compound 26 (0.1 g, 0.3 mmol), potassium carbonate (0.1 g, 0.7 mmol), and pyrrolidine (0.08 mL, 1.0 mmol) were dissolved in 0.5 mL of DMF. The reaction was then performed according to general procedure B to obtain pure compound 8 as semisolid (93%). 1H NMR (400 MHz, $CDCl_3$): δ 8.30 (s, 1H), 7.74 (s, 1H), 4.38–4.28 (m, 4H), 4.25 (t, J = 6.8 Hz, 2H), 2.55 (t, J = 5.2 Hz, 4H), 2.48–2.41 (m, 8H), 2.08–2.00 (m, 2H), 1.77–1.72 (m, 4H), 1.10 (t, J = 7.2 Hz, 3H). ^{13}C NMR (100 MHz, $CDCl_3$): δ 153.9, 152.4, 150.9, 138.9, 120.0, 54.1, 53.0, 52.6, 52.5, 41.7, 28.7, 23.5, 12.0. HRMS (ESI) m/z : (M + H) calcd for $C_{18}H_{30}N_7$, 344.2563; found, 344.2569. HPLC purity 95.8%.

6-(4-Ethylpiperazin-1-yl)-9-propyl-9H-purine (31). Compound 25 (1.0 g, 4.3 mmol) and potassium carbonate (1.2 g, 8.6 mmol) were dissolved in 1 mL of DMF, and the reaction mixture was heated at 50 °C for 2 h. 3-Bromopropane (0.7 mL, 6.5 mmol) was added to the reaction mixture at rt and stirred for 12 h. The solvent was then removed, and reaction was partitioned between $CHCl_3$ and water. Organic layer was then dried, and column chromatography was performed to get pure compound 5 as semisolid (78%). 1H NMR (400 MHz, $CDCl_3$): δ 8.35 (s, 1H), 7.73 (s, 1H), 4.44–4.26 (m, 4H), 4.14 (t, J = 7.2 Hz, 2H), 2.61–2.57 (m, 4H), 2.51–2.44 (m, 2H), 1.94–1.87 (m, 2H), 1.13 (t, J = 7.2 Hz, 3H), 0.96 (t, J = 7.2 Hz, 3H). ^{13}C NMR (100 MHz, $CDCl_3$): δ 153.9, 152.3, 150.9, 138.4, 119.9, 52.9, 52.5, 45.4, 23.4, 11.9, 11.2. HRMS (ESI) m/z : (M + H) calcd for $C_{14}H_{23}N_6$, 275.1984; found, 275.1977. HPLC purity 96.9%.

■ ASSOCIATED CONTENT

Supporting Information

The Supporting Information is available free of charge at <https://pubs.acs.org/doi/10.1021/acs.jmedchem.0c00011>.

TLR7 antagonistic assay, TLR7 agonistic assay, TLR8 antagonistic assay, cytotoxicity assay, X-ray crystallographic structure of HCl salt of compound 16, LC–MS/

MS spectrum analysis of compound **23**, aqueous solubility assay table, Caco-2 permeability assay table, plasma stability assay table, microsomal stability assay table, molecular docking, HPLC data, and ^1H NMR and ^{13}C NMR spectra of compounds **1–31** (PDF)

Molecular formula strings (CSV)

Human TLR7 homology model (PDB)

AUTHOR INFORMATION

Corresponding Authors

Dipayan Ganguly – IICB-Translational Research Unit of Excellence, CSIR-Indian Institute of Chemical Biology, Kolkata 700032, India; Academy of Scientific and Innovative Research (AcSIR), Ghaziabad 201002, India; Email: dipayan@iicb.res.in

Arindam Talukdar – Department of Organic and Medicinal Chemistry, CSIR-Indian Institute of Chemical Biology, Kolkata 700032, West Bengal, India; Academy of Scientific and Innovative Research (AcSIR), Ghaziabad 201002, India; orcid.org/0000-0002-7831-1795; Email: atalukdar@iicb.res.in

Authors

Ayan Mukherjee – Department of Organic and Medicinal Chemistry, CSIR-Indian Institute of Chemical Biology, Kolkata 700032, West Bengal, India; Academy of Scientific and Innovative Research (AcSIR), Ghaziabad 201002, India

Deblina Raychaudhuri – IICB-Translational Research Unit of Excellence, CSIR-Indian Institute of Chemical Biology, Kolkata 700032, India

Bishnu Prasad Sinha – IICB-Translational Research Unit of Excellence, CSIR-Indian Institute of Chemical Biology, Kolkata 700032, India

Biswajit Kundu – Department of Organic and Medicinal Chemistry, CSIR-Indian Institute of Chemical Biology, Kolkata 700032, West Bengal, India

Mousumi Mitra – IICB-Translational Research Unit of Excellence, CSIR-Indian Institute of Chemical Biology, Kolkata 700032, India

Barnali Paul – Department of Organic and Medicinal Chemistry, CSIR-Indian Institute of Chemical Biology, Kolkata 700032, West Bengal, India; Academy of Scientific and Innovative Research (AcSIR), Ghaziabad 201002, India

Purbita Bandopadhyay – IICB-Translational Research Unit of Excellence, CSIR-Indian Institute of Chemical Biology, Kolkata 700032, India; Academy of Scientific and Innovative Research (AcSIR), Ghaziabad 201002, India

Complete contact information is available at:

<https://pubs.acs.org/10.1021/acs.jmedchem.0c00011>

Author Contributions

[†]A.M., D.R., and B.P.S. contributed equally.

Notes

The authors declare no competing financial interest.

ACKNOWLEDGMENTS

The project was supported by grant no. EMR/2016/003021 from Science and Engineering Research Board (SERB), Department of Science & Technology (DST), Govt. of India, to D.G. and A.T. Acknowledging University Grant Commission (UGC), Govt. of India by A.M., B.P. and B.K. for fellowship. D.R. would like to acknowledge Council of

Scientific and Industrial Research (CSIR) for her SPM senior research fellowship. P.B. would like to acknowledge Council of Scientific and Industrial Research (CSIR). B.P.S. is supported by the SyMeC Biocluster project from Department of Biotechnology (DBT), Govt. of India. Authors would like to acknowledge Central Instrument Facility of CSIR-IICB and Santu Paul for the LTQ Orbitrap XL mass spectrometer.

ABBREVIATIONS

pDC, plasmacytoid dendritic cell; SLE, systemic lupus erythematosus; hPBMC, human peripheral blood mononuclear cell; LC–MS, liquid chromatography–mass spectrometry; ISG15, interferon-stimulated gene 15; DMEM, Dulbecco's modified Eagle medium; HBSS, Hank's balanced salt solution; SEAP, secreted alkaline phosphatase; IFN, interferon

REFERENCES

- (1) Pandey, S.; Kawai, T.; Akira, S. Microbial sensing by toll-like receptors and intracellular nucleic acid sensors. *Cold Spring Harbor Perspect. Biol.* **2015**, *7*, a016246.
- (2) Takeda, K.; Kaisho, T.; Akira, S. Toll-like receptors. *Annu. Rev. Immunol.* **2003**, *21*, 335–376.
- (3) Akira, S.; Uematsu, S.; Takeuchi, O. Pathogen recognition and innate immunity. *Cell* **2006**, *124*, 783–801.
- (4) Gilliet, M.; Cao, W.; Liu, Y.-J. Plasmacytoid dendritic cells: sensing nucleic acids in viral infection and autoimmune diseases. *Nat. Rev. Immunol.* **2008**, *8*, 594–606.
- (5) Akira, S.; Takeda, K. Toll-like receptor signalling. *Nat. Rev. Immunol.* **2004**, *4*, 499–511.
- (6) Gay, N. J.; Symmons, M. F.; Gangloff, M.; Bryant, C. E. Assembly and localization of toll-like receptor signalling complexes. *Nat. Rev. Immunol.* **2014**, *14*, 546–558.
- (7) Lande, R.; Gregorio, J.; Facchinetti, V.; Chatterjee, B.; Wang, Y.-H.; Homey, B.; Cao, W.; Wang, Y.-H.; Su, B.; Nestle, F. O.; Zal, T.; Mellman, I.; Schröder, J.-M.; Liu, Y.-J.; Gilliet, M. Plasmacytoid dendritic cells sense self-DNA coupled with antimicrobial peptide. *Nature* **2007**, *449*, 564–569.
- (8) Ganguly, D.; Chamilos, G.; Lande, R.; Gregorio, J.; Meller, S.; Facchinetti, V.; Homey, B.; Barrat, F. J.; Zal, T.; Gilliet, M. Self-RNA-antimicrobial peptide complexes activate human dendritic cells through TLR7 and TLR8. *J. Exp. Med.* **2009**, *206*, 1983–1994.
- (9) Lande, R.; Ganguly, D.; Facchinetti, V.; Frasca, L.; Conrad, C.; Gregorio, J.; Meller, S.; Chamilos, G.; Sebasigari, R.; Ricciardi, V.; Bassett, R.; Amuro, H.; Fukuhara, S.; Ito, T.; Liu, Y.-J.; Gilliet, M. Neutrophils activate plasmacytoid dendritic cells by releasing self-DNA-peptide complexes in systemic lupus erythematosus. *Sci. Transl. Med.* **2011**, *3*, 73ra19.
- (10) Ganguly, D.; Haak, S.; Sisirak, V.; Reizis, B. The role of dendritic cells in autoimmunity. *Nat. Rev. Immunol.* **2013**, *13*, 566–577.
- (11) Ganguly, D. Do type I interferons link systemic autoimmunities and metabolic syndrome in a pathogenetic continuum? *Trends Immunol.* **2018**, *39*, 28–43.
- (12) Czarnecki, M. Small molecule modulators of toll-like receptors. *J. Med. Chem.* **2008**, *51*, 6621–6626.
- (13) Lipford, B.; Forsbach, D.; Zepp, C. M. Small Molecule Toll-like Receptor (TLR) Antagonists. U.S. Patent 20,070,232,622 A1, 2007.
- (14) Zhang, L.; Dewan, V.; Yin, H. Discovery of small molecules as multi-toll-like receptor agonists with proinflammatory and anticancer activities. *J. Med. Chem.* **2017**, *60*, 5029–5044.
- (15) Van der Fits, L.; Mourits, S.; Voerman, J. S. A.; Kant, M.; Boon, L.; Laman, J. D.; Cornelissen, F.; Mus, A.-M.; Florença, E.; Prens, E. P.; Lubberts, E. Imiquimod-induced psoriasis-like skin inflammation in mice is mediated via the IL-23/IL-17 axis. *J. Immunol.* **2009**, *182*, 5836–5845.
- (16) Balak, D. M. W.; van Doorn, M. B. A.; Arbeit, R. D.; Rijnveld, R.; Klaassen, E.; Sullivan, T.; Brevard, J.; Thio, H. B.; Prens, E. P.;

- Burggraaf, J.; Rissmann, R. IMO-8400, a Toll-like receptor 7, 8, and 9 antagonist, demonstrates clinical activity in a phase 2a, randomized, placebo-controlled trial in patients with moderate-to-severe plaque psoriasis. *Clin. Immunol.* **2017**, *174*, 63–72.
- (17) Dosa, P. I.; Amin, E. A. Tactical approaches to interconverting GPCR agonists and antagonists. *J. Med. Chem.* **2016**, *59*, 810–840.
- (18) Shukla, N. M.; Kimbrell, M. R.; Malladi, S. S.; David, S. A. Regioisomerism-dependent TLR7 agonism and antagonism in an imidazoquinoline. *Bioorg. Med. Chem. Lett.* **2009**, *19*, 2211–2214.
- (19) Zhang, S.; Hu, Z.; Tanji, H.; Jiang, S.; Das, N.; Li, J.; Sakaniwa, K.; Jin, J.; Bian, Y.; Ohto, U.; Shimizu, T.; Yin, H. Small-molecule inhibition of TLR8 through stabilization of its resting state. *Nat. Chem. Biol.* **2018**, *14*, 58–64.
- (20) Black, J. A life in new drug research. *Br. J. Pharmacol.* **2010**, *160*, S15–S25.
- (21) Ganellin, R. Medicinal chemistry and dynamic structure–activity analysis in the discovery of drugs acting at histamine H₂-receptors. *J. Med. Chem.* **1981**, *24*, 913–920.
- (22) Martin, W. History and development of mixed opioid agonists, partial agonists and antagonists. *Br. J. Clin. Pharmacol.* **1979**, *7*, 273S–279S.
- (23) Biggadike, K.; Ahmed, M.; Ball, D. I.; Coe, D. M.; Dalmas Wilk, D. A.; Edwards, C. D.; Gibbon, B. H.; Hardy, C. J.; Hermitage, S. A.; Hessey, J. O.; Hillegas, A. E.; Hughes, S. C.; Lazarides, L.; Lewell, X. Q.; Lucas, A.; Mallett, D. N.; Price, M. A.; Priest, F. M.; Quint, D. J.; Shah, P.; Sitaram, A.; Smith, S. A.; Stocker, R.; Trivedi, N. A.; Tsitoura, D. C.; Weller, V. Discovery of 6-amino-2-[[[(1S)-1-methylbutyl]oxy]-9-[5-(1-piperidinyl)pentyl]-7,9-dihydro-8H-purin-8-one (GSK2245035), a highly potent and selective intranasal toll-like receptor 7 agonist for the treatment of asthma. *J. Med. Chem.* **2016**, *59*, 1711–1726.
- (24) Jones, P.; Pryde, D. C.; Tran, T.-D.; Adam, F. M.; Bish, G.; Calo, F.; Ciaramella, G.; Dixon, R.; Duckworth, J.; Fox, D. N. A.; Hay, D. A.; Hitchin, J.; Horscroft, N.; Howard, M.; Laxton, C.; Parkinson, T.; Parsons, G.; Proctor, K.; Smith, M. C.; Smith, N.; Thomas, A. Discovery of a highly potent series of TLR7 agonists. *Bioorg. Med. Chem. Lett.* **2011**, *21*, S939–S943.
- (25) Hirota, K.; Kazaoka, K.; Niimoto, I.; Kumihara, H.; Sajiki, H.; Isobe, Y.; Takaku, H.; Tobe, M.; Ogita, H.; Ogino, T.; Ichii, S.; Kurimoto, A.; Kawakami, H. Discovery of 8-hydroxyadenines as a novel type of interferon inducer. *J. Med. Chem.* **2002**, *45*, S419–S422.
- (26) Tran, T.-D.; Pryde, D. C.; Jones, P.; Adam, F. M.; Benson, N.; Bish, G.; Calo, F.; Ciaramella, G.; Dixon, R.; Duckworth, J.; Fox, D. N. A.; Hay, D. A.; Hitchin, J.; Horscroft, N.; Howard, M.; Gardner, I.; Jones, H. M.; Laxton, C.; Parkinson, T.; Parsons, G.; Proctor, K.; Smith, M. C.; Smith, N.; Thomas, A. Design and optimisation of orally active TLR7 agonists for the treatment of hepatitis C virus infection. *Bioorg. Med. Chem. Lett.* **2011**, *21*, 2389–2393.
- (27) Zhang, Z.; Ohto, U.; Shibata, T.; Krayukhina, E.; Taoka, M.; Yamauchi, Y.; Tanji, H.; Isobe, T.; Uchiyama, S.; Miyake, K.; Shimizu, T. Structural analysis reveals that toll-like receptor 7 is a dual receptor for guanosine and single-stranded RNA. *Immunity* **2016**, *45*, 737–748.
- (28) Zhang, Z.; Ohto, U.; Shibata, T.; Taoka, M.; Yamauchi, Y.; Sato, R.; Shukla, N. M.; David, S. A.; Isobe, T.; Miyake, K.; Shimizu, T. Structural analyses of toll-like receptor 7 reveal detailed RNA sequence specificity and recognition mechanism of agonistic ligands. *Cell Rep.* **2018**, *25*, 3371–3381.
- (29) Isobe, Y.; Tobe, M.; Ogita, H.; Kurimoto, A.; Ogino, T.; Kawakami, H.; Takaku, H.; Sajiki, H.; Hirota, K.; Hayashi, H. Synthesis and structure–activity relationships of 2-substituted-8-hydroxyadenine derivatives as orally available interferon inducers without emetic side effects. *Bioorg. Med. Chem.* **2003**, *11*, 3641–3647.
- (30) Bazin, H. G.; Li, Y.; Khalaf, J. K.; Mwakwari, S.; Livesay, M. T.; Evans, J. T.; Johnson, D. A. Structural requirements for TLR7-selective signaling by 9-(4-piperidinylalkyl)-8-oxoadenine derivatives. *Bioorg. Med. Chem. Lett.* **2015**, *25*, 1318–1323.
- (31) Smith, A. J.; Li, Y.; Bazin, H. G.; St-Jean, J. R.; Larocque, D.; Evans, J. T.; Baldridge, J. R. Evaluation of novel synthetic TLR7/8 agonists as vaccine adjuvants. *Vaccine* **2016**, *34*, 4304–4312.
- (32) Isobe, Y.; Kurimoto, A.; Tobe, M.; Hashimoto, K.; Nakamura, T.; Norimura, K.; Ogita, H.; Takaku, H. Synthesis and biological evaluation of novel 9-substituted-8-hydroxyadenine derivatives as potent interferon inducers. *J. Med. Chem.* **2006**, *49*, 2088–2095.
- (33) Roethle, P. A.; McFadden, R. M.; Yang, H.; Hrvatin, P.; Hui, H.; Graupe, M.; Gallagher, B.; Chao, J.; Hesselgesser, J.; Duatschek, P.; Zheng, J.; Lu, B.; Tumas, D. B.; Perry, J.; Halcomb, R. L. Identification and optimization of pteridinone toll-like receptor 7 (TLR7) agonists for the oral treatment of viral hepatitis. *J. Med. Chem.* **2013**, *56*, 7324–7333.
- (34) Lamphier, M.; Zheng, W.; Latz, E.; Spyvee, M.; Hansen, H.; Rose, J.; Genest, M.; Yang, H.; Shaffer, C.; Zhao, Y.; Shen, Y.; Liu, C.; Liu, D.; Mempel, T. R.; Rowbottom, C.; Chow, J.; Twine, N. C.; Yu, M.; Gusovsky, F.; Ishizaka, S. T. Novel small molecule inhibitors of TLR7 and TLR9: mechanism of action and efficacy in vivo. *Mol. Pharmacol.* **2014**, *85*, 429–440.
- (35) Paul, B.; Rahaman, O.; Roy, S.; Pal, S.; Satish, S.; Mukherjee, A.; Ghosh, A. R.; Raychaudhuri, D.; Bhattacharya, R.; Goon, S.; Ganguly, D.; Talukdar, A. Activity-guided development of potent and selective toll-like receptor 9 antagonists. *Eur. J. Med. Chem.* **2018**, *159*, 187–205.
- (36) Gerster, J. F.; Lindstrom, K. J.; Miller, R. L.; Tomai, M. A.; Birmachou, W.; Bomersine, S. N.; Gibson, S. J.; Imbertson, L. M.; Jacobson, J. R.; Knafla, R. T.; Maye, P. V.; Nikolaidis, N.; Oneyemi, F. Y.; Parkhurst, G. J.; Pecore, S. E.; Reiter, M. J.; Testerman, L. S.; Thompson, N. J.; Wagner, T. L.; Weeks, C. E.; Andre, J.-D.; Lagain, D.; Bastard, Y.; Lupu, M. Synthesis and structure–activity-relationships of 1H-Imidazo[4,5-c] quinolines that induce interferon production. *J. Med. Chem.* **2005**, *48*, 3481–3491.
- (37) Laxer, A.; Major, D. T.; Gottlieb, H. E.; Fischer, B. (¹⁵N)-Labeled adenine derivatives: synthesis and studies of tautomerism by ¹⁵N NMR spectroscopy and theoretical calculations. *J. Org. Chem.* **2001**, *66*, 5463–5481.
- (38) Carson, D. A.; Takabayashi, K.; Cottam, H. B.; Chan, M.; Wu, C. C. N. TLR Agonists. U.S. Patent 71,033,705 P, Aug 22, 2005.
- (39) He, L.; Gangwar, S.; Poudel, Y. B.; Sivaprakasam, P. Toll-like Receptor 7 (TLR7) Agonists Having Heteroatom-Linked Aromatic Moieties, Conjugates Thereof, and Methods and Uses Therefor. U.S. Patent 20,190,055,247 A1, Feb 21, 2019.
- (40) Hirota, K.; Kazaoka, K.; Sajiki, H. Synthesis and biological evaluation of 2,8-disubstituted 9-benzyladenines: discovery of 8-mercaptoadenines as potent interferon-inducers. *Bioorg. Med. Chem.* **2003**, *11*, 2715–2722.
- (41) Karroum, N. B.; Moarbess, G.; Guichou, J.-F.; Bonnet, P.-A.; Patinote, C.; Bouharoun-Tayoun, H.; Chamat, S.; Cuq, P.; Diab-Assaf, M.; Kassab, I.; Deleuze-Masquefa, C. Novel and selective TLR7 antagonists among the imidazo[1,2-a]pyrazines, imidazo[1,5-a]-quinoxalines, and pyrazolo[1,5-a]quinoxalines series. *J. Med. Chem.* **2019**, *62*, 7015–7031.
- (42) Shukla, N. M.; Mutz, C. A.; Malladi, S. S.; Warshakoon, H. J.; Balakrishna, R.; David, S. A. toll-like receptor (TLR)-7 and -8 modulatory activities of dimeric imidazoquinolines. *J. Med. Chem.* **2012**, *55*, 1106–1116.
- (43) Veber, D. F.; Johnson, S. R.; Cheng, H.-Y.; Smith, B. R.; Ward, K. W.; Kopple, K. D. Molecular properties that influence the oral bioavailability of drug candidates. *J. Med. Chem.* **2002**, *45*, 2615–2623.
- (44) Smith, D. A.; Beaumont, K.; Maurer, T. S.; Di, L. Volume of distribution in drug design. *J. Med. Chem.* **2015**, *58*, S691–S698.
- (45) Hawkes, J. E.; Adalsteinsson, J. A.; Gudjonsson, J. E.; Ward, N. L. Research techniques made simple: murine models of human psoriasis. *J. Invest. Dermatol.* **2018**, *138*, e1–e8.

Development, Optimization, and In Vivo Validation of New Imidazopyridine Chemotypes as Dual TLR7/TLR9 Antagonists through Activity-Directed Sequential Incorporation of Relevant Structural Subunits

Nirmal Das,^{||} Purbita Bandopadhyay,^{||} Swarnali Roy,^{||} Bishnu Prasad Sinha, Uddipta Ghosh Dastidar, Oindrila Rahaman, Sourav Pal, Dipyaman Ganguly,^{*} and Arindam Talukdar^{*}Cite This: *J. Med. Chem.* 2022, 65, 11607–11632

Read Online

ACCESS |



Metrics & More



Article Recommendations



Supporting Information

ABSTRACT: Undesirable activation of endosomal toll-like receptors TLR7 and TLR9 present in specific immune cells in response to host-derived ligands is implicated in several autoimmune diseases and other contexts of autoreactive inflammation, making them important therapeutic targets. We report a drug development strategy identifying a new chemotype for incorporating relevant structural subunits into the basic imidazopyridine core deemed necessary for potent TLR7 and TLR9 dual antagonism. We established minimal pharmacophoric features in the core followed by hit-to-lead optimization, guided by in vitro and in vivo biological assays and ADME. A ligand–receptor binding hypothesis was proposed, and selectivity studies against TLR8 were performed. Oral absorption and efficacy of lead candidate **42** were established through favorable in vitro pharmacokinetics and in vivo pharmacodynamic studies, with IC_{50} values of 0.04 and 0.47 μM against TLR9 and TLR7, respectively. The study establishes imidazopyridine as a viable chemotype to therapeutically target TLR9 and TLR7 in relevant clinical contexts.



INTRODUCTION

The human innate immune system serves as the first line of defense against invading pathogens. The innate recognition of pathogens is carried out by germline-encoded pathogen recognition receptors known as toll-like receptors (TLRs) which are abundantly expressed in antigen-presenting cells such as the dendritic cells.^{1–4} These receptors recognize conserved patterns associated with microbes to be followed by the innate immune response in the context of health and disease.^{2,5,6} The structure of TLRs comprises three units, namely, the leucine-rich repeat containing ligand-binding ectodomain (ECD), a transmembrane domain, and a cytoplasmic TIR (toll/IL-1 receptor) through which the downstream signaling is initiated.^{2,7,8} In human immune cells, four TLRs, viz., TLR3, 7, 8, and 9, are known to be endosomally located where the pH ranges between 4.5 and 6.5.^{9–12} Among them, TLR7 and TLR8 are associated with single-stranded RNA recognition and TLR9 identifies hypomethylated CpG DNA motifs of not only pathogenic but also self-origin.^{13–17} In humans, plasmacytoid dendritic cells (pDCs) and B lymphocytes are known to selectively express TLR7 and TLR9 in healthy contexts.¹⁸ One of the most

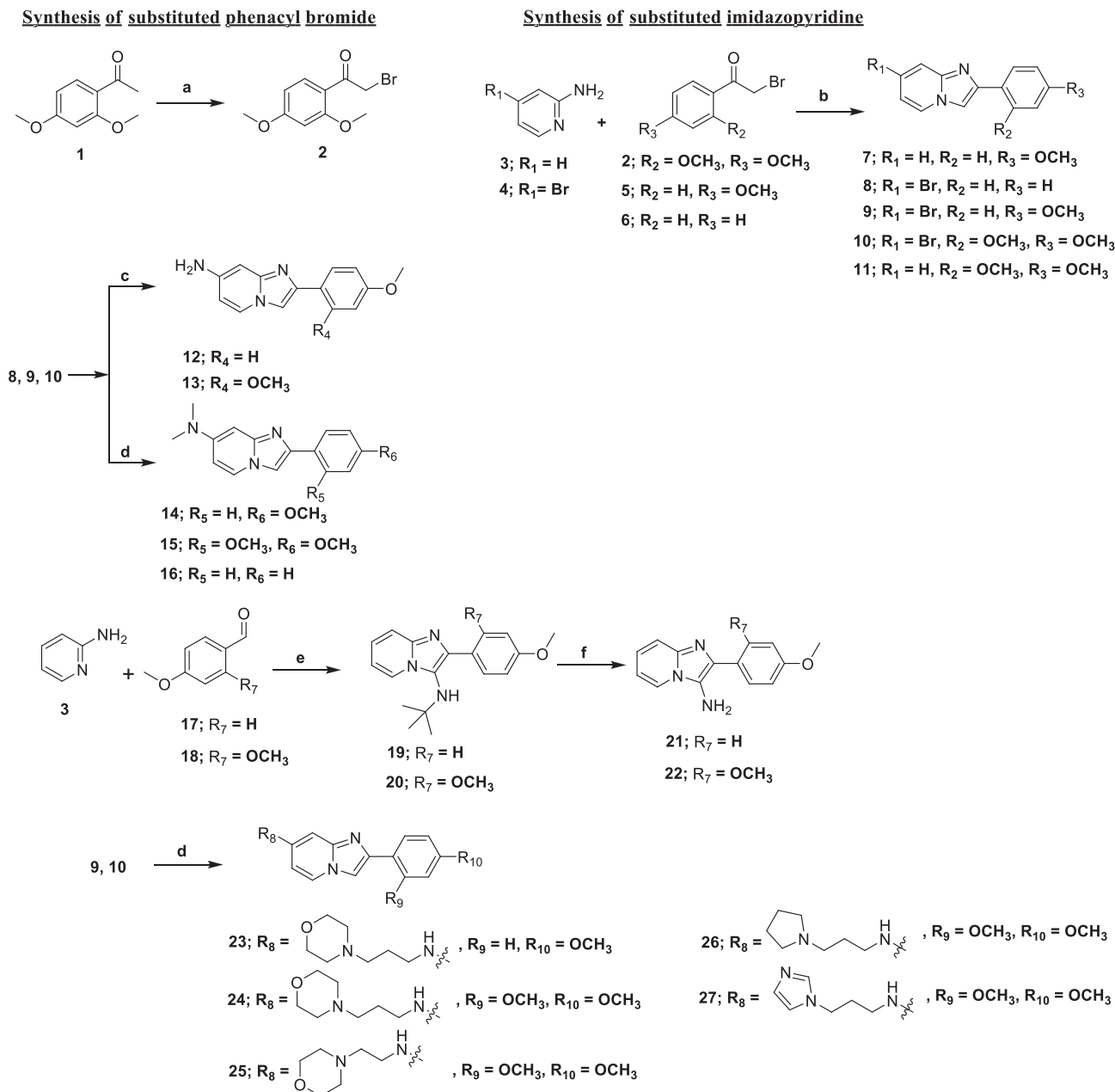
significant outcomes of their activation is type I interferon (IFN) production from pDCs.^{15,18,19}

Interestingly, when self-origin RNA or DNA molecules get access to endosomes, they can also activate TLR7/8/9 receptors, thus initiating autoreactive inflammation. The aberrant activation of TLR7/9 by self-nucleic acids leads to the induction of type I IFN in immune cells such as pDCs which triggers the onset and ultimate pathogenesis of several autoimmune disorders such as systemic lupus erythematosus (SLE), Sjögren's syndrome, psoriasis, and systemic sclerosis. Since the role of TLRs has been well established in the context of the initiation and subsequent exacerbation of inflammatory and autoimmune disorders, they serve as ideal therapeutic targets for novel drug discovery, leading to amelioration of disease and their associated symptoms.^{20–25}

Received: March 11, 2022

Published: August 12, 2022

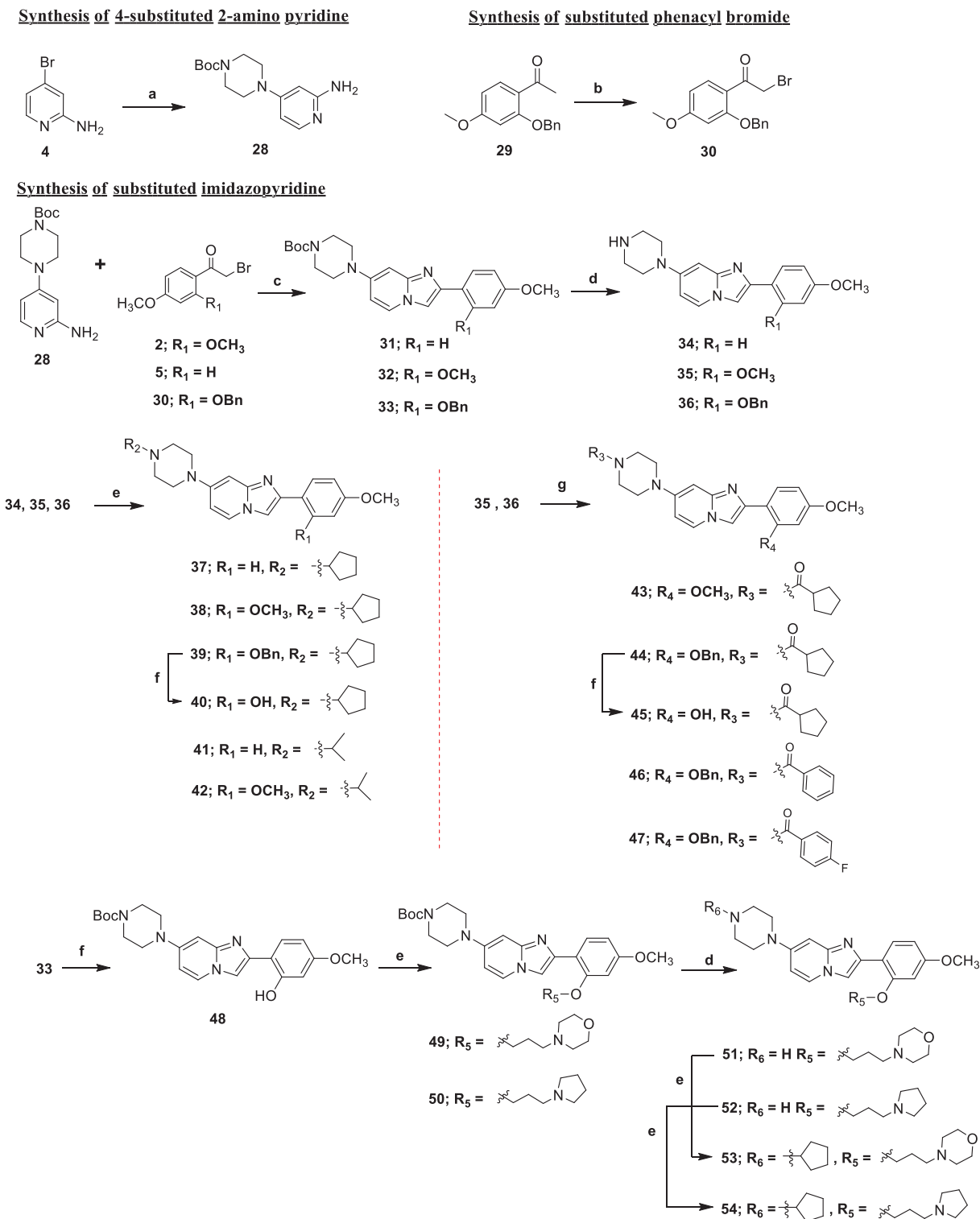


Scheme 1. Reagents and Conditions^a

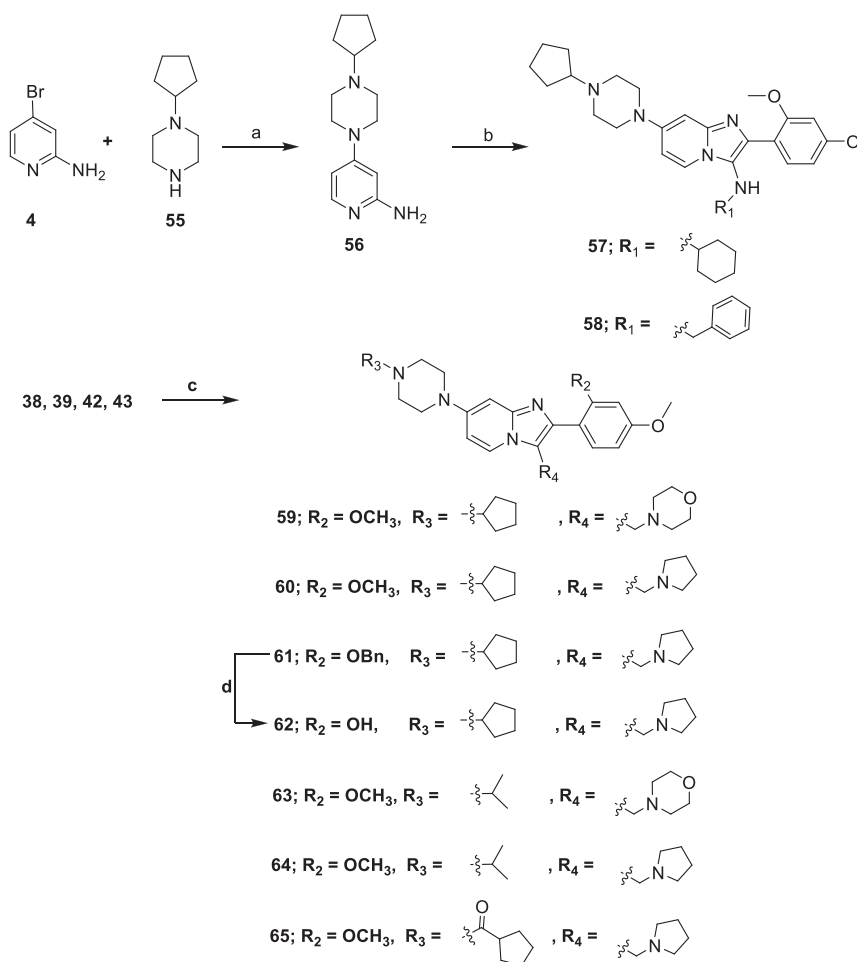
^aReagents and conditions: (a) TBATB (1.05 equiv), dry THF, room temperature, 14 h, (yield 82%); (b) NaHCO₃ (2.0 equiv), acetone, reflux, 4–6 h, (yield 85–92%); (c) Cu₂O (0.2 equiv), excess NH₄OH, NMP, 120 °C, 15–16 h (yield 62–66%); (d) amine (1.3 equiv), Na^tOBu (4.0 equiv), (±) BINAP (0.1 equiv), Pd₂(dba)₃ (0.05 equiv), toluene, 110 °C, 8–10 h (yield 65–75%); (e) *tert*-butyl isocyanide (1.02 equiv), *p*-toluenesulfonic acid (PTSA) (0.2 equiv), dry MeOH, room temperature, 16–18 h (yield 76–83%); (f) tetrabutylammonium bromide (TBAB) (0.05 equiv), DCE, 12 N HCl (1:1), 25–30 °C, 72 h (yield 88–91%).

TLR7 and TLR9 activation with their respective ligands lead to identical downstream signaling pathways initiated by the association with their adaptor protein Myd88 and culminating in the transcriptional activation of several inflammatory genes such as type I interferons or pro-inflammatory cytokines depending on the cell type and the endosomal localization of the ligands.^{26,27} Dual antagonists targeting TLR7/9 serve as important tools to prevent undesirable activation and production of type I interferons in various inflammatory disease contexts. Antimalarial drugs chloroquine and hydroxy-chloroquine,²⁸ with established inhibitory action on endosomal

TLR activation, have been in clinical use against several major autoimmune diseases such as rheumatoid arthritis.^{29,30} Several oligonucleotide TLR7/TLR9 antagonists such as IMO-8400, IMO-3100, and IMO-9200 have undergone evaluation in clinical trials to monitor their safety and efficacy in patients diagnosed with autoimmune disorders.^{31–37} Pfizer initiated a clinical trial of a small molecule (CpG-52364) with a quinazoline core, but it failed to pass the phase I stage.^{20,38,39} Several groups along with us have also previously demonstrated systematic development of potent TLR7 and TLR9 small-molecule antagonists based on benzoxazole,^{40,41}

Scheme 2. Reagents and Conditions^a

^aReagents and conditions: (a) 1-Boc-piperazine (1.1 equiv), DIPEA (2.0 equiv), ^tBuOH, 120 °C, 24 h (yield: 86–88%); (b) TBATB (1.02 equiv), dry THF, room temperature, 14 h (yield: 78%); (c) NaHCO₃ (2.0 equiv), acetone, reflux, 4–6 h (yield: 85–89%); (d) 4 (M) HCl in 1,4-dioxane, room temperature, 12–14 h (yield: 83–86%); (e) bromocyclopentane (1.3 equiv for 37, 38, 39, 53, and 54), 2-iodopropane (1.2 equiv for 41 and 42), 4-(3-chloropropyl)morpholine (1.3 equiv for 49), 1-(3-chloropropyl)pyrrolidine (1.3 equiv for 50), K₂CO₃ (2.0 equiv), dry DMF, 50–55 °C, 8–12 h (yield: 62–86%); (f) Pd(OH)₂, H₂ gas, MeOH, balloon pressure, 12–14 h (yield: 74–78%); (g) cyclopentanecarbonyl chloride (1.2 equiv for 43 and 44), benzoyl chloride (1.2 equiv for 46), 4-fluorobenzoyl chloride (1.2 equiv for 47), DIPEA (3.0 equiv), dry DCM, room temperature, 2–3 h (yield: 76–81%).

Scheme 3. Reagents and Conditions^a

^aReagents and conditions: (a) 1-cyclopentylpiperazine (1.1 equiv), DIPEA (2.0 equiv), ^tBuOH, 120 °C, 24 h (yield: 86–88%); (b) isocyanocyclohexane (1.02 equiv for **57**), (isocyanomethyl)benzene (1.02 equiv for **58**), 2,4-dimethoxybenzaldehyde (1.0 equiv), NH₄Cl (1.0 equiv), microwave heating at 130 °C (at 100 W power), 1 h (yield: 60–62%); (c) morpholine (1.2 equiv for **59** and **63**), pyrrolidine (1.2 equiv for **60**, **61**, **64**, and **65**), formaldehyde (1.15 equiv), glacial AcOH, room temperature, 14–16 h (yield: 51–56%); (d) Pd(OH)₂, H₂ gas, balloon pressure, MeOH, 12 h (yield: 53%).

quinazoline,^{42–44} imidazoquinoline,⁴⁵ and purine^{46–48} scaffolds by employing different medicinal chemistry strategies.^{49–53} Through agonist-to-antagonist strategy, we identified a chemical switch in the purine scaffold leading to a switch from TLR7 agonism to antagonism.⁴⁶ An activity-guided strategy was employed for the development of selective TLR9 and dual TLR7/TLR9 antagonists in the quinazoline scaffold.^{42,43}

Designing a drug candidate is more complex than the development of biologically active molecules. In the present study, we report the development of a new chemotype “imidazopyridine” as dual TLR7/TLR9 antagonists. The exploration put forth an interesting medicinal chemistry approach starting from imidazopyridine as a basic molecular framework and deducing the chemical spaces through sequentially incorporating relevant structural subunits to identify minimal pharmacophoric features, thereby sculpting the structure–activity relationship (SAR). The screenings of the compounds were performed based on inhibition in primary human immune cells and in reporter cells. We identified the structural subunits required for exhibiting selective TLR9 antagonism as well as dual TLR7/9 antagonism. The hit

molecules depicted excellent selectivity against TLR8. The optimization provided potential lead molecules with favorable in vitro pharmacokinetic parameters as in vivo TLR9 antagonism efficacy, depicting therapeutic potential. Modern drug discovery strategies such as high-throughput screening to identify new chemotypes are often out of the reach of academics. Our strategy described herein can be considered as a template for conceptually developing basic chemotypes into a possible drug candidate.

CHEMISTRY

Schemes 1–3 describe the synthetic protocol and strategies for the synthesis of designed imidazopyridine derivatives. The synthesis was initiated from commercially available 2',4'-dimethoxy acetophenone (**1**), 2-aminopyridine (**3**), 2-amino-4-bromopyridine (**4**), 4'-methoxyphenyl bromide (**5**), phenacyl bromide (**6**), and 1-(2-(benzyloxy)-4-methoxyphenyl)-ethanone (**29**) (Scheme 1). To start with, we performed α -bromination of **1** with the TBATB brominating reagent in dry THF at 25–30 °C for 14 h to obtain **2**. Compounds 7–11 were synthesized by reacting with the appropriate 2-aminopyridines **3** and **4** along with suitable phenacyl bromide **2**, **5**,

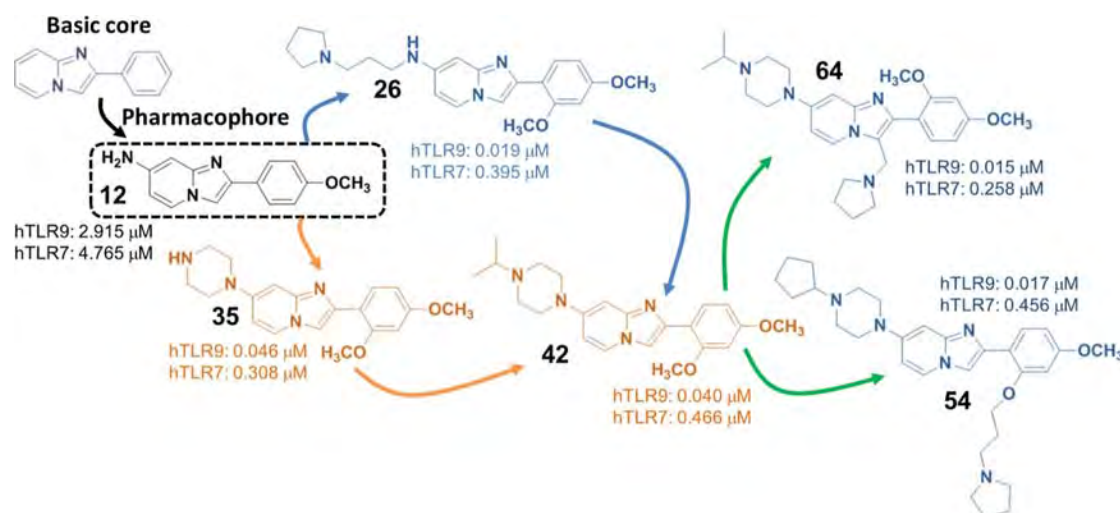


Figure 1. Identification of basic pharmacophores in the imidazopyridine chemotype and structural optimization toward dual TLR7/9 antagonists.

and **6** under refluxing conditions for 4–6 h using NaHCO_3 as a base. To substitute the $-\text{Br}$ group at the C-7 position of imidazopyridine with the $-\text{NH}_2$ group, **9** and **10** were treated with excess NH_4OH in the presence of catalytic Cu_2O in the NMP solvent at 120°C for 15–16 h to obtain **12** and **13**, respectively.⁵⁴

To prepare **14–16** and **23–27**, where the C-7 position of imidazopyridine is substituted with a different type of amine, the Buchwald–Hartwig amination reaction was performed, where the appropriate aryl bromides **8**, **9**, and **10** were reacted with a suitable amine in the presence of Na^tOBu as a base, $\text{Pd}_2(\text{dba})_3$ as a catalyst, and (\pm) BINAP as a ligand in toluene at 110°C for 8–10 h (Scheme 1). Compounds **19** and **20** were synthesized in a single step, where **3** was initially treated with suitable benzaldehydes **17** and **18** in the presence of *tert*-butyl isocyanide and PTSA in dry MeOH at $25\text{--}30^\circ\text{C}$ for 16–18 h.⁵⁵ Compounds **19** and **20** were treated with 12 (N) HCl and DCE (1:1) in the presence of TBAB at $25\text{--}30^\circ\text{C}$ for 72 h to get **21** and **22** (Scheme 1).

We made some imidazopyridine derivatives to understand the chemical space and geometry with an aliphatic chain having different chain lengths linked to the morpholine, pyrrolidine at the C-2' position, and piperazine ring at the C-7 position of imidazopyridine, as shown in Scheme 2. The next set of compounds described in Scheme 2 were prepared with Boc-piperazine at the C7 position of the imidazopyridine ring. Accordingly, the Boc-piperazine moiety was initially attached to the 2-aminopyridine ring to prepare **28** from **4** via an ArSN_2 type of reaction. 1-Boc-piperazine is used as a nucleophile in the presence of DIPEA as an organic base in the $n\text{-BuOH}$ solvent at 120°C for 24 h in a pressure tube. The required phenacyl bromide intermediate **30** was prepared by treating **29** with TBATB in dry THF at $25\text{--}30^\circ\text{C}$ for 14 h. Various phenacyl bromides **2**, **5**, and **30** were refluxed with **28** in the acetone solvent using NaHCO_3 as a base for 4–6 h to obtain advanced intermediates **31–33**. Deprotection of the Boc group of **31–33** using 4(N) HCl in 1,4-dioxane yielded **34–36**, which were then further treated with various alkyl halides to obtain **37**, **38**, **39**, **41**, and **42**.

Compounds **35** and **36** were treated with the appropriate acid chloride in dry DCM solvent in the presence of DIPEA as a base at $25\text{--}30^\circ\text{C}$ for 2–3 h to obtain **43**, **44**, **46**, and **47**. Deprotection of the benzyl group of **39**, **44**, and **33** was carried

out in the presence of a catalytic amount of $\text{Pd}_2(\text{OH})_2$ and H_2 gas at balloon pressure in a MeOH solvent for 12–14 h to provide **40**, **45**, and **48**, respectively. The $-\text{OH}$ group in **48** was then substituted with 4-(3-chloropropyl)morpholine and 1-(3-chloropropyl)pyrrolidine in the presence of K_2CO_3 and dry DMF at $50\text{--}55^\circ\text{C}$ for 12 h to give **49** and **50**, respectively. Deprotection of the Boc group from **49** and **50** using 4(N) HCl in 1,4-dioxane yielded **51** and **52**. A subsequent reaction with bromocyclopentane in the presence of K_2CO_3 in dry DMF yielded **53** and **54** (Scheme 2).

Scheme 3 focused on the synthesis of C3-substituted derivatives of imidazopyridine through a Mannich reaction. Initially, we prepared an important intermediate **56** from **4** by replacing the $-\text{Br}$ group with 1-cyclopentylpiperazine (**55**) in the presence of DIPEA in a $n\text{-BuOH}$ solvent. **57** and **58** had been synthesized in a single step where **56** was treated with 2,4-dimethoxybenzaldehyde (**18**) in the presence of a suitable isocyanide and NH_4Cl at 130°C in a CEM microwave reactor (100 W power was applied) for 1 h.⁵⁶ The Mannich reaction was done on the **38**, **39**, **42**, and **43** with the suitable amine in the presence of formaldehyde and glacial AcOH at $25\text{--}30^\circ\text{C}$ for 14–16 h to get **59**, **60**, **61**, **63**, **64**, and **65**. Compound **62** was synthesized by treating **61** with a catalytic amount of $\text{Pd}_2(\text{OH})_2$ and H_2 gas at balloon pressure in MeOH for 14 h (Scheme 3).

RESULTS AND DISCUSSION

Development and Optimization of Antagonists. We conceptualized 2-phenylimidazopyridine as a basic molecular framework for sequential incorporation of relevant structural subunits for the design and development of potent TLR7 and TLR9 antagonists (Figure 1). Our initial objective was to explore minimal pharmacophoric features that are essential to instigate TLR7 and TLR9 antagonism.^{51,57,58} Thereafter, we intended to delve into the structural aspects that impart dual and selective TLR7/9 antagonism and the chemical spaces around these basic subunits. Figure 1 depicts the snapshot of the sequential development of imidazopyridine chemotype through initial identification of the basic pharmacophore, followed by structural optimization as dual TLR7 and TLR9 antagonists. The possible ligand–receptor interaction and selectivity studies were conducted through molecular docking

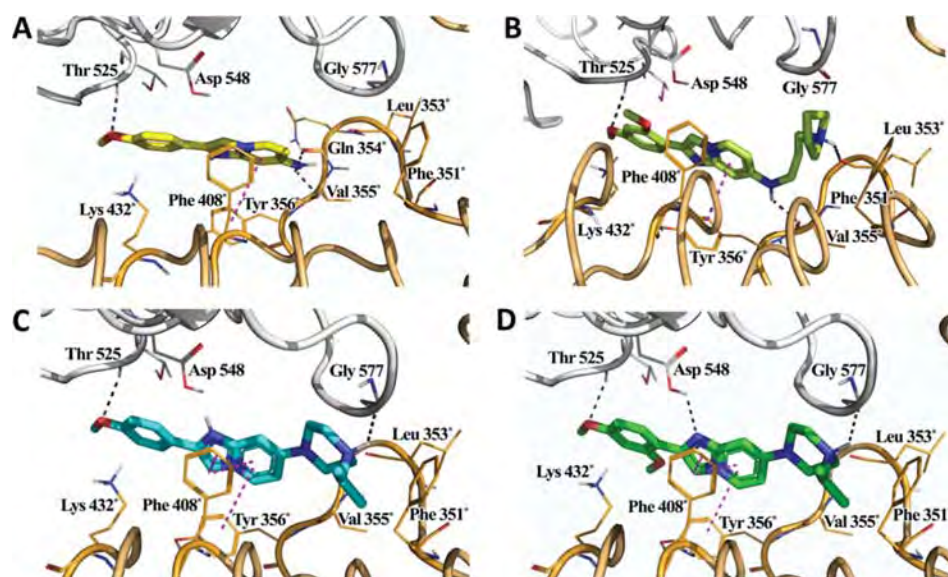


Figure 2. (A–D). Homology model of homodimerized TLR7 ECD was constructed using human TLR8 crystal structure (PDB 3W3J) as a template. (A–D) depict the molecular interactions between **12**, **26**, **41**, and **42** with the TLR7 active-site residues. (A) Compound **12** is represented in yellow stick representation; (B) compound **26** is represented in lime stick representation; (C) compound **41** is represented in cyan stick representation; (D) compound **42** is represented in green stick representation. Hydrophobic π – π interactions are shown by magenta dashed lines, whereas hydrogen bonds are shown by black dashed lines. *Indicates residues in chain B.

analysis (Figures 2 and 3). Lastly, our goal is to develop the initial hits into leads, guided by in vitro and in vivo biological



Figure 3. Homology model of homodimerized TLR7 ECD was constructed using template PDB ID: 3W3J. The figure depicts the molecular interactions between amide **43** with the TLR7 active-site residues. Compound **43** is represented in greenish cyan color. Hydrophobic π – π stacking interactions are shown by magenta dashed lines. *Indicates residues in chain B.

assays supported by ADME profiles. The activity profile guided rational development of the TLR7 and TLR9 antagonists in this study was evaluated by in vitro assays using reporter cell lines expressing TLRs, namely, HEK-BlueTLR9, a HEK293 cell line transfected with human TLR9, HEK-BlueTLR7, a HEK293 cell line transfected with human TLR7, and HEK-BlueTLR8, a HEK293 cell line transfected with human TLR8, which quantify TLR-induced NF- κ B activation in a colorimetric assay. In the reporter assays, CpGB, CL264, and CL075 were used as TLR9, TLR7, and TLR8 ligands, respectively, against which the inhibitory potency of the compounds was evaluated by calculating their IC_{50} values in the assayed cells (Figure 4; Supporting Information, Figures S1 and S2).⁵⁹ To further validate the inhibitory potential of our lead compound, we also assessed the antagonist activity of compound **42** in a more physiologically significant setting, whereupon TLR9 induction IFN α was measured in human pDCs (Figure 5)

which are known to be the major source of type I interferons in humans.

The conceptual design of the compounds was influenced by our previous experience with the essential structural features and geometrical arrangements in different chemotypes such as benzoxazole,^{40,41} oxoadenine,^{46–48} imidazoquinoline,⁴⁵ quina-zoline,^{42–44} and other cores.^{49–53} To identify the minimal substitutions required to attain TLR7/9 antagonism, initially, **7–11** were prepared with small substituents at the C4' and C2' positions. The C2' substitution was to impart obvious geometrical restrictions in the molecule. A halogen group was substituted at the C7 position for further derivatization. To our great surprise, the C2' and C4' bi-substituted **11** showed selective TLR9 inhibition with an IC_{50} of 10.43 μ M (Table 1). However, a similar compound **10** with bromo substitution at C7 did not show significant inhibition at 10 μ M. Next, the –Br groups in **9** and **10** were converted to –NH₂ (**12** and **13**) and –N(CH₃)₂ (**14** and **15**). The initial conversion of –Br to the –NH₂ group was influenced by our knowledge of TLR7/9 target-dependent biases toward amino groups. All the compounds showed moderate-to-potent inhibition against both TLR7 and TLR9 proteins. The initial success revealed the effectiveness of 2-phenylimidazopyridine as a possible chemotype with incredible potential. The nature of the amine substitution at C7 influences the TLR9 inhibition, with the –N(CH₃)₂ group showing more potent inhibition compared to the –NH₂ group. Another observation was the set of **13** and **15** with disubstitution at C2' and C4' showed more potent inhibition against both TLR7 and TLR9 as compared to **12** and **14** with monosubstitution at C4'. Interestingly, **16** with only C7 amine substitution and unsubstituted C2 phenyl showed potent TLR9 inhibition with an IC_{50} value of 2.19 μ M (Table 1). We presumed that **12** is the basic pharmacophore structure in our 2-phenylimidazopyridine chemotype. To understand the basis of inhibition of the early hit compounds, we docked **12** in our recently developed TLR7 binding model (Figure 2A).⁴³ The proposed binding hypothesis of structurally

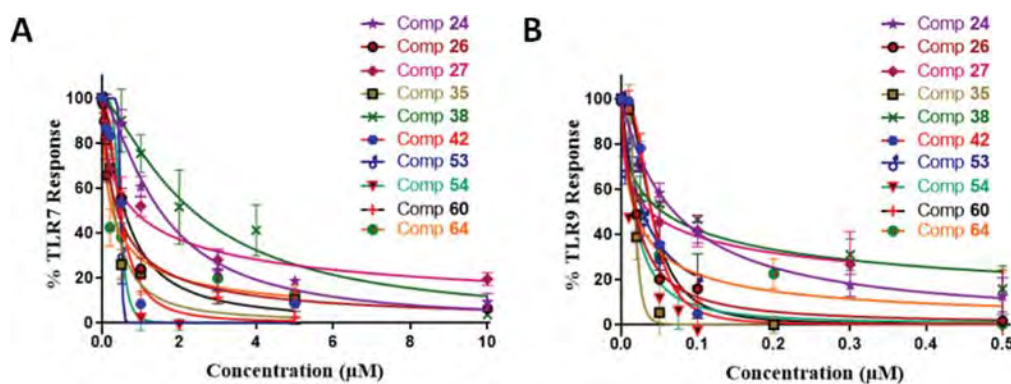


Figure 4. Reporter assay of potent TLR7 and TLR9 antagonists. (A) The compounds were assessed for dose-dependent inhibition of TLR7, using a HEK-Blue TLR7 cell line expressing a TLR7-responsive, NF- κ B-inducible SEAP. Data are shown as mean \pm SD, $n = 3$. (B) The compounds were assessed for dose-dependent inhibition of TLR9, using a HEK-Blue TLR9 cell line expressing a TLR9-responsive, NF- κ B-inducible SEAP. Data are shown as mean \pm SD, $n = 3$.

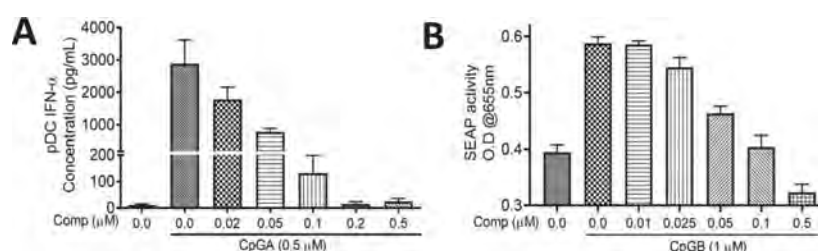


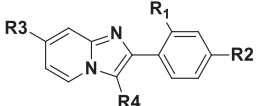
Figure 5. Dose–response experiment of compound 42. The compound was assessed for dose (μM)-dependent inhibition of TLR9 in (A) pDCs and the (B) reporter assay.

diverse antagonists with hTLR7 revealed the significance of different hydrophobic pockets and grooves, where specific hydrophobic and hydrogen bond interactions contribute toward TLR7 antagonist activity.⁴³ Evidently, the antagonist-TLR7 receptor binding model proposed by our group can be substantiated by the report from another group through the TLR7 antagonist co-crystal structure.^{60–62} The docking analysis of compound 12 showed that the imidazopyridine ring occupied the central hydrophobic cavity-forming- π interaction with Tyr356* (Figure 2A). The oxygen atom of the methoxy group present at the C4' position forms a hydrogen bond with an important Thr525 residue at the active site. The $-\text{NH}_2$ group at the C7 position acts as both hydrogen bond donor and acceptor to form interaction with Gln354* and Val355*. Both C7 $-\text{NH}_2$ and C4' $-\text{OCH}_3$ groups establish important interactions to stabilize the pharmacophore 12 in the active site. To support the binding hypothesis, we switched the amino group from the C7 position to the C3 position in 21 and 22. These compounds did not show any significant inhibition in TLR9 and TLR7 at 10 μM , substantiating the significance of proper positioning of the structural subunits on the core. Compound 12 was identified as our basic pharmacophore upon which further systematic lead development can be conducted.

Next, we extended the C7 amine substitution with a flexible alkyl chain containing basic nitrogen in compounds 23–27 by varying the chain length and the nature of the basic nitrogen-containing group. Compounds 24 and 23 contain three-carbon morpholine units at C7 but differ in monosubstitution at C4' (23) and disubstitution (24) at C2' and C4', whereas 23 and 25 contain morpholine groups with different chain lengths. All of the three compounds showed <100 nM inhibitory potency in TLR9, with no preference for mono- or disubstitution at the

C2 phenyl ring. As the three-carbon chain length showed more potent TLR7 inhibition, we further prepared two compounds with pyrrolidine (26) and imidazole (27) substituents. Both compounds showed sub-micromolar potency in both TLR7 and TLR9, with compound 26 showing the most potent activity in TLR9 ($\text{IC}_{50} = 19$ nM) and TLR7 ($\text{IC}_{50} = 395$ nM) (Table 1 and Figure 4). Next, we performed a docking analysis of compound 26 in TLR7. The template for the human TLR7 homology model contains the homodimeric chain that was built from the human TLR8 crystal structure [Protein Data Bank (PDB) ID: 3W3J]. The docking analysis of 26 in the active site similarly showed the π – π interaction of the imidazopyridine ring with Tyr356* along with the hydrogen bond between the C4' group and Thr525 (Figure 2B) as that of 12. The secondary $-\text{NH}$ group at C7 acts as a hydrogen bond donor and retains the hydrogen bond interaction with Val355*. Similarly, the protonated nitrogen atom of the pyrrolidine ring acts as a hydrogen bond donor to form a hydrogen bond with Leu353*. In vitro, ADME assays of 24 and 26 showed both compounds with good plasma stability with moderate aqueous solubility at pH 7.4 (Table 5). The low efflux ratio of 24 suggested that the compound is not a substrate of p-glycoprotein. However, the log D value of compound 26 was found to be <1 , which may not be ideal for oral absorption.^{63,64}

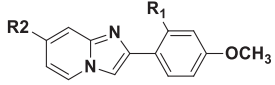
The result obtained from the compounds mentioned in Table 1 prompted further lead optimization. The main focus of the next stage of the development was to optimize the lipophilic bulk and decrease the flexibility at C7 by incorporating a conformationally constrained ring structure containing similar basic amine. Accordingly, we incorporated piperazine at the C7 position to incorporate suitable lipophilic substituents at the terminal amine of piperazine. The C2

Table 1. SAR Modification of the Imidazopyridine Core^c


Comp. No.	R1	R2	R3	R4	TLR9 IC ₅₀ (μM)	TLR7 IC ₅₀ (μM)
7	H	OCH ₃	H	H	no inhibition at 40 μM	37% inhibition at 40 μM
8	H	H	Br	H	no inhibition at 10 μM	NT
9	H	OCH ₃	Br	H	no inhibition at 10 μM	NT
10	OCH ₃	OCH ₃	Br	H	no inhibition at 10 μM	NT
11	OCH ₃	OCH ₃	H	H	10.43 ± 0.99	42% inhibition at 40 μM
12	H	OCH ₃	NH ₂	H	2.92 ± 0.17	4.77 ± 0.86
13	OCH ₃	OCH ₃	NH ₂	H	1.57 ± 0.15	2.55 ± 0.33
14	H	OCH ₃	N(CH ₃) ₂	H	1.48 ± 0.07	6.74 ± 0.44
15	OCH ₃	OCH ₃	N(CH ₃) ₂	H	0.766 ± 0.108	3.78 ± 0.27
16	H	H	N(CH ₃) ₂	H	2.19 ± 0.143	NT
21	H	OCH ₃	H	NH ₂	no inhibition at 10 μM	36% inhibition at 30 μM
22	OCH ₃	OCH ₃	H	NH ₂	no inhibition at 10 μM	40% inhibition at 30 μM
23	H	OCH ₃		H	0.067 ± 0.005	1.06 ± 0.12
24	OCH ₃	OCH ₃		H	0.069 ± 0.017	1.53 ± 0.14
25	OCH ₃	OCH ₃		H	0.049	3.39 ± 0.39
26	OCH ₃	OCH ₃		H	0.019 ± 0.004	0.395 ± 0.06
27	OCH ₃	OCH ₃		H	0.038 ± 0.018	0.819 ± 0.09

^aIC₅₀ values were derived from reporter assays using HEK293 cells transfected with hTLR9 (mean ± SD, *n* = 3). ^bIC₅₀ values were derived from reporter assays using HEK293 cells transfected with hTLR7 (mean ± SD, *n* = 3). ^cCommercially available TLR agonists (CpGB for TLR9 and CL264 for TLR7) were used as positive controls.

substitutions of the imidazopyridine core remain the same in the initial set of compounds with C2'/C4' bisubstitution and C4' monosubstitution at the phenyl ring. The dimethoxy derivative **35** showed excellent TLR9 (IC₅₀ = 46 nM) and TLR7 (IC₅₀ = 308 nM) inhibition. The inhibitory profile of **35** is similar to the best active **26** from Table 1, indicating our strategic modification. The monomethoxy derivative **34** (TLR9: IC₅₀ = 803 nM; TLR7: IC₅₀ = 559 nM) displayed lesser potency in both TLR9 and TLR7 than **35** (Table 2). Incorporating a bulky hydrophobic substituent at C2' in **36** led to a slight decrease in both TLR9 and TLR7 inhibition in comparison to **35**. Next, logically, we extended the terminal nitrogen of the piperazine unit with small hydrophobic groups in **37**, **38**, **40**, **41**, and **42**. Compounds **37** and **38** were prepared with a cyclopentyl group attached to the piperazine ring. Expectedly, the dimethoxy derivative **38** showed slightly better antagonism in both TLR7 and TLR9 as compared to

Table 2. SAR Development and Lead Optimization^c


Comp No.	R1	R2	TLR9 IC ₅₀ (μM) ^a	TLR7 IC ₅₀ (μM) ^b
34	H		0.803 ± 0.095	0.559 ± 0.03
35	OCH ₃		0.046 ± 0.002	0.308 ± 0.03
36	OBn		0.055 ± 0.08	1.13 ± 0.18
37	H		0.071 ± 0.008	3.33 ± 0.40
38	OCH ₃		0.049 ± 0.015	2.34 ± 0.26
39	OBn		0.153 ± 0.017	5.56 ± 0.60
40	OH		0.79 ± 0.33	20.82 ± 5.98
41	H		0.044 ± 0.019	1.23 ± 0.06
42	OCH ₃		0.040 ± 0.004	0.466 ± 0.03
43	OCH ₃		2.91 ± 0.63	8.70 ± 0.84
44	OBn		5.13 ± 0.72	no inhibition up to 30 μM
45	OH		2.12 ± 0.222	no inhibition up to 30 μM
46	OBn		1.06 ± 0.521	24.90 ± 3.23
47	OBn		2.19 ± 0.304	10.95 ± 2.11
49		Boc-N-	0.314 ± 0.024	2.95 ± 0.24
50		Boc-N-	0.157 ± 0.033	2.95 ± 0.43
51			0.035 ± 0.004	1.35 ± 0.20
52			0.094 ± 0.014	0.659 ± 0.08
53			0.028 ± 0.003	0.478
54			0.017 ± 0.004	0.456 ± 0.02

^aIC₅₀ values were derived from reporter assays using HEK293 cells transfected with hTLR9 (mean ± SD, *n* = 3). ^bIC₅₀ values were derived from reporter assays using HEK293 cells transfected with hTLR7 (mean ± SD, *n* = 3). ^cCommercially available TLR agonists (CpGB for TLR9 and CL264 for TLR7) were used as positive controls.

monomethoxy derivative **37**. Although the TLR9 inhibition (IC₅₀ = 49 nM) of **38** was excellent, the TLR7 inhibition became moderate with an IC₅₀ value of 2.34 μM. Interestingly, replacing the C2' methoxy group with the hydroxyl group led to a drastic change in both TLR7 and TLR9 inhibitions in **40** (TLR9: IC₅₀ = 0.79 μM; TLR7: IC₅₀ = 20.82 μM) (Table 2). Furthermore, the cyclopentyl group was replaced by the isosteric isopropyl group in **41** and **42**. The result displayed a similar pattern as previously observed for mono- and

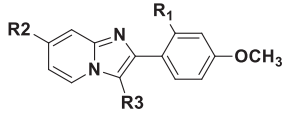
disubstitution. **41** displayed TLR9 and TLR7 inhibition with IC_{50} values of 44 nM and 1.23 μ M, whereas the bisubstituted derivative **42** exhibited TLR9 and TLR7 inhibition with IC_{50} values of 40 and 466 nM, respectively (Table 2 and Figure 4). The antagonism profile of bi-substituted derivative **42** against TLR7 and TLR9 is very encouraging and similar to the other potent compounds **26** and **35**.

The docking analysis of **41** and **42** provided important insight into the ligand–receptor binding (Figure 2C,D). Both **41** and **42** showed similar hydrogen bond interactions with Thr525 and Gly577, whereas the imidazopyridine ring stabilized through π – π hydrophobic interactions with Tyr356* and Phe408*. Specifically, the terminal protonated nitrogen atom of the piperazine forms a similar hydrogen bond interaction with Gly577 as that of pyrrolidine protonated nitrogen in **26**. Expectedly, the previously observed hydrogen bond between C7 amine acting as the donor and Val355* acting as the acceptor was absent in both **41** and **42** as their C7 nitrogen is tertiary-substituted and devoid of hydrogen donor property. The difference in the binding mode of mono-substituted (C4') **41** and di-substituted (C2' and C4') **42** was observed at the N1 nitrogen of the imidazopyridine core. In **42**, the N1 nitrogen remains unprotonated, which enables it to act as a hydrogen bond acceptor forming interaction with Asp548. However, in **41**, due to the absence of C2' substituents, the N1 nitrogen becomes protonated and, thus, can act only as a hydrogen bond donor. Thus, the strategic replacement of the flexible chain containing a basic amine with conformationally constrained piperazine and the requisite substitution pattern on the C2 aromatic ring was substantiated through a comparative docking analysis of **42** with **26** (Figure 2B–D). These compounds were stabilized in the active site through hydrogen bond interactions at both the terminal ends and hydrophobic interactions with the imidazopyridine core. In a comparison of the ADME profile of **38**, **41**, and **42**, it can be stated that all three compounds have an ideal log *D* value of oral absorption with good plasma stability in both humans and mice.^{63,64} Compound **42** showed a good aqueous solubility of 130.9 μ g/mL, whereas **41** and **38** showed moderate-to-poor solubility. Compound **42** also depicted good Caco-2 permeability with low efflux potential.

The next stage of development provided important revelation about the sensitivity of substituents that can be incorporated at the terminal amine of the piperazine ring at C7. The installation of the amide group in **43**, **44**, and **45** led to a dramatic change in both TLR7 and TLR9 antagonisms. In a comparison of TLR7 and TLR9 antagonism for **42** and **43**, an almost 72-fold decrease in TLR9 potency and an 18-fold decrease in TLR7 potency were observed for **43**. The loss in the potency could be envisaged through docking experiments of **43** in the TLR7 active site (Figure 3). The analysis showed that the terminal nitrogen at the piperazine ring of **43** could not get protonated due to the presence of an electron-withdrawing carbonyl group. As a result, the essential hydrogen bond interaction was absent in **43**. Also, the conformation of the piperazine ring was different when compared to **42**. For **44** and **45**, no significant TLR7 antagonism was observed up to 30 μ M. A similar decrease in the antagonist activity was observed when the cyclopentyl amide was replaced by aromatic amide in **46** and **47**. Thus, it can be stated that the terminal nitrogen of the piperazine can tolerate directly attached hydrophobic alkyl substituents but is sensitive toward electron-withdrawing substituents that can modulate the basicity of that nitrogen.

The role of basic amine to instigate TLR7 and TLR9 antagonism is well documented. Until now, we were able to optimize our lead through the replacement of the flexible linker at C7 with a conformationally constrained basic amine. We were tempted to explore the role of an additional basic amine center on TLR7 and TLR9 antagonism. A comparison of the SAR between **38**, **39**, and **40** showed hydrophobic groups at the C2' position provide better TLR9 antagonism. Thus, we expected that the C2' position would be ideal to install a flexible group with a basic amine. Compounds **51**, **52**, **53**, and **54** were synthesized containing pyrrolidine and morpholine substituents installed at the C2' position with a three-carbon flexible linker. To our satisfaction, all the four compounds showed excellent potency <100 nM against TLR9 with **54** containing three-carbon pyrrolidine rings at the C2' position and cyclopentyl piperazine at the C7 position, showing an IC_{50} value of 17 nM for TLR9 antagonism. Compounds **53** and **54** showed similar TLR7 antagonism with an IC_{50} value of \sim 0.5 μ M (Table 2). Compounds **51** and **52** did not have any hydrophobic substituent at the C7 terminal amine of the piperazine ring. Comparing **51** and **52** with their complementary compounds containing a hydrophobic cyclopentyl ring with **53** and **54** depicted that hydrophobicity at that position does not have a significant effect. The results are similar to those observed initially for set **34**–**39**. However, as observed before, the C7 piperazine terminal amine is sensitive to electron-withdrawing groups in amide-containing compounds **43**–**47**. To further validate, we investigated the precursor –Boc group-containing compounds **49** and **50**. The result showed a significant decrease in both TLR9 and TLR7 antagonisms, which substantiated the previous findings. Although the potency decrease is not as profound as observed for **43**–**47**, we assume that both TLR7 and TLR9 antagonisms were balanced by the presence of an additional basic center at the C2' position. Although **53** and **54** showed excellent potency against both TLR7 and TLR9, the aqueous solubility of both compounds was poor at 2.6 and 0.8 μ g/mL, respectively. Compound **54** showed poor permeability in the Caco-2 permeability assay with a high efflux ratio, suggesting that the compound may be a substrate of *p*-glycoprotein.

The introduction of the amine group at C3 in **22** was not encouraging, unlike **12** and **13**, where similar substitution provided the template for further SAR development and optimization. The basic compound **22** did not show any inhibition against TLR9 at 10 μ M, whereas **13** depicted an IC_{50} value of 1.57 μ M. We further incorporated aliphatic and aromatic substituents in **57** and **58**. Expectedly, **57** and **58** showed moderate potency (Table 3) in both TLR9 and TLR7. The result substantiates that amine substitution at C7 and subsequent derivatization were preferable. Next, we introduced a methylene spacer at the C3 of the imidazopyridine ring and the amine substitution to further modulate the basicity of the amine in **59** and **60**. Satisfactorily, the results were very encouraging; especially, **60** showed excellent inhibition in both TLR9 and TLR7 (TLR9: IC_{50} = 39 nM; TLR7: IC_{50} = 0.58 μ M) (Table 3 and Figure 4). Replacing the –OCH₃ group at C2' with benzyl and –OH in **61** and **62** provided a similar loss of inhibition as observed for **39** and **40**. Together, the results substantiate the importance of the –OCH₃ group at the C2' position. Further optimization of the cyclopentyl group at the C7 terminal piperazine ring in **59** and **60** with the isopropyl group in **63** and **64** expectedly displayed excellent TLR9 and TLR7 antagonism. Compound **64** exhibited TLR9 and TLR7

Table 3. Effect of R3 Substitution on TLR7 and TLR9 Antagonism^c


Comp No.	R1	R2	R3	TLR9 IC ₅₀ (μM) ^a	TLR7 IC ₅₀ (μM) ^b
22	OCH ₃	H	NH ₂	no inhibition at 10 μM	>30 (40% inhibition at 30 μM)
57	OCH ₃			2.11 ± 0.29	6.70 ± 0.62
58	OCH ₃			0.526 ± 0.044	4.81 ± 0.46
59	OCH ₃			0.142 ± 0.013	2.12 ± 0.20
60	OCH ₃			0.039 ± 0.007	0.58 ± 0.05
61	OBn			0.24 ± 0.039	15% inhibition at 20 μM
62	OH			0.245 ± 0.027	24.89 ± 6.7
63	OCH ₃			0.040 ± 0.009	2.49 ± 0.31
64	OCH ₃			0.015 ± 0.004	0.258 ± 0.06
65	OCH ₃			1.12	2.55 ± 0.42

^aIC₅₀ values were derived from reporter assays using HEK293 cells transfected with hTLR9 (mean ± SD, *n* = 3). ^bIC₅₀ values were derived from reporter assays using HEK293 cells transfected with hTLR7 (mean ± SD, *n* = 3). ^cCommercially available TLR agonists (CpGB for TLR9 and CL264 for TLR7) were used as positive controls.

inhibition with IC₅₀ values of 15 and 258 nM, respectively (Table 3 and Figure 4). As observed in Table 2, the terminal nitrogen of the piperazine is sensitive toward electron-withdrawing substituents (43–47) and led to the loss in TLR9 and TLR7 antagonism. To further validate the result in a different set of substitutions, the isopropyl moiety in 64 was replaced with cyclopentyl amide in 65. The installation of the amide group in 65 led to the loss in both TLR7 and TLR9 antagonism with almost 62-fold decreases in TLR9 potency and 10-fold decreases in TLR7 potency; the observation was similar to that of 42 and 43.

The TLR9 antagonist activity of our lead compound 42 was again validated in human pDC which are a major source of type I interferon and play an important role in the immune system. TLR9 is highly expressed in pDCs, and it is widely used to find the antagonist activity against TLRs. Antagonist activity against TLR9 of our lead compound 42 in human pDCs was obtained by taking the average values of three individual donors and finding the IC₅₀^{pDC}: 0.028 μM (Figure 5A), which is very good and resembled our reporter assay result (IC₅₀^{reporter}: 0.040 μM) (Figure 5B).

Selectivity of Antagonists against TLR8. Selected compounds from different substitution patterns (26, 38, 41, 42, 52, 54, 57, 59, 60, and 64) were evaluated for selectivity against hTLR8. Out of all the molecules evaluated for hTLR8 antagonism, 26, 42, and 54 showed hTLR8 antagonism (Supporting Information, Figure S3). The lead compound 42 showed hTLR8 antagonism with an IC₅₀ value of 8.32 μM. Compound 26, with a flexible alkyl linker with a pyrrolidine group at C7, also showed TLR8 inhibition with 17.18 μM. Compound 54 showed ~35% inhibition at 20 μM, and the rest of the compounds showed less than 20% inhibition at 20 μM. To understand the selective antagonism in TLR7 and TLR8, the antagonist binding site of both TLR7 and TLR8 sequences were aligned to identify the differences such as the amino acid residue present (Figure 6; Supporting Information S4) at the active site.^{43,65–67} The analysis revealed the difference such as many amino acids at their active site such as Thr406* (polar) of TLR7 is complementary with Ile403* (nonpolar bulky) in TLR8 (Figure 6A). Table 4 describes the changes in the corresponding amino acid residues at the active site of both TLR7 and TLR8. As result, the shape and nature of both TLR7 and TLR8 showed characteristic differences in the active site with the TLR7 pocket being more hydrophobic. Also, TLR8 contains shallow and smaller pockets as compared to TLR7 with bigger pockets and grooves (Figure 6B,C). A distinct difference like an amino acid was observed specifically in chain B of TLR7 when compared with the complementary residue of chain B of TLR8. As an example, the hydrophobic residues of TLR7 have changed to hydrophilic residues in TLR8 such as Leu353* (TLR7) changed to Lys350* (TLR8) and Val355* (TLR7) changed to Ser352* (TLR8) (Figure 6B,C). These differences may account for the selective antagonist activity between TLR8 and TLR7.

Isothermal Titration Calorimetry Experiment. As proposed earlier by Gao et al.,³⁴ the mechanism of antagonism may be either by (a) interacting with the agonist oligonucleotide CpG or nucleic acid derivatives and preventing the agonists to interact with the receptor or (b) by interacting directly with the ECD and not permitting the agonist to interact with the receptor.³⁴ To provide mechanistic insight into the nature of the binding, isothermal titration calorimetry (ITC) was used to determine the interaction of the lead antagonist 42 with commercially available TLR9/7 agonists—CpGB/CL264. The binding capacity was analyzed by titration of compound 42 into CpGB (TLR9 agonist) and CL264 (TLR7 agonist). The heat signals indicate that there is no significant interaction between the antagonists and CpGB and CL264 (Figure 7). The binding constant (*K_d*) between our lead compound 42 and CL264 and CpGB was also found too low, that is, 0.0001 and 0.01, respectively. Hence, through the exclusion of direct interaction between antagonists with TLR9/7 agonists, indirect binding of compound 42 to human TLR9/TLR7 can be logically stated. The ITC experiment conclusively rules out direct binding between the antagonist and agonist due to the reason behind the observed antagonist activity. Through logical extrapolation, we can assume that the antagonist activity is most likely due to the interaction between the antagonists with the TLR7/9 protein.

In Vitro ADME Study. Sequential incorporation of relevant structural subunits in a basic molecular framework of imidazopyridine at C7, C3, C2, and C2' positions provided compounds 13, 16, 22, 25, 26, 36, 37, and 41 as the prospective lead candidate. To further optimize these lead

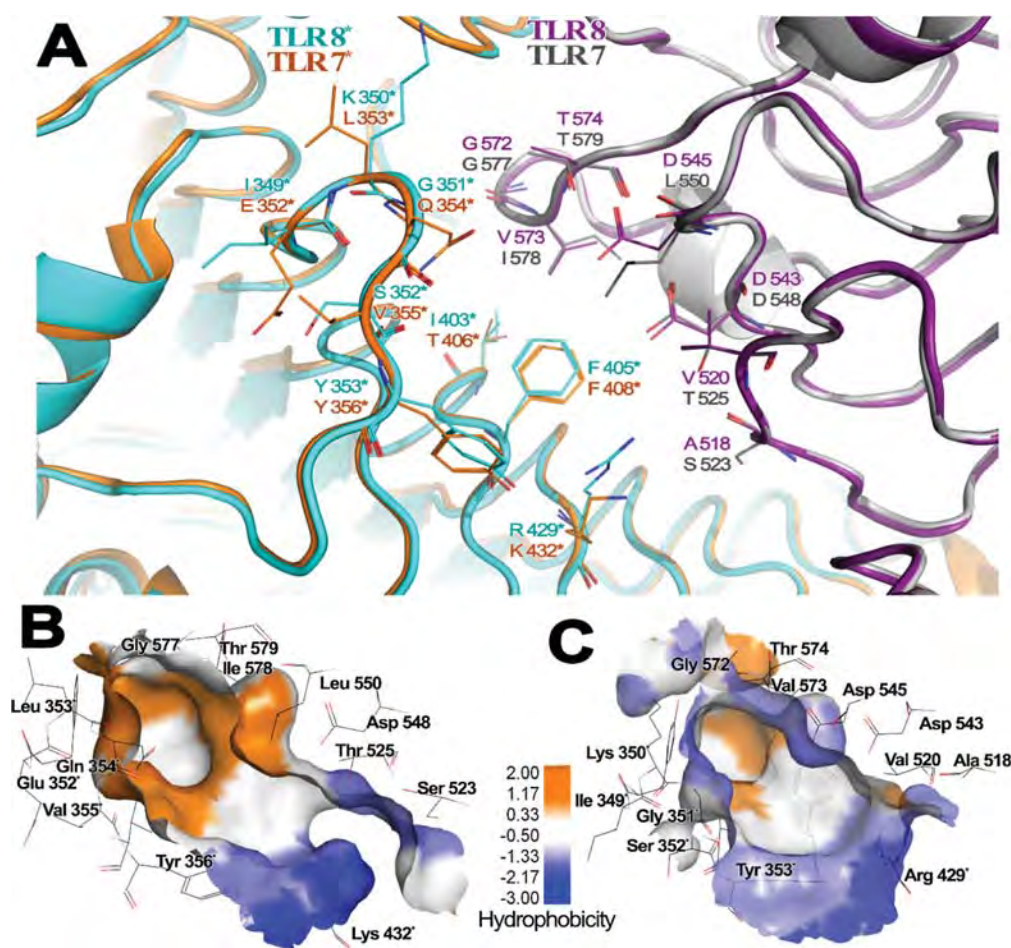


Figure 6. (A) The antagonist binding site of both TLR7 and TLR8 protein was superimposed. The A chain of TLR7 is colored gray, and the B chain is orange; the A chain of TLR8 is colored purple and the B chain is cyan. Asterisk indicates the second monomeric chain. (B) Surface representation of the active site of TLR7; (C) surface representation of the active site of TLR8. The blue color represents low hydrophobicity, and the brown areas represent a highly hydrophobic region.

Table 4. Difference in the Corresponding Amino Acid Residue in the Active Site of TLR7 and TLR8

s no.	A chain		B chain (denoted with *)	
	TLR7 residue (nature)	TLR8 residue (nature)	TLR7 residue (nature)	TLR8 residue (nature)
1	Ser 523 (hydroxylic, polar)	Ala 518 (aliphatic, nonpolar)	Phe 351 (aromatic, nonpolar)	Tyr 348 (aromatic, Brønsted acid)
2	Thr 525 (hydroxylic, polar)	Val 520 (aliphatic, nonpolar)	Glu 352 (anion, Brønsted base)	Ile 349 (aliphatic, nonpolar)
3	Leu 550 (aliphatic, nonpolar)	Asp 545 (anion, Brønsted base)	Leu 353 (aliphatic, nonpolar)	Lys 350 (cation, Brønsted acid)
4	Ile 578 (aliphatic, nonpolar)	Val 573 (aliphatic, nonpolar)	Gln 354 (amide, polar)	Gly 351 (aliphatic, nonpolar)
5			Val 355 (aliphatic, nonpolar)	Ser 352 (hydroxylic, polar)
6			Thr 406 (hydroxylic, polar)	Ile 403 (aliphatic, nonpolar)
7			Lys 432 (cation, Brønsted acid)	Arg 429 (fixed cation, basic polar)

candidates we evaluated them in a panel of in vitro ADME assays (Tables 5 and 6).^{47,63,68,69} These compounds have different substitutions at C7, C3, and C2' positions. Thus, this would provide an understanding of the correlation between in vitro pharmacokinetic properties and different structural modifications in the imidazopyridine scaffold for lead selection. We experimentally evaluated kinetic solubility (pH 7.4), log *D*, plasma stability (human and mouse), microsomal stability (human and mouse), and Caco-2 permeability.^{70,71}

Plasma Stability. Compounds 24, 26, 38, 41, 42, 53, 54, and 60 showed good plasma stability in both human and mouse plasma (Table 5).

Microsomal Stability. Mouse and human microsomal stability assays of lead candidates were carried out at 5 μ M at 37 $^{\circ}$ C for 60 min (Table 5). Except for compound 13, all the other compounds showed moderate-to-good human microsomal stability. Similarly, all the compounds except 60 showed moderate-to-good mouse microsomal stability (Table 5).

Aqueous Solubility. The compounds 42, 41, and 60 showed good aqueous solubility, whereas compounds 53 and 54 showed poor solubility with <5 μ g/mL value (Table 5).

Caco-2 Permeability. Compounds 24, 42, 53, 54, and 60 were evaluated for Caco-2 permeability. All the compounds except 54 showed good permeability in the Caco-2 permeability assay with low efflux potential (Table 6).

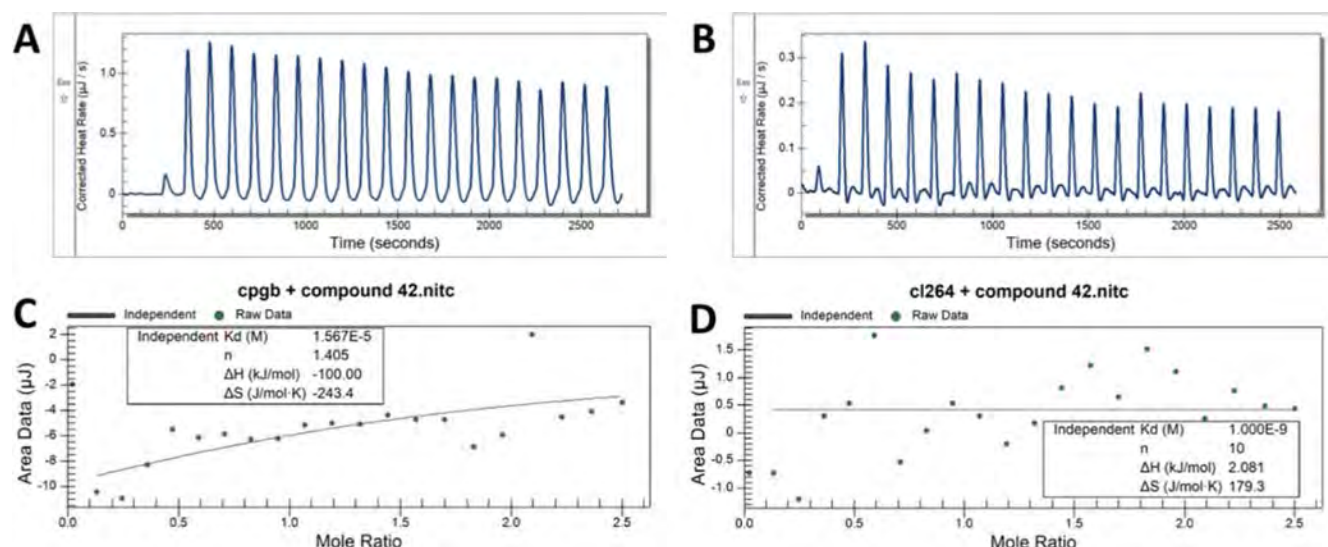


Figure 7. (A,B) ITC thermograms of compound **42** into CpGB and CL264, respectively. (C,D) Respective representations of the binding constant (K_d) value, which suggests that there is insignificant interaction between our lead compound **42** and nucleic acid analogues, i.e., CpGB and CL264.

Table 5. In Vitro Pharmacokinetic Profile of Potent Compounds

comp.	PSA ^a (Å ²)	log <i>D</i>	aq. solubility pH = 7.4 (μg/mL)	plasma stability ^b		metabolic stability half-life (<i>t</i> _{1/2}) (min)	
				human	mouse	human	mouse
24	58.56		22.3	95.7	105.5	16.2	114.5
26	49.33	0.82	29.69	72.0	82.9	28.7	103.3
38	40.54	2.13	10.22	64.9	93.4	37.6	31.8
41	31.31	1.64	46.07	60.4	92.8	66.0	29.4
42	40.54	2.21	130.92	89.4	69.7	28.2	144.5
53	53.01		2.6	94.3	90.6	NA	NA
54	43.78		0.8	103.6	97.1	11.8	26.0
60	43.78		22.6	90.0	103.9	9.5	38.8
64	43.78	1.77	162.9	43.0	20.9	32.1	17.9
ketoconazole ^c	66.84	3.54					
albendazole ^d	62.72		2.2				
propantheline ^e	35.53			0.0	0.0		
verapamil ^f	63.95					6.4	5.5

^aPolar surface area. ^bMean % remaining after 2 h. ^cKetoconazole was taken as the standard for log *D* determination. ^dAlbendazole was taken as the standard for the aqueous solubility test. ^ePropantheline was taken as the standard for human and mice plasma stability experiments. ^fVerapamil was taken as the standard for metabolic stability experiments in both humans and mice.

Table 6. Caco-2 Permeability of the Antagonists

comp.	mean parameters		
	<i>P</i> _{app} (10 ^{−6} cm/s)		efflux ratio
	apical to basal	basal to apical	
24	23.50	20.10	0.9
42	19.73	19.10	0.97
53	15.43	8.17	0.5
54	0.35	3.54	10.2
60	33.58	57.53	1.7
propranolol ^a	14.36	17.30	1.2
atenolol ^a	0.71	1.50	2.1

^aPropranolol and atenolol were taken as standards.

In Vitro Cellular Toxicity Assay. From our library, we selected 10 hit compounds **24**, **26**, **27**, **35**, **38**, **42**, **53**, **54**, **60**, and **64** for cytotoxicity assessment. We checked the in vitro toxicity in various cell lines of different tissue origins, for

example, human peripheral blood mononuclear cells (PBMCs) (hematopoietic origin) and HEK293 cells, by propidium iodide (PI) staining. To our satisfaction, none of our hit molecules showed appreciable toxicity in the above-mentioned cell lines up to 20 μM concentration of the compounds except for compound **54** in the HEK293 cell (Figure 8A,B).

We further decided to perform the pharmacodynamic study with compound **42** to explore the in vivo efficacy in the mouse model developed in our laboratory.

In Vivo TLR9 Antagonism Efficacy. The abundance of self-nucleic acids in tissues leads to the aberrant activation of TLR9, resulting in the production of copious amounts of type I IFN by recruited pDCs, which drives the onset and subsequent clinical pathogenesis of various autoimmune disorders. Upregulation of interferon signature genes (ISGs) in tissues is established by markers of local type I interferon release which is known to promote inflammation and disease severity in clinical contexts.⁷² The in vivo efficacy of compound **42** was

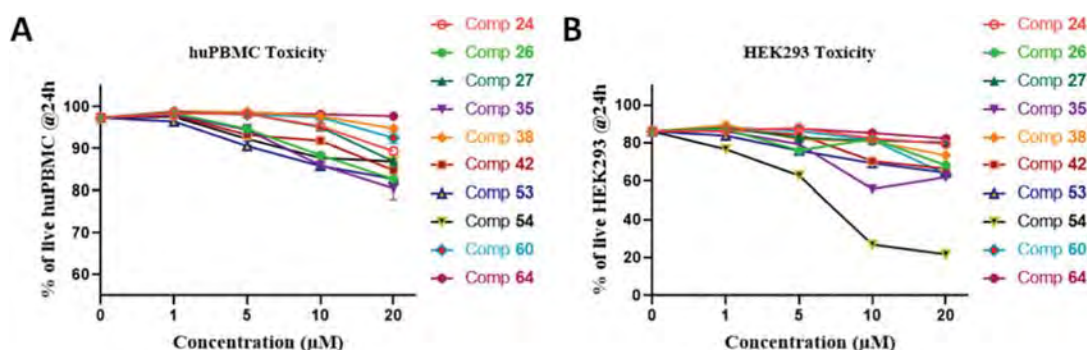


Figure 8. Determination of in vitro cytotoxicity of potent TLR9 antagonists. (A) Human PBMCs and (B) HEK293 cells were treated with the mentioned concentrations of the compounds overnight and assessed by PI staining and flow cytometry to determine the percentage of live/dead cells.

estimated by testing it in a suitable clinical murine model reported in previous studies.^{42,47}

In brief, 8–10 weeks-old female C57BL/6 mice were orally administered with the vehicle or **42** and then intraperitoneally injected with PBS or a mixture of bona fide TLR9 ligands CpGA and CpGB. 18 h postinjection recruitment of pDCs (Figure 9B) and the local abundance of IFN- α protein were quantified from the peritoneal fluid (Figure 9C), while the relative expression of ISGs (Figure 9D,E) was measured in cells isolated from the peritoneal cavity, that is, the site of inflammation. Significant downregulation of IFN- α protein was observed in the mice that were fed **42** as compared to those that were not (Figure 9C). Moreover, mRNA expression of two ISGs, namely, IFIT1 and IRF7, which are reliable biomarkers of interferon signaling in clinical contexts, were significantly downregulated in the **42** fed group (Figure 9D,E). Together, this data suggests **42** to be a potent antagonist of TLR9 in an in vivo setting.

In Vivo TLR7 Antagonism Efficacy. The in vivo efficacy of **42** was also estimated by testing it in a suitable clinical murine model of TLR7. In brief, 8–10 weeks old female C57BL/6 mice were orally administered with the vehicle or compound **42** and then intraperitoneally injected with PBS or the TLR7 ligand CL264 (Figure 10A). 18 h postinjection recruitment of pDCs (Figure 10B) and the local abundance of IFN- α protein (Figure 10C) were quantified from the peritoneal fluid. A significant reduction of IFN- α protein was observed in the mice that were fed **42** before CL264 injection as compared to those that were not (Figure 10C). Together, this data suggests that **42** also shows antagonistic activity against TLR7 in an in vivo setting.

CONCLUSIONS

The study reported the development of a new chemotype “imidazopyridine” as dual TLR7/TLR9 antagonists. The exploration put forth an interesting approach through systematic SAR studies by sequentially incorporating relevant structural subunits in a basic molecular framework necessary for instigating potent TLR7 and TLR9 dual antagonism. We established minimal pharmacophoric features in the imidazopyridine core and subsequent hits to lead optimization, guided by in vitro and in vivo biological assays supported by ADME profiles. We illustrate here the importance of C7, C3, C2, and C2' substitutions in imidazopyridine core for antagonism to TLR7 and TLR9 through SAR studies. We considered **12** as a basic pharmacophore with the -NH₂ group at the C7 position.

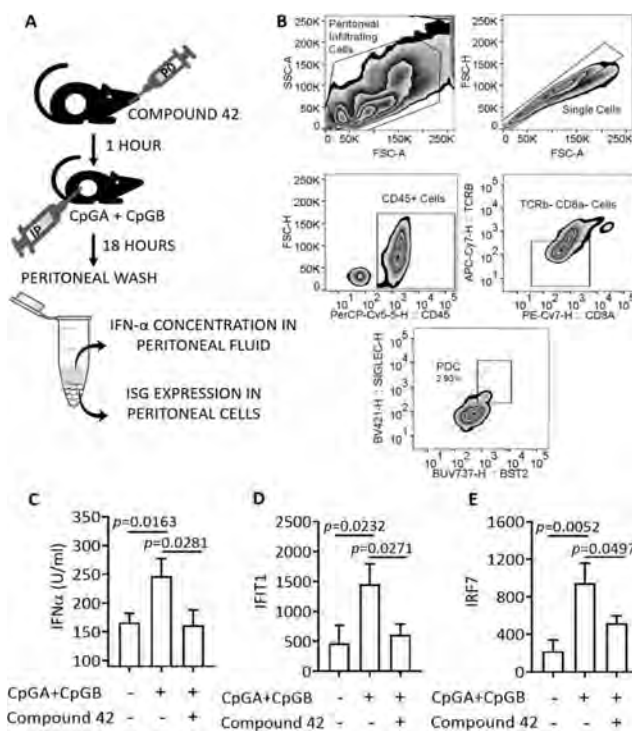


Figure 9. Study of in vivo efficacy of **42** in the context of TLR9 antagonism: (A) compound **42** was administered to the assigned group of mice ($n = 7$ –8 per group), orally, at a dose of 10 mg/kg body weight. 1 h post administration of a mixture of TLR9 ligands CpGA and CpGB were injected intraperitoneally. 18 h postinjection peritoneal wash was collected. Sandwich ELISA was performed to measure IFN- α protein concentrations, whereas the relative expression of ISGs was quantified from mRNA isolated from peritoneal cells. (B) The peritoneal cells were subjected to flow cytometric analysis to evaluate the infiltration of immune cells, specifically pDCs, into the peritoneal cavity. (C) IFN- α protein concentration was measured in the peritoneal fluid of mice w/o **42** by sandwich ELISA (2 independent experiments). (D,E) Relative mRNA expression levels of IFIT1 (D) and IRF7 (E) in the peritoneal infiltrating cells of mice w/o exposure to **42** was quantified by real-time PCR (two independent experiments). The p values were determined by the unpaired Student t -test.

The inactivity of **21** validated the proper positioning of the structural subunit on the imidazopyridine ring, where the -NH₂ group was shifted from the C7 to C3 position.

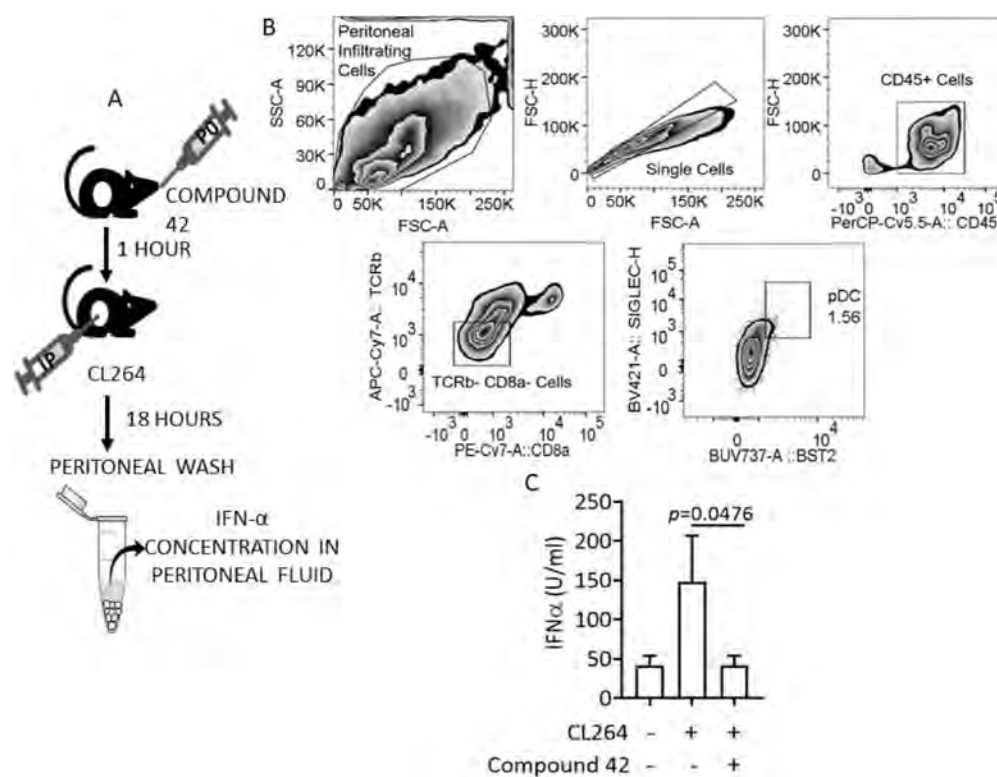


Figure 10. Study of in vivo efficacy of **42** in the context of TLR7 antagonism: (A) compound **42** was administered to the assigned group of mice ($n = 4-5$ per group), orally, at a dose of 10 mg/kg body weight. 1 h postadministration, the TLR7 ligand CL264 was injected intraperitoneally. 18 h postinjection peritoneal wash was collected. Sandwich ELISA was performed to measure IFN- α protein concentrations. (B) The peritoneal cells were isolated and subjected to flow cytometric analysis to evaluate the infiltration of immune cells, specifically pDCs, into the peritoneal cavity. (C) IFN- α protein concentration was measured in the peritoneal fluid of mice w/o **42** by sandwich ELISA. The p values were determined by the unpaired Student t -test.

Generally, disubstitution at C2' and C4' showed more potent inhibition against both TLR7 and TLR9 as compared to C4' monosubstitution. The possible ligand–receptor interactions and selectivity studies were performed through molecular docking analysis. The ITC experiment excluded direct binding between TLR agonist and antagonist due to the reason behind the observed antagonist activity. The lead candidate **42** showed a log D value of 2.21 ideal for oral absorption with excellent aqueous solubility at pH 7.4. The observation was supported by good Caco-2 permeability with an efflux ratio of <1, ruling out the possibility of **42** being a P-gp substrate. Compound **42** also showed good-to-moderate plasma and microsomal stability in both mice and humans. The oral absorption and efficacy of lead **42** were established through in vitro pharmacokinetic studies and in vivo pharmacodynamic studies in mice, with IC_{50} values of 0.04 and 0.47 μ M against TLR9 and TLR7, respectively. The findings establish imidazopyridines as viable chemotypes for exploring potential therapeutic candidates in relevant clinical contexts. Our strategy described herein can be considered as a template for conceptually developing basic chemotypes into a possible drug candidate.

EXPERIMENTAL SECTION

Log D Determination Assay. 10 mM primary stocks of test compounds were prepared in dimethyl sulfoxide (DMSO). 500 μ L of 1-octanol which is saturated with 10 mM phosphate buffer of pH 7.4 was added to each well of a 2 mL deep-well plate, and 15 μ L of test compounds was added to each well containing the organic phase in two replicates and vortexed for 10 min on a plate shaker at 1200 rpm;

then, 500 μ L of phosphate buffer of pH 7.4 which was presaturated with 1-octanol was added to each well of a 2 mL deep-well plate and vortexed for 4 h on a plate shaker at 1200 rpm; and then, the plate was incubated at room temperature on a plate shaker at 1200 rpm. After incubation, the samples were allowed to equilibrate for 20 min and then centrifuged at 4000 rpm for 30 min. After centrifugation of a 1-octanol layer and phosphate, the buffer layer is separated and the sample is injected into the HPLC column and analyzed by HPLC-UV (Table S3).

Aqueous Solubility Assay. 50 mM primary stocks of test compounds were prepared in DMSO. 4.0 μ L of this prepared stock solution was added to the deep-well plate containing 396 μ L of pH 7.4 phosphate buffer, mixed, and incubated for 24 h at room temperature with constant mixing at 300 rpm. The DMSO content in the sample was 1.0%, and 500 μ M was the final concentration of the compound in a deep-well plate. The plate was sealed properly during the incubation process. The samples were centrifuged for 20 min at 4000 rpm after incubation. The supernatant was analyzed by HPLC-UV spectroscopy. The spectrum was read using a Shimadzu UV spectrophotometer at 254 nm (Table S2).

Caco-2 Permeability Assay. A 10 mM stock solution of test compounds was prepared in DMSO, and this stock was diluted with Hank's balanced salt solution (HBSS) buffer of pH 7.4 to a final concentration of 10 μ M. Cell proliferation was carried out by adding 250 μ L of Dulbecco's modified Eagle's medium (DMEM) to the basal compartment of a 96-well multiscreen Caco-2 plate and seeded 12,000 cells/well (0.16×10^6 cells/mL) in all the apical wells required and one well with only media as blank without cells. The Caco-2 plate was placed in a CO₂ incubator at 37 °C for the proliferation of cells. On the day of assay, the medium was removed and washed twice with HBSS buffer followed by incubation with HBSS buffer for 30 min in a CO₂ incubator at 37 °C. To determine apical-to-basal permeability,

75 μL of test compound and 250 μL of 2% bovine serum albumin (BSA) containing HBSS buffer were added to apical wells and basal wells, respectively. 25 μL of basal samples was collected after 120 min to analyze. Now, to determine basal-to-apical permeability, 250 μL of the test compound and 75 μL of 2% BSA containing HBSS buffer were added to basal wells and apical wells, respectively. 25 μL of apical samples were collected after 120 min to analyze. A single-point calibration curve in an HBSS buffer containing 2% BSA was used. Donor samples were diluted 1:1 with HBSS containing 2% BSA, whereas receiver samples were diluted with 1:1 HBSS buffer only. It was then precipitated with 200 μL of acetonitrile (ACN) containing the internal standard, vortexed for 5 min at 1000 rpm, and further centrifuged at 4000 rpm for 10 min. 100 μL of the supernatant was diluted with 200 μL of water and analyzed using liquid chromatography–mass spectrometry (LC–MS)/MS analysis (Table S6).

Plasma Stability Assay. A 10 mM stock solution was prepared in DMSO, which was then diluted to 1 mM stock of test compounds by 1:9 dilutions with DMSO. Then, 10 μL of 1 mM stock was diluted with 90 μL of water to obtain a 100 μM final concentration with 10% DMSO. On the other hand, the frozen plasma was thawed at room temperature and centrifuged at $1400 \times \text{RCF}$ at 4°C for 15 min. Around 90% of the clear supernatant fraction was transferred to a separate tube which was then used for the experiment. The final working stock of 1 μM of the test compounds was obtained by diluting 3 μL of 100 μM with 297 μL of plasma. Plasma containing the test compound was incubated for 120 min at 37°C in a shaker with gentle shaking. 50 μL aliquots of the sample at 0, 15, 30, 60, and 120 min were precipitated with 200 μL of acetonitrile containing the internal standard and centrifuged at 4000 rpm and 4°C for 20 min. 150 μL of the supernatant was analyzed on LC–MS/MS (Table S4 and S5).

Microsomal Stability Assay. A 1 mM stock solution of the test compounds in DMSO was diluted with 1:1 water and methanol to get a 100 μM working concentration of the test compounds. 100 mL of Milli-Q water was added to K_2HPO_4 (1.398 g) and KH_2PO_4 (0.27 g) to get a final pH of 7.4 of the buffer. A 2.5 mM 1-nicotinamide adenine dinucleotide phosphate (NADPH) cofactor solution was prepared by diluting 468.75 μL of 16 mM NADPH stock to 2531.25 μL with the above-prepared buffer. 75 μL of 3.33 mg/mL working stock of liver microsomes (diluted by phosphate buffer from 16 mg/mL initial stock solution) and 85 μL of the buffer of pH 7.4 was added to 2.5 μL of the test compound (100 μM), and this mixture was preincubated for 10 min at 37°C . In the absence of the NADPH cofactor, 32.5 μL of this mixture was added to 17.5 μL of phosphate buffer and incubated for 60 min. For the 0 min sample, 16.25 μL of the preincubated mixture and 8.75 μL of the cofactor were added to 150 μL of the ACN-containing internal standard. 62 μL of the cofactor was added to the remaining preincubated mixture and kept at 37°C . 25 μL of this incubation mixture at different time points (0, 5, 15, 30, and 60 min) were precipitated with 150 μL of the ACN-containing internal standard and vortexed for 5 min at 1200 rpm and then centrifuged at 4000 rpm and 4°C for 20 min. 150 μL of the supernatant was diluted with 150 μL of water and analyzed by LC–MS/MS (Tables S7 and S8).

Isothermal Titration Calorimetry. ITC experiments were performed in a buffer composed of 25 mM MES pH 5.5, 0.20 M NaCl, and 1% DMSO at 298 K using a MicroCal iTC200 (GE Healthcare). The titration sequence included a single 0.4 μL injection followed by 20 injections, 2 μL each, with a spacing of 120 s between the injections. The titration conditions were as follows: 100 μM **42** into 10 μM CpGB and 100 μM **42** into 10 μM CL264. NanoAnalyze software was used to analyze the raw ITC data (Figure 7).

Molecular Docking Study. *Ligand Preparation.* Two-dimensional (2D) forms of structurally diverse imidazopyridine class of TLR7/9 antagonist molecules were drawn on ChemDraw Ultra and converted to their three-dimensional (3D) structures by Accelrys Discovery Studio 4.1 (DS). All the compounds were energy-minimized by performing 2000 steps of steepest descent followed by conjugate gradient algorithms, which conserved an RMSD gradient

of 0.01 Å.^{43,73} All the compounds were processed in the pH range of pH 5.5–6.5.

Protein Preparation. The 3D structure of human TLR7 ECD used in the docking calculation was solved by homology building using the template hTLR8 crystal structure by the Discovery Studio MODELER suite. The human TLR8 ECD crystal structure (PDB ID: 3W3J) was extracted from the PDB. The cocrystallized water and heteroatoms were removed. The protein preparation was done at pH 5.5 to mimic the endosomal environment using the CHARMM force field.

Molecular Docking. Molecular docking was performed using the LibDock module in Discovery Studio 4.1 client (DS). The designed compounds were docked on the predefined active site⁴³ on the homodimeric interface with a 10 Å radius sphere by selecting the active site residues of the protein hTLR7. To explore probable ligand conformational flexibility and rotational flexibilities, the default genetic algorithm module was implemented during the docking program.^{74,75} The energy-minimized ligands were docked by applying the CAESAR conformational strategy in which a limit of 255 adaptations for each compound was permitted inside an energy range of 20 kcal/mol above the global energy minimum threshold.⁴³

Reporter Assay to Measure TLR9, TLR7, and TLR8 Antagonism. The antagonist potential of synthesized small-molecule compounds against TLR9, TLR7, or TLR8 was measured using human HEK-Blue TLR9, HEK-Blue TLR7, and HEK-Blue TLR8 reporter cell lines, respectively. The cell line-specific TLRs are overexpressed in these reporter cells which on binding to their respective ligands/agonists cause downstream activation of NF- κ B which in turn stimulate activation and release of secreted embryonic alkaline phosphatase (SEAP) into the culture supernatant. The addition of this supernatant to the detection medium, that is, QUANTI-Blue solution, changes its color from pink to blue which can be quantitated spectrophotometrically by measuring the O.D. at 655 nm. Antagonists inhibit this activation of NF- κ B and the subsequent release of SEAP into the culture medium, which is then unable to change the color of the detection solution. The assay involves seeding reporter cells at a density of 70,000 cells per well in a 96-well plate in 200 μL of complete DMEM supplemented with 100 $\mu\text{g}/\text{mL}$ Normocin. The cells are incubated at 37°C and 5% CO_2 for 5 h to allow adherence to the plates. Postincubation increasing doses of the designated compounds are added in triplicate to the assigned wells and incubated for an additional hour. The ligands specific for the respective reporter cells, that is, CpGB (1 μM) for HEK-Blue TLR9, CL264 (5 $\mu\text{g}/\text{mL}$) for HEK-Blue TLR7, and CL075 (3 $\mu\text{g}/\text{mL}$) for HEK-Blue TLR8 are added after 1 h to each well with the compounds, as well as triplicate wells without compounds which serve as the positive control. Wells with no compound or ligand serve as the negative control. The next day, the supernatant is collected and added to QUANTI-Blue detection solution and observed for change in color which is then quantitated by measuring the O.D. at 655 nm using a spectrophotometer.⁷⁶ HEK-Blue hTLR9, HEK-Blue hTLR7, HEK-Blue hTLR8 reporter cells, QUANTI-Blue detection solution, Normocin, CpGB (ODN 2006), CL264, and CL075 were all purchased from Invivogen, USA. DMEM was purchased from Gibco, Thermo Fisher Scientific.

TLR9 Antagonism Assay in Human pDCs. Human pDCs are enriched in TLR9 and served as ideal primary cells to assess the TLR9 antagonist activity of the synthesized lead small molecule **42**. First, PBMCs were isolated by Ficoll density gradient centrifugation from buffy coats of healthy donors collected from the Tata Medical Center Blood Bank, Kolkata, India, after obtaining institutional ethical committee clearance following the guidelines of the Declaration of Helsinki. pDCs were then isolated from PBMCs by performing magnetic-activated cell sorting through positive selection using CD304 (BDCA-4/Neuropilin-1) microbeads (Miltenyi Biotec). The isolated pDCs were then resuspended in complete RPMI 1640 media (Gibco, Thermo Fisher Scientific) and seeded at a density of 2×10^5 cells in 100 μL per well in a 96-well U bottom plate. Compound **42** was added to the designated wells at indicated doses and incubated for 1 h. Following incubation, the TLR9 ligand CpGA (ODN 2216,

Invivogen, USA) was added (500 nM) to each well with the compound, as well as the positive control wells. Negative control wells had only pDCs but no compound or CpGA. The cells were incubated at 37 °C and 5% CO₂ for 18 h, following which the supernatant was collected for measuring the IFN- α level using a human IFN-alpha pan ELISA kit (Mabtech) using the manufacturer's protocol.

Cytotoxicity Assay in PBMCs. Selected compounds were assessed for possible cytotoxicity in primary human PBMCs. PBMCs were isolated by Ficoll density gradient centrifugation, from buffy coats of healthy donors collected from the Tata Medical Center Blood Bank, Kolkata, India, after obtaining institutional ethical committee clearance following the guidelines of the Declaration of Helsinki. 2×10^5 PBMCs were resuspended in complete RPMI 1640 medium. Selected compounds were added to designated wells at increasing doses of 1, 5, 10, and 20 μ M and incubated overnight. The next day, the cells were washed and resuspended in 200 μ L of fresh PBS, stained with 2.5 μ g/mL PI for 1 min, and acquired immediately in a flow cytometer. 25% of DMSO was used as a positive control. The percentage of PI-positive cells indicated the proportion of dead cells.

Cytotoxicity Assay in HEK293 Cell Lines. The cytotoxicity of the compounds was also assayed in human embryonic kidney HEK293A cells. 7×10^4 HEK293A cells were seeded in a complete DMEM medium at 37 °C and 5% CO₂ and allowed to adhere for 5 h, following which the designated compounds were added at the doses of 1, 5, 10, and 20 μ M to the assigned wells and incubated overnight. The next day, the cells were washed and resuspended in fresh PBS and stained with 2.5 μ g/mL PI for 1 min and acquired immediately in a flow cytometer. 25% of DMSO was used as a positive control. The percentage of PI-positive cells indicated the proportion of dead cells.

In Vivo Inhibition Assay. The in vivo efficacy assay was performed in C57BL/6 mice after obtaining requisite approval from the CSIR-IICB Animal Ethics Committee. In brief, for the TLR9 model, 8–10 weeks old female C57BL/6 mice were taken and divided into three groups (seven to eight mice per group from two independent experiments). The first group was intraperitoneally injected with PBS, the second group was intraperitoneally injected with 25 μ g of CpGA and 25 μ g of CpGB mixtures which are bona fide TLR9 ligands, while the third group was orally administered with **42** at a dose of 10 mg/kg body weight 1 h before intraperitoneal (i.p.) injection of 25 μ g of CpGA and 25 μ g of CpGB mixtures. For the TLR7 model, 8–10 weeks old female C57BL/6 mice were taken (4–5 per group) and divided into three groups. The first group was intraperitoneally injected with PBS, the second group was intraperitoneally injected with 80 μ g of CL264 which is a TLR7-specific ligand, while the third group was orally administered with **42** at a dose of 10 mg/kg body weight 1 h before i.p. injection of 80 μ g of CL264. 18 h post-i.p. injection, the mice were sacrificed and the peritoneal fluid was collected after peritoneal wash with PBS. The i.p. cells were pelleted down to stain for evaluating pDC infiltration and performing mRNA relative expression studies, while the supernatant was stored to measure IFN- α levels in the peritoneal fluid.

Mouse IFN α ELISA. The IFN- α concentration was measured in the peritoneal fluid collected after peritoneal wash by performing sandwich ELISA. Wells were coated with 1:1000 dilution of antimouse interferon- α (IFN- α) rat monoclonal antibody (RMMA1) from PBL Assay Science and incubated at 4 °C overnight. The next morning, the plate was washed in PBS and blocked for 1 h in PBS containing 0.05% Tween 20 (PBST) and 0.1% BSA. Peritoneal fluid was added to assigned wells after PBST wash and incubated for another 2.5 h. After another round of washing with PBST, a 1:500 dilution of polyclonal rabbit IgG antibody detecting mouse IFN α was added, incubated for 1 h, and washed again, and a 1:2000 dilution of tertiary antibody (horseradish peroxidase-conjugated antirabbit IgG) was added for 1 h. To measure IFN- α levels, a TMB substrate was added after PBST wash and O.D. was measured at 455 and 655 nm (reference) spectrophotometrically once the color developed, and the reaction was stopped with 1 N HCl.

Quantitative PCR. Total RNA was isolated from peritoneal cells using RNAiso Plus, total RNA extraction reagent (Takara) following

the manufacturer's protocol, and subjected to cDNA synthesis by reverse transcription using a high-capacity cDNA Reverse Transcription Kit (Applied Biosystems). qPCR was done using BioRad SyBR Green to monitor the expression of the indicated genes: MuIRF7 (forward primer: reverse primer), MuFIT1 (forward primer: AGGCTGGAGTGTGCTGAGAT, reverse primer: TCTGGATTAAACCGGACAGC), and Mu18S (forward primer: GTTGGTTTTCGGAACTGAGG, reverse primer: TCGTTTATGGTCGGAACACTACG, housekeeping gene).

Flow Cytometry. Peritoneal cells isolated after peritoneal wash were assessed for pDC infiltration following i.p. injection with CpGA and CpGB mixtures. The cells were stained with antimouse CD45 PerCP-Cy5.5 (BD Biosciences), TCRb APC-Cyanine7 (eBioscience), Bst2 BUV737 (BD Biosciences), CD8a PE-Cyanine7 (eBioscience), and SiglecH BV421 ((BD Biosciences) and acquired using a BD Fortessa flow cytometer and analyzed using FlowJo software (version 10).

Chemical Synthesis and Methods. General Methods. All starting materials, reagents, and solvents were purchased from commercial suppliers and used without further purification. Dry solvents were either commercially purchased or dried using a standard protocol. Reactions that had a sensitivity toward moisture or oxygen were carried out under a dry nitrogen or argon atmosphere. All the TLC experiments were performed on silica gel plates (Merck silica gel 60, F₂₅₄). The spots were visualized under UV light (λ = 254 and 365 nm) or by using the appropriate stain. Compounds were purified using a Teledyne ISCO CombiflashRf system using a 230–400 mesh size silica gel. Microwave-assisted reactions were performed in CEM explorer. ¹H NMR was recorded at 300 MHz (Bruker-DPX), 400 MHz (JEOL), and 600 MHz (Bruker AVANCE) frequencies, and ¹³C NMR spectra were recorded at 75 MHz (Bruker-DPX), 100 MHz (JEOL), and 150 MHz (Bruker AVANCE) frequencies in CDCl₃ or CD₃OD or DMSO-*d*₆ using tetramethylsilane as the internal standard. The following abbreviations were used to explain multiplicities: s = singlet, d = doublet, t = triplet, q = quartet, p = pentate, m = multiplet, br. = broad. The coupling constant, *J*, was reported in Hertz unit (Hz). High-resolution mass spectroscopy, HRMS (*m/z*), was carried out using EI (JEOL-JMS 700 mass spectrometer), ESI (Q-ToF Micro mass spectrometer), and ESI (LTQ Orbitrap XL mass spectrometer). The purity of all the compounds was determined to be >95%, analyzed using an Agilent Infinity Prep. HPLC system using a BioSuite Phenyl reverse-phase column (75 \times 7.5 mm, 10 μ m particle size, 1000 Å pore size). Mobile phase A was composed of 0.1% TFA in water and mobile phase B of 10% water in acetonitrile. A Hitachi HPLC system equipped with a column Xtimate C18 (4.6 mm \times 150 mm, 5.0 μ m) was used for HPLC using a gradient elution of acetonitrile in water 0–90% for 8–20 min and a flow rate of 1 mL/min with detection at 220, 210, and 254 nm wavelengths.

General Procedure A: Phenacyl Bromide Synthesis. Appropriate acetophenone (1.0 equiv) was charged with TBATB (1.05 equiv) in dry THF under a nitrogen atmosphere at 25–30 °C for 14–16 h. Progress of the reaction was thoroughly monitored by checking TLC at 5% EtOAc in hexane (V/V). After full consumption of the starting material, the solvent was evaporated under reduced pressure and the crude was washed with cold water and extracted by Et₂O, which was then dried over Na₂SO₄. Column chromatography was performed using a hexane/EtOAc solvent system to get pure compounds with a yield of 78–82%.

General Procedure B: 4-Substituted 2-Amino Pyridine Synthesis. To a mixture of 2-amino-4-bromo pyridine (1.0 equiv) and suitable N-substituted piperazine (1.1 equiv) taken in a pressure tube, ^tBuOH was added, followed by the addition of DIPEA (2.0 equiv). Then, the reaction mixture was allowed to heat at 120 °C for 24–26 h. After completion of the reaction, confirmed by TLC, ^tBuOH was evaporated in a vacuum and the crude was washed with cold water and our desired compound was extracted with 5% MeOH/CHCl₃ (V/V). The compound was purified using a Teledyne ISCO CombiflashRf system using 230–400 mesh size silica gel and CHCl₃, MeOH, and NH₃ solution was used as eluents. A pure compound isolated with a yield of 86–88%.

General Procedure C: Imidazo[1,2-*a*]pyridine Synthesis. A mixture of appropriate phenacyl bromide (1.05 equiv) and suitable 2-amino pyridine (1.0 equiv) was dissolved in acetone and NaHCO₃ (2.0 equiv) was added to it. Resultant reaction mixture was refluxed for 4–6 h. Full consumption of both starting materials was confirmed by TLC; then, the reaction mixture was dried under reduced pressure; the crude was washed with cold water and extracted by CHCl₃, dried over Na₂SO₄, and concentrated under reduced pressure; the crude was then purified by column chromatography using a CHCl₃/MeOH solvent system. A pure compound was isolated with a yield of 85–92%.

General Procedure D: Cu-Catalyzed Aryl Amination Reaction. To a solution of appropriate aryl bromide in NMP in a pressure tube, excess ammonia was added, followed by Cu₂O, and then the resultant reaction mixture was heated at 115–120 °C for 15–16 h. TLC confirmed the consumption of the starting material, then the reaction mixture was diluted with ammonia, and the compound was extracted with CHCl₃. The organic layer was dried over Na₂SO₄, and the solvent was evaporated under vacuum to obtain the crude, which was then purified in a flash column using a CHCl₃/MeOH solvent system in a 230–400 mesh size silica gel to get the pure compounds with a yield of 62–66%.

General Procedure E: Buchwald–Hartwig Amination Reaction. To a solution of appropriate aryl bromide in toluene in a pressure tube, a suitable amine (1.5 equiv) was added followed by Na⁺OBu (4.0 equiv) to the reaction mixture and the resultant reaction mixture was purged with Ar gas for 25–30 min. Pd₂(dba)₃ (0.05 equiv) was added as a catalyst to the reaction mixture, followed by (±) BINAP as a ligand, and the resulting reaction mixture was allowed to heat at 120 °C for 8–10 h. The progress of the reaction mixture was monitored by TLC, which confirmed the consumption of the starting material, and then the reaction mixture was filtered through a Celite bed and washed with CHCl₃; the organic layer was washed with brine solution and dried over Na₂SO₄, and the solvent was evaporated under vacuum to obtain the crude, which was then purified in flash column using CHCl₃, MeOH, and NH₃ solutions as eluents in 230–400 mesh size silica gel to obtain the pure compounds with a yield of 65–75%.

General Procedure F: Synthesis of the 3-Substituted Imidazopyridine Core. To a solution of 2-amino pyridine (1.0 equiv) in dry MeOH, appropriate benzaldehyde (1.2 equiv) and *tert*-butyl isocyanide (1.02 equiv) were added at 25–30 °C. PTSA was added to it at 25–30 °C, and the reaction mixture was stirred well for 16–18 h at 25–30 °C. Completion of the reaction was confirmed by TLC; then, the reaction mixture was dried under vacuum; normal water workup was carried out, and the product was extracted with CHCl₃, which was then dried over Na₂SO₄ and concentrated under reduced pressure to obtain the crude, which was purified using a flash column using a 230–400 mesh size silica gel and CHCl₃, MeOH, and NH₃ solutions as eluents to obtain the pure compounds with a yield of 76–83%.

General Procedure G: Deprotection of the *tert*-Butyl Group. To a solution of *N*-(*tert*-butyl)-2-substituted imidazo[1,2-*a*]pyridin-3-amine (1.0 mmol) in DCE (3.0 mL), 12 N HCl (3.0 mL) was added at 0–5 °C, followed by TBAB, and the reaction mixture was stirred at 25–30 °C for 72 h. TLC confirmed the completion of the reaction, the reaction mixture was neutralized with a saturated NaHCO₃ solution, the product was extracted with CHCl₃, and the organic layer was dried over Na₂SO₄ and concentrated under reduced pressure to obtain the crude, which was purified in a flash column using a 230–400 mesh size silica gel and CHCl₃, MeOH, and NH₃ solutions as eluents to get the pure compounds with a yield of 88–91%.

General Procedure H: Deprotection of the –Boc Group. To a solution of Boc-protected substituted imidazopyridine (1.0 mmol) in 1,4-dioxane (4.0 mL), 4 M HCl in 1,4-dioxane (2.0 mL) was added at 0–5 °C and the reaction mixture was stirred at 25–30 °C for 12 h. Completion of the reaction was confirmed by TLC, and then, a NaHCO₃ solution was added at 0–5 °C to the reaction mixture to neutralize and extracted with CHCl₃, which was then dried over Na₂SO₄ and CHCl₃ was removed under vacuum and the crude was

purified in flash column using CHCl₃, MeOH, and NH₃ solutions as eluents in a 230–400 mesh size silica gel to get the pure compounds with a yield of 67–86%.

General Procedure I: Substitution Reaction. To a solution of appropriately substituted piperazine (1.0 equiv) or appropriate substituted phenols (1.0 equiv) in dry DMF, K₂CO₃ (2.0 equiv) was added at 25–30 °C and stirred at 25–30 °C for 30 min; then, appropriate alkyl halide (1.02–1.4 equiv) was added to the reaction mixture, and the resultant reaction mixture was stirred well for 8–12 h at 25–30 °C. Consumption of the starting material was confirmed by TLC; then, the reaction mixture was poured into ice-cold water, and the product was extracted by EtOAc, which was then dried over Na₂SO₄. EtOAc was removed under reduced pressure to obtain the crude, which was purified in a flash column using 230–400 mesh size silica gel to get the pure compounds with a yield of 62–86%.

General Procedure J: Amidation Reaction. To a solution of appropriately substituted piperazine (1.0 equiv) in dry DCM, appropriate acid chloride (1.2 equiv) was added to it at 0–5 °C, followed by DIPEA (3.0 equiv) to the reaction mixture, and then the resultant reaction mixture was stirred well at 25–30 °C for 2–3 h. Progress of the reaction was thoroughly monitored through TLC, and after completion of the reaction, the reaction mixture was poured into ice-cold water and the product was extracted by EtOAc, which was then dried over Na₂SO₄. The solvent was evaporated in a rotary evaporator under reduced pressure to obtain the crude which was purified in a flash column using 230–400 mesh size silica gel and CHCl₃, MeOH, and NH₃ solution as eluents to get the pure compounds with a yield of 76–81%.

General Procedure K: Deprotection of the Benzyl Group. Pd(OH)₂ was added to a solution of the benzyl-protected compound in methanol, and the reaction mixture was allowed to stir at 25–30 °C for 12–14 h under the constant pressure of H₂ gas. Progress of the reaction was monitored through TLC. After completion of the reaction, it was filtered through a Celite bed and washed with 10% MeOH in CHCl₃ (V/V). Solvents were removed under a vacuum. The product was purified in a flash column using CHCl₃, MeOH, and NH₃ solution as eluents and 230–400 mesh size silica gel as stationary phase to get the pure compounds with a yield of 53–78%.

General Procedure L: Groebke–Blackburn–Bienaymé Reaction. Compound 56 (1.0 equiv) and compound 18 (1.0 equiv) were taken in a microwave vial. To this mixture, appropriate isocyanide (1.05 equiv) was added, followed by the addition of NH₄Cl (1.0 equiv) to the reaction mixture. The microwave vial was then sealed, and the reaction was allowed to proceed under microwave conditions, where we used 100 W power to reach the temperature which was set at 130 °C. The reaction proceeded under solvent-free conditions, and it took around 60 min to complete. Then, the compound was extracted with CHCl₃; flash chromatography was done to get the purified product using a 230–400 mesh size silica gel, and CHCl₃, MeOH, and NH₃ solutions were used as eluents to get the pure compounds with a yield of 60–62%.

General Procedure M: Mannich Reaction. To a solution of HCHO (1.15 equiv) in glacial AcOH, morpholine (1.2 equiv) or pyrrolidine (1.2 equiv) was added at 25–30 °C and stirred at 25–30 °C for 1 h and then appropriate substituted imidazopyridine (1.0 equiv) was added to the reaction mixture at 25–30 °C and stirred for 14–16 h at 25–30 °C. Completion of the reaction was confirmed by TLC, and then the reaction was poured in ice-cold water and neutralized with a saturated solution of NaHCO₃ and extracted with CHCl₃, which was dried over Na₂SO₄ and concentrated under reduced pressure to obtain the crude which was purified using a C18 column; water and ACN were used as eluents for the reverse-phase column to get the pure compounds with a yield of 51–56%.

2-Bromo-1-(2,4-dimethoxyphenyl)ethenone (2). TBATB (14.05 g, 29.13 mmol) was added to a solution of compound 1 (5.0 g, 27.75 mmol) in dry THF (30.0 mL), and the reaction was performed according to general procedure A. Pure compound 2 appeared as a brown gummy solid (82%). ¹H NMR (600 MHz, CDCl₃): δ 7.91 (d, *J* = 9.0 Hz, 1H), 6.57 (dd, *J* = 9.0 Hz, 2.4 Hz, 1H), 6.46 (d, *J* = 2.4 Hz, 1H), 4.58 (s, 2H), 3.93 (s, 3H), 3.87 (s, 3H). ¹³C NMR (75 MHz,

CDCl_3): δ 190.3, 165.5, 161.0, 133.9, 117.9, 105.9, 98.3, 55.8, 55.6, 25.7.

2-(4-Methoxyphenyl)imidazo[1,2-*a*]pyridine (7). Compound 5 (1.28 g, 5.58 mmol) was added to a solution of compound 3 (0.50 g, 5.31 mmol) in acetone (5.0 mL) followed by the addition of NaHCO_3 (0.89 g, 10.63 mmol), and the reaction was performed according to general procedure C. Pure compound 7 appeared as a faint yellowish-white solid (92%, mp 132 °C). ^1H NMR (400 MHz, CDCl_3): δ 8.06 (d, J = 6.7 Hz, 1H), 7.89–7.86 (m, 2H), 7.74 (s, 1H), 7.60 (d, J = 9.1 Hz, 1H), 7.15–7.11 (m, 1H), 6.98–6.94 (m, 2H), 6.73 (dt, J = 6.7 Hz, 0.9 Hz, 1H), 3.84 (s, 3H). ^{13}C NMR (100 MHz, CDCl_3): δ 159.7, 145.8, 145.7, 127.4, 126.6, 125.5, 124.5, 117.4, 114.2, 112.3, 107.3, 55.4. HRMS (ESI) m/z ($M + \text{H}$) $^+$ calcd for $\text{C}_{14}\text{H}_{13}\text{N}_2\text{O}$, 225.1028; found, 225.1030. HPLC purity: 99.22%.

7-Bromo-2-phenylimidazo[1,2-*a*]pyridine (8). To a solution of compound 4 (0.5 g, 2.89 mmol) in acetone (5.0 mL), compound 6 (0.6 g, 3.03 mmol) and NaHCO_3 (0.49 g, 5.78 mmol) were added and the reaction was performed according to general procedure C. Pure compound 8 appeared as a white crystalline solid (85%, mp 192 °C). ^1H NMR (400 MHz, CDCl_3): δ 7.95–7.90 (m, 3H), 7.81–7.79 (m, 2H), 7.45–7.41 (m, 2H), 7.36–7.32 (m, 1H), 6.87–6.84 (m, 1H). ^{13}C NMR (100 MHz, CDCl_3): δ 146.7, 145.8, 133.3, 128.9, 128.4, 126.2, 125.8, 119.8, 118.3, 116.4, 108.4. HRMS (ESI) m/z ($M + \text{H}$) $^+$ calcd for $\text{C}_{13}\text{H}_{10}\text{BrN}_2$, 273.0027; found, 273.0042. HPLC purity: 99.52%.

7-Bromo-2-(4-methoxyphenyl)imidazo[1,2-*a*]pyridine (9). Compound 5 (1.39 g, 6.07 mmol) and NaHCO_3 (0.7 g, 11.56 mmol) were added to a solution of compound 4 (1.0 g, 5.78 mmol) in acetone (10.0 mL), and the reaction was performed according to general procedure C. Pure compound 9 appeared as a very off-white solid (88%, mp 210 °C). ^1H NMR (400 MHz, CDCl_3): δ 7.93 (dd, J = 7.1 Hz, 0.7 Hz, 1H), 7.86–7.82 (m, 2H), 7.79–7.76 (m, 1H), 7.72 (d, J = 0.6 Hz, 1H), 6.98–6.94 (m, 2H), 6.84 (dd, J = 7.1, 1.9 Hz, 1H), 3.85 (s, 3H). ^{13}C NMR (100 MHz, CDCl_3): δ 159.9, 146.7, 145.8, 127.5, 126.0, 125.7, 119.6, 118.1, 116.2, 114.3, 107.5, 55.4. HRMS (ESI) m/z ($M + \text{H}$) $^+$ calcd for $\text{C}_{14}\text{H}_{12}\text{BrN}_2\text{O}$, 303.0133; found, 303.0125. HPLC purity: 99.35%.

7-Bromo-2-(2,4-dimethoxyphenyl)imidazo[1,2-*a*]pyridine (10). To a solution of compound 4 (1.0 g, 5.78 mmol) in acetone (10.0 mL), compound 2 (1.57 g, 6.07 mmol) and NaHCO_3 (0.97 g, 11.56 mmol) were added, and the reaction was performed according to general procedure C. Pure compound 10 appeared as a faint yellowish solid (86%, mp >250 °C). ^1H NMR (400 MHz, $\text{CDCl}_3 + 1$ drop CD_3OD): δ 8.06 (d, J = 8.4 Hz, 1H), 7.98 (s, 1H), 7.93 (d, J = 7.2 Hz, 1H), 7.70 (s, 1H), 6.79 (dd, J = 7.2 Hz, 2.0 Hz, 1H), 6.57 (dd, J = 8.8 Hz, 2.4 Hz, 1H), 6.47 (d, J = 2.4 Hz, 1H), 3.87 (s, 3H), 3.78 (s, 3H). ^{13}C NMR (100 MHz, $\text{CDCl}_3 + 1$ drop CD_3OD): δ 161.0, 158.0, 144.1, 141.2, 129.4, 125.9, 118.9, 118.3, 116.3, 114.1, 111.6, 105.1, 98.6, 55.4, 55.4. HRMS (ESI) m/z ($M + \text{H}$) $^+$ calcd for $\text{C}_{15}\text{H}_{14}\text{BrN}_2\text{O}_2$, 333.0239; found, ($M + \text{H}$) $^+$ 333.0228. HPLC purity: 99.02%.

2-(2,4-Dimethoxyphenyl)imidazo[1,2-*a*]pyridine (11). Compound 2 (0.58 g, 2.23 mmol) was added to a mixture of compound 3 (0.2 g, 2.15 mmol) in acetone (5.0 mL) and NaHCO_3 (0.36 g, 4.25 mmol), and the reaction was performed according to general procedure C. Pure compound 11 appeared as a brown solid (90%, mp 228 °C). ^1H NMR (600 MHz, $\text{DMSO}-d_6$): δ 8.86 (d, J = 5.5 Hz, 1H), 8.63 (s, 1H), 7.90 (t, J = 8.3 Hz, 2H), 7.85 (t, J = 7.6 Hz, 1H), 7.43 (t, J = 6.9 Hz, 1H), 6.79 (s, 2H), 4.00 (s, 3H), 3.85 (s, 3H). ^{13}C NMR (150 MHz, $\text{DMSO}-d_6$): δ 162.5, 158.5, 139.8, 129.2, 129.0, 117.0, 112.6, 112.4, 106.7, 99.5, 56.5, 56.1. HRMS (ESI) m/z ($M + \text{H}$) $^+$ calcd for $\text{C}_{15}\text{H}_{15}\text{N}_2\text{O}_2$, 255.1134; found, 255.1142. HPLC purity: 99.59%.

2-(4-Methoxyphenyl)imidazo[1,2-*a*]pyridin-7-amine (12). In a pressure tube, compound 9 (0.1 g, 0.33 mmol), NMP (2.0 mL), and NH_4OH (0.7 mL) were taken and Cu_2O (0.01 g, 0.07 mmol) was added, and the reaction was performed according to general procedure D. Pure compound 12 appeared as a greenish-yellow solid (62%). ^1H NMR (400 MHz, CD_3OD): δ 8.01 (d, J = 7.2 Hz, 1H), 7.73 (d, J = 8.3 Hz, 2H), 7.68 (s, 1H), 6.95 (d, J = 8.8 Hz, 2H),

6.52 (s, 1H), 6.43 (dd, J = 7.2 Hz, 2.1 Hz, 1H), 3.82 (s, 3H). ^{13}C NMR (100 MHz, CD_3OD): δ 159.5, 148.1, 147.7, 143.2, 126.6, 126.4, 113.7, 106.7, 105.6, 92.1, 70.1, 54.4. HRMS (ESI) m/z ($M + \text{H}$) $^+$ calcd for $\text{C}_{14}\text{H}_{14}\text{N}_3\text{O}$, 240.1137; found, 240.1137. HPLC purity: 95.86%.

2-(2,4-Dimethoxyphenyl)imidazo[1,2-*a*]pyridin-7-amine (13). In a pressure tube, compound 10 (0.1 g, 0.3 mmol), NMP (2.0 mL), NH_4OH (0.65 mL) was taken and Cu_2O (0.009 g, 0.06 mmol) was added, and the reaction was performed according to general procedure D. Pure compound 13 appeared as a brown solid (66%, mp 236 °C). ^1H NMR (600 MHz, $\text{DMSO}-d_6$): δ 8.19 (d, J = 6.9 Hz, 1H), 7.99 (d, J = 8.3 Hz, 1H), 7.92 (s, 1H), 6.65 (s, 1H), 6.63 (d, J = 8.5 Hz, 1H), 6.44 (d, J = 7.2 Hz, 1H), 6.41 (s, 1H), 6.01 (s, 2H), 3.92 (s, 3H), 3.80 (s, 3H). ^{13}C NMR (150 MHz, $\text{DMSO}-d_6$): δ 160.4, 157.8, 128.7, 127.7, 114.0, 109.7, 107.1, 105.7, 100.0, 98.9, 90.5, 56.0, 55.7. HRMS (ESI) m/z ($M + \text{H}$) $^+$ calcd for $\text{C}_{15}\text{H}_{16}\text{N}_3\text{O}_2$, 270.1243; found, 270.1248. HPLC purity: 95.31%.

2-(4-Methoxyphenyl)-*N,N*-dimethylimidazo[1,2-*a*]pyridin-7-amine (14). Compound 9 (0.15 g, 0.50 mmol), *N,N*-dimethyl amine (2 M in THF) (0.32 mL, 0.64 mmol), and Na^tOBu (0.19 g, 1.98 mmol) were taken in a pressure tube and toluene (2.0 mL) was added, then the reaction mixture was purged with N_2 gas for 25 min, then $\text{Pd}_2(\text{dba})_3$ (0.023 g, 0.025 mmol) and (\pm) BINAP (0.031 g, 0.05 mmol) were added, and the reaction was performed according to general procedure E. Pure compound 14 appeared as a dark-brown solid (70%, mp 170 °C). ^1H NMR (600 MHz, CDCl_3): δ 7.86 (s, 1H), 7.84 (d, J = 2.4 Hz, 2H), 7.50 (s, 1H), 6.94 (d, J = 9.0 Hz, 2H), 6.62 (d, J = 1.8 Hz, 1H), 6.47 (dd, J = 7.8 Hz, 2.4 Hz, 1H), 3.84 (s, 3H), 3.01 (s, 6H). ^{13}C NMR (150 MHz, CDCl_3): δ 159.1, 148.0, 126.9, 125.3, 113.9, 104.4, 103.9, 93.1, 55.2, 40.2. HRMS (ESI) m/z ($M + \text{H}$) $^+$ calcd for $\text{C}_{16}\text{H}_{18}\text{N}_3\text{O}$, 268.1450; found, 268.1451. HPLC purity: 99.76%.

2-(2,4-Dimethoxyphenyl)-*N,N*-dimethylimidazo[1,2-*a*]pyridin-7-amine (15). *N,N*-dimethyl amine (2 M in THF) (0.29 mL, 0.59 mmol), compound 10 (0.15 g, 0.45 mmol), and Na^tOBu (0.17 g, 1.8 mmol) were taken in a pressure tube and toluene (2.0 mL) was added, then the reaction mixture was purged with N_2 gas for 25 min, $\text{Pd}_2(\text{dba})_3$ (0.021 g, 0.023 mmol) and (\pm) BINAP (0.028 g, 0.045 mmol) were added, and the reaction was performed according to general procedure E. Pure compound 15 appeared as yellow gummy solid (71%). ^1H NMR (600 MHz, $\text{CDCl}_3 + \text{CD}_3\text{OD}$): δ 8.02 (d, J = 7.8 Hz, 1H), 7.69–7.68 (m, 2H), 6.66 (s, 1H), 6.64 (d, J = 7.8 Hz, 1H), 6.54 (dd, J = 8.4 Hz, 1.2 Hz, 1H), 6.45 (s, 1H), 3.86 (s, 3H), 3.75 (s, 3H), 3.02 (s, 6H). ^{13}C NMR (150 MHz, $\text{CDCl}_3 + \text{CD}_3\text{OD}$): δ 161.9, 157.8, 151.6, 141.9, 130.5, 128.2, 127.3, 108.6, 108.0, 105.8, 105.4, 98.7, 86.3, 55.5, 55.4, 39.9. HRMS (ESI) m/z ($M + \text{H}$) $^+$ calcd for $\text{C}_{17}\text{H}_{20}\text{N}_3\text{O}_2$, 298.1556; found 298.1555. HPLC purity: 96.99%.

***N,N*-Dimethyl-2-phenylimidazo[1,2-*a*]pyridin-7-amine (16).** Compound 8 (0.15 g, 0.55 mmol), Na^tOBu (0.21 g, 2.20 mmol), and *N,N*-dimethyl amine (2 M in THF) (0.36 mL, 0.71 mmol) were taken in a pressure tube and toluene (2.0 mL) was added, then the reaction mixture was purged with N_2 gas for 25 min, $\text{Pd}_2(\text{dba})_3$ (0.025 g, 0.028 mmol) and (\pm) BINAP (0.034 g, 0.055 mmol) were added, and the reaction was performed according to general procedure E. Pure compound 16 appeared as a deep-brown gummy solid (65%). ^1H NMR (300 MHz, CDCl_3): δ 7.90 (d, J = 7.2 Hz, 2H), 7.81 (d, J = 7.5 Hz, 1H), 7.55 (s, 1H), 7.38 (t, J = 7.8 Hz, 3H), 6.59 (d, J = 2.1 Hz, 1H), 6.43 (dd, J = 7.8 Hz, 2.4 Hz, 1H), 2.98 (s, 6H). ^{13}C NMR (150 MHz, CDCl_3): δ 148.6, 147.1, 132.4, 131.9, 128.6, 127.7, 125.7, 105.6, 104.4, 40.2. (ESI) m/z ($M + \text{H}$) $^+$ calcd for $\text{C}_{15}\text{H}_{16}\text{N}_3$, 238.1344; found, 238.1448. HPLC purity: 100.0%.

***N*-(*tert*-Butyl)-2-(4-methoxyphenyl)imidazo[1,2-*a*]pyridin-3-amine (19).** To a mixture of compound 3 (0.4 g, 4.25 mmol), compound 17 (0.62 mL, 5.1 mmol), and *tert*-butyl isocyanide (0.49 mL, 4.34 mmol), PTSA (0.16 g, 0.85 mmol) was added, and the reaction was performed according to general procedure F. Pure compound 19 appeared as a white solid (83%). ^1H NMR (400 MHz, CDCl_3): δ 8.19 (d, J = 5.7 Hz, 1H), 7.84 (d, J = 8.9 Hz, 2H), 7.50 (d, J = 9.0 Hz, 1H), 7.12–7.06 (m, 1H), 6.96 (d, J = 8.9 Hz, 2H), 6.74 (td, J = 6.7, 1.1 Hz, 1H), 3.84 (s, 3H), 3.04 (s, 1H), 1.03 (s, 9H). ^{13}C

NMR (100 MHz, CDCl₃) 159.0, 142.0, 139.6, 129.4, 128.0, 123.8, 123.4, 123.0, 117.2, 113.8, 111.2, 56.4, 55.3, 30.4. HRMS (ESI) *m/z* (M + H)⁺ calcd for C₁₈H₂₂N₃O, 296.1763; found, 296.1763.

N-(tert-Butyl)-2-(2,4-dimethoxyphenyl)imidazo[1,2-*a*]pyridin-3-amine (20). To a mixture of compound 3 (0.4 g, 4.25 mmol), compound 18 (0.85 g, 5.1 mmol), and *tert*-butyl isocyanide (0.49 mL, 4.34 mmol), PTSA (0.16 g, 0.85 mmol) was added, and the reaction was performed according to general procedure F. Pure compound 20 appeared as a white solid (76%). ¹H NMR (400 MHz, CDCl₃): δ 8.25 (dt, *J* = 6.9, 1.1 Hz, 1H), 7.74 (d, *J* = 8.5 Hz, 1H), 7.49 (dt, *J* = 9.0, 1.0 Hz, 1H), 7.06 (ddd, *J* = 9.0, 6.7, 1.3 Hz, 1H), 6.71 (td, *J* = 6.8, 1.0 Hz, 1H), 6.64 (dd, *J* = 8.5, 2.4 Hz, 1H), 6.53 (d, *J* = 2.4 Hz, 1H), 3.84 (s, 3H), 3.83 (s, 3H), 3.69 (br s, 1H), 0.93 (s, 9H). ¹³C NMR (100 MHz, CDCl₃) 160.7, 157.0, 142.3, 136.2, 132.4, 125.5, 123.5, 123.3, 118.0, 117.0, 110.9, 105.7, 99.2, 55.9, 55.9, 55.5, 30.0. HRMS (ESI) *m/z* (M + H)⁺ calcd for C₁₉H₂₄N₃O₂, 326.1869; found, 326.1873.

2-(4-Methoxyphenyl)imidazo[1,2-*a*]pyridin-3-amine (21). To a solution of compound 19 (0.15 g, 0.51 mmol) in DCE (2.0 mL), 12 N HCl (2.0 mL) and TBAB (0.008 g, 0.025 mmol) were added following general procedure G. Pure compound 21 appeared as a brownish-yellow solid (88%, mp 143 °C). ¹H NMR (400 MHz, DMSO-*d*₆): δ 8.17 (d, *J* = 6.9 Hz, 1H), 7.95 (d, *J* = 8.9 Hz, 2H), 7.35 (d, *J* = 9.0 Hz, 1H), 7.02–6.98 (m, 1H), 6.95 (d, *J* = 9.0 Hz, 2H), 6.78 (t, *J* = 6.7 Hz, 1H), 4.93 (s, 2H), 3.75 (s, 3H). ¹³C NMR (100 MHz, DMSO-*d*₆) 158.3, 139.3, 128.7, 128.2, 128.0, 125.7, 122.9, 122.3, 116.7, 114.3, 111.3, 55.6. HRMS (ESI) *m/z* (M + H)⁺ calcd for C₁₄H₁₄N₃O, 240.1137; found, 240.1136. HPLC purity: 97.70%.

2-(2,4-Dimethoxyphenyl)imidazo[1,2-*a*]pyridin-3-amine (22). TBAB (0.007 g, 0.023 mmol) and 12 N HCl (2.0 mL) were added to a solution of compound 20 (0.15 g, 0.46 mmol) in DCE (2.0 mL) following general procedure G. Pure compound 22 appeared as a reddish-orange solid (91%, mp 149 °C). ¹H NMR (400 MHz, DMSO-*d*₆): δ 8.11 (d, *J* = 6.8 Hz, 1H), 7.55 (d, *J* = 8.4 Hz, 1H), 7.38 (d, *J* = 9.0 Hz, 1H), 7.02 (t, *J* = 6.8 Hz, 1H), 6.82 (t, *J* = 6.7 Hz, 1H), 6.67–6.63 (m, 2H), 4.76 (br s, 2H), 3.86 (s, 3H), 3.81 (s, 3H). ¹³C NMR (100 MHz, DMSO-*d*₆) 160.4, 157.1, 139.1, 132.1, 127.4, 125.0, 122.6, 121.6, 117.0, 116.7, 111.2, 106.2, 99.1, 56.2, 55.8. HRMS (ESI) *m/z* (M + H)⁺ calcd for C₁₅H₁₆N₃O₂, 270.1243; found, 270.1242. HPLC purity: 98.07%.

2-(4-Methoxyphenyl)-N-(3-morpholinopropyl)imidazo[1,2-*a*]pyridin-7-amine (23). Pd₂(dba)₃ (0.023 g, 0.025 mmol) and (±) BINAP (0.031 g, 0.05 mmol) were added to a N₂ gas-purged reaction mixture of compound 9 (0.15 g, 0.50 mmol), 3-morpholinopropan-1-amine (0.094 mL, 0.64 mmol), and Na^tOBu (0.19 g, 1.32 mmol) in toluene (2.0 mL) following general procedure E. Pure compound 23 appeared as an off-white solid (73%, mp 125 °C). ¹H NMR (400 MHz, CDCl₃): δ 7.82 (d, *J* = 8.8 Hz, 2H), 7.75 (d, *J* = 7.2 Hz, 1H), 7.47 (s, 1H), 6.93 (d, *J* = 8.8 Hz, 2H), 6.47 (d, *J* = 1.8 Hz, 1H), 6.15 (dd, *J* = 7.2, 2.2 Hz, 1H), 5.27 (s, 1H), 3.83 (s, 3H), 3.75–3.72 (m, 4H), 3.22 (t, *J* = 5.5 Hz, 2H), 2.52–2.48z (m, 6H), 1.83 (p, *J* = 6.3 Hz, 2H). ¹³C NMR (100 MHz, CDCl₃): δ 159.2, 148.3, 146.2, 144.5, 127.1, 127.0, 125.5, 114.1, 106.4, 105.1, 91.1, 67.2, 57.9, 55.4, 53.8, 43.3, 24.6. HRMS (ESI) *m/z* (M + H)⁺ calcd for C₂₁H₂₇N₄O₂, 367.2134; found, 367.2143. HPLC purity: 100.0%.

2-(2,4-Dimethoxyphenyl)-N-(3-morpholinopropyl)imidazo[1,2-*a*]pyridin-7-amine (24). Compound 24 was synthesized following general procedure E, where (±) BINAP (0.028 g, 0.045 mmol) and Pd₂(dba)₃ (0.021 g, 0.023 mmol) were added to a mixture of compound 10 (0.15 g, 0.45 mmol), 3-morpholinopropan-1-amine (0.086 mL, 0.59 mmol), and Na^tOBu (0.173 g, 1.8 mmol) in toluene (2.0 mL). Pure compound 24 appeared as a light-brown solid (70%, mp 153 °C). ¹H NMR (600 MHz, CDCl₃): δ 8.24 (d, *J* = 8.6 Hz, 1H), 7.76 (d, *J* = 7.0 Hz, 1H), 7.74 (s, 1H), 6.62–6.61 (m, 1H), 6.58 (s, 1H), 6.52 (d, *J* = 2.0 Hz, 1H), 6.29 (d, *J* = 6.1 Hz, 1H), 3.93 (s, 3H), 3.83 (s, 3H), 3.73 (br s, 4H), 3.21 (s, 2H), 2.51 (t, *J* = 6.2 Hz, 2H), 2.48 (br s, 4H), 1.82 (t, *J* = 6.1 Hz, 2H). ¹³C NMR (150 MHz, CDCl₃): δ 160.6, 157.8, 129.4, 125.9, 109.2, 107.1, 105.0, 100.1, 98.8, 89.3, 67.2, 57.8, 55.6, 53.8, 49.6, 43.3, 27.1. HRMS (ESI) *m/z* (M + H)⁺ calcd for C₂₂H₂₉N₄O₃, 397.2240; found, 397.2257. HPLC purity: 99.59%.

2-(2,4-Dimethoxyphenyl)-N-(2-morpholinoethyl)imidazo[1,2-*a*]pyridin-7-amine (25). To a mixture of compound 10 (0.15 g, 0.45 mmol), 2-morpholinoethanamine (0.076 mL, 0.59 mmol), and Na^tOBu (0.173 g, 1.8 mmol) in toluene (2.0 mL), Pd₂(dba)₃ (0.021 g, 0.023 mmol) and (±) BINAP (0.028 g, 0.045 mmol) were added following general procedure E. Pure compound 25 appeared as a greenish-brown solid (72%, mp 137 °C). ¹H NMR (400 MHz, CDCl₃): δ 8.26 (d, *J* = 8.6 Hz, 1H), 7.99 (d, *J* = 4.8 Hz, 1H), 7.79 (s, 1H), 6.62 (dd, *J* = 8.6, 2.3 Hz, 1H), 6.54 (s, 2H), 6.25 (dd, *J* = 7.2, 2.0 Hz, 1H), 3.94 (s, 3H), 3.84 (s, 3H), 3.73–3.71 (m, 4H), 3.20–3.19 (m, 2H), 2.67–2.64 (m, 2H), 2.49–2.47 (m, 4H). ¹³C NMR (100 MHz, CDCl₃): δ 160.2, 157.7, 146.4, 146.3, 145.3, 129.3, 125.7, 109.3, 106.4, 104.8, 98.7, 90.8, 67.0, 56.6, 55.5, 55.5, 53.4, 39.4. HRMS (ESI) *m/z* (M + H)⁺ calcd for C₂₁H₂₇N₄O₃, 383.2083; found, 383.2088. HPLC purity: 99.95%.

2-(2,4-Dimethoxyphenyl)-N-(3-(pyrrolidin-1-yl)propyl)imidazo[1,2-*a*]pyridine-7-amine (26). To a mixture of compound 10 (0.15 g, 0.45 mmol), 3-(pyrrolidin-1-yl)propan-1-amine (0.083 mL, 0.59 mmol), and Na^tOBu (0.173 g, 1.8 mmol) in toluene (2.0 mL), Pd₂(dba)₃ (0.021 g, 0.023 mmol) and (±) BINAP (0.028 g, 0.045 mmol) were added following general procedure E. Pure compound 26 appeared as a light-brown solid (75%, mp 116 °C). ¹H NMR (600 MHz, CDCl₃): δ 8.26 (d, *J* = 8.5 Hz, 1H), 7.79 (s, 1H), 7.75 (d, *J* = 7.1 Hz, 1H), 6.61 (dd, *J* = 8.5, 2.3 Hz, 1H), 6.54 (d, *J* = 2.4 Hz, 1H), 6.45 (s, 1H), 6.13 (dd, *J* = 7.3, 2.3 Hz, 1H), 3.94 (s, 3H), 3.85 (s, 3H), 3.22 (t, *J* = 6.3 Hz, 2H), 2.65 (t, *J* = 6.6 Hz, 2H), 2.57 (br s, 4H), 1.87 (p, *J* = 6.4 Hz, 2H), 1.81 (br s, 4H). ¹³C NMR (150 MHz, CDCl₃): δ 159.4, 157.1, 146.5, 145.7, 139.2, 128.7, 125.0, 115.5, 108.7, 105.7, 104.2, 98.1, 90.0, 55.0, 54.9, 54.5, 53.7, 42.6, 26.4, 23.0. HRMS (ESI) *m/z* (M + H)⁺ calcd for C₂₂H₂₉N₄O₂, 381.2291; found, 381.2285. HPLC purity 100.0%.

N-(3-(1H-Imidazole-1-yl)propyl)-2-(2,4-dimethoxyphenyl)imidazo[1,2-*a*]pyridin-7-amine (27). Pd₂(dba)₃ (0.021 g, 0.023 mmol) and (±) BINAP (0.028 g, 0.045 mmol) were added to a mixture of compound 10 (0.15 g, 0.45 mmol), 3-(1H-imidazole-1-yl)propan-1-amine (0.070 mL, 0.59 mmol), and Na^tOBu (0.173 g, 1.8 mmol) in toluene (2.0 mL) following general procedure E. Pure compound 27 appeared as a brownish-green sticky solid (72%). ¹H NMR (400 MHz, CDCl₃): δ 8.22 (d, *J* = 8.6 Hz, 1H), 7.79 (s, 1H), 7.76 (d, *J* = 7.0 Hz, 1H), 7.47 (s, 1H), 7.05 (s, 1H), 6.90 (s, 1H), 6.60 (dd, *J* = 8.5, 2.0 Hz, 1H), 6.54 (s, 1H), 6.46 (s, 1H), 6.18 (d, *J* = 6.4 Hz, 1H), 4.38 (s, 1H), 4.04 (t, *J* = 6.4 Hz, 2H), 3.93 (s, 3H), 3.84 (s, 3H), 3.12 (br s, 2H), 2.11–2.06 (m, 2H). ¹³C NMR (100 MHz, CDCl₃): δ 160.2, 157.7, 146.5, 145.7, 139.7, 129.2, 125.9, 118.9, 115.6, 109.5, 106.1, 104.8, 98.7, 91.0, 55.5, 55.5, 44.7, 40.5, 30.0. HRMS (ESI) *m/z* (M + H)⁺ calcd for C₂₁H₂₄N₅O₂, 378.1930; found, 378.1936. HPLC purity: 99.96%.

tert-Butyl 4-(2-Aminopyridin-4-yl)piperazine-1-carboxylate (28). DIPEA (10.06 mL, 57.8 mmol) was added to a mixture of compound 4 (5.0 g, 28.9 mmol), 1-Boc-piperazine (5.92 g, 31.79 mmol), and ⁿBuOH following general procedure B. Compound 28 appeared as a light-yellow solid (86%, mp 135 °C). ¹H NMR (400 MHz, CDCl₃): δ 7.79 (d, *J* = 6.1 Hz, 1H), 6.16 (dd, *J* = 6.2, 2.3 Hz, 1H), 5.82 (d, *J* = 2.2 Hz, 1H), 3.53–3.50 (m, 4H), 3.25–3.22 (m, 4H), 1.46 (s, 9H). ¹³C NMR (100 MHz, CDCl₃): δ 159.7, 156.9, 154.7, 148.6, 101.7, 91.7, 80.2, 46.3, 28.5. HRMS (ESI) *m/z* (M + H)⁺ calcd for C₁₄H₂₃N₄O₂, 279.1821; found, 279.1810.

1-(2-(Benzyloxy)-4-methoxyphenyl)-2-bromoethanone (30). To a solution of compound 29 (5.0 g, 19.51 mmol) in dry THF (30.0 mL), TBATB (9.88 g, 20.48 mmol) was added, and the reaction was performed according to general procedure A. Pure compound 30 appeared as purple gummy solid (78%). ¹H NMR (300 MHz, CDCl₃): δ 8.09–8.05 (m, 1H), 7.62–7.55 (m, 5H), 6.77–6.67 (m, 2H), 5.29 (s, 2H), 4.65 (s, 2H), 3.98 (s, 3H). ¹³C NMR (150 MHz, CDCl₃): δ 190.2, 165.1, 159.8, 135.3, 133.7, 128.7, 128.4, 127.7, 117.9, 106.1, 99.2, 70.9, 55.5, 37.7.

tert-Butyl 4-(2-(4-Methoxyphenyl)imidazo[1,2-*a*]pyridin-7-yl)piperazine-1-carboxylate (31). To a solution of compound 28 (2.0 g, 7.19 mmol) in acetone (20.0 mL), compound 5 (1.73 g, 7.54 mmol) and NaHCO₃ (1.21 g, 14.37 mmol) were added, and the

reaction was performed according to general procedure C. Pure compound **31** appeared as a white crystalline solid (85%, mp 192 °C). ¹H NMR (400 MHz, CHCl₃): δ 7.99 (d, *J* = 7.6 Hz, 1H), 7.83 (d, *J* = 8.8 Hz, 2H), 7.54 (s, 1H), 7.05 (d, *J* = 2.1 Hz, 1H), 6.93 (d, *J* = 8.9 Hz, 2H), 6.65 (dd, *J* = 7.6, 2.4 Hz, 1H), 3.83 (s, 3H), 3.60–3.57 (m, 4H), 3.31–3.29 (m, 4H), 1.49 (s, 9H). ¹³C NMR (100 MHz, CDCl₃): δ 160.2, 154.6, 150.0, 145.2, 127.4, 126.5, 114.5, 106.9, 105.5, 80.5, 55.4, 28.5. HRMS (ESI) *m/z* (*M* + *H*)⁺ calcd for C₂₃H₂₉N₄O₃, 409.2240; found, 409.2230.

tert-Butyl 4-(2-(2,4-dimethoxyphenyl)imidazo[1,2-*a*]pyridine-7-yl)piperazine-1-carboxylate (**32**). To a solution of compound **28** (2.0 g, 7.19 mmol) in acetone (20.0 mL), compound **2** (1.95 g, 7.54 mmol) and NaHCO₃ (1.21 g, 14.37 mmol) were added, and the reaction was performed according to general procedure C. Pure compound **32** appeared as a faint greenish solid (89%). ¹H NMR (400 MHz, CHCl₃): δ 8.26 (d, *J* = 8.6 Hz, 1H), 7.89 (d, *J* = 7.5 Hz, 1H), 7.86 (s, 1H), 6.83 (d, *J* = 1.9 Hz, 1H), 6.62 (dd, *J* = 8.7, 2.3 Hz, 1H), 6.54 (d, *J* = 2.3 Hz, 1H), 6.51 (dd, *J* = 7.6, 2.4 Hz, 1H), 3.94 (s, 3H), 3.84 (s, 3H), 3.59–3.57 (m, 4H), 3.18–3.16 (m, 4H), 1.48 (s, 9H). ¹³C NMR (100 MHz, CHCl₃): δ 160.3, 157.8, 154.7, 148.6, 145.9, 140.6, 129.4, 125.7, 115.6, 109.7, 106.4, 104.9, 98.7, 97.7, 80.2, 55.5, 48.7, 28.5. HRMS (ESI) *m/z* (*M* + *H*)⁺ calcd for C₂₄H₃₁N₄O₄, 439.2345; found, 439.2340.

tert-Butyl 4-(2-(2-(Benzyloxy)-4-methoxyphenyl)imidazo[1,2-*a*]pyridin-7-yl)piperazine-1-carboxylate (**33**). To a solution of compound **28** (2.5 g, 8.98 mmol) in acetone (25.0 mL), compound **30** (3.16 g, 9.43 mmol) and NaHCO₃ (1.51 g, 17.96 mmol) were added, and the reaction was performed according to general procedure C. Pure compound **33** appeared as a faint yellowish solid (88%). ¹H NMR (400 MHz, CD₃OD): δ ¹H NMR (400 MHz, CD₃OD): δ 8.27 (d, *J* = 7.7 Hz, 1H), 7.68 (d, *J* = 8.6 Hz, 1H), 7.50–7.34 (m, 6H), 7.10 (dd, *J* = 7.7, 2.2 Hz, 1H), 6.76 (t, *J* = 2.3 Hz, 2H), 6.69 (dd, *J* = 8.7, 2.2 Hz, 1H), 5.33 (s, 2H), 3.82 (s, 3H), 3.62–3.61 (m, 4H), 3.53–3.51 (m, 4H), 1.50 (s, 9H). ¹³C NMR (100 MHz, CD₃OD): δ 162.2, 157.2, 155.0, 152.3, 136.6, 128.5, 128.5, 128.5, 128.3, 128.2, 128.1, 128.0, 127.5, 109.8, 107.1, 106.1, 100.2, 88.3, 80.4, 70.5, 54.7, 27.3. HRMS (ESI) *m/z* (*M* + *H*)⁺ calcd for C₃₀H₃₅N₄O₄ [*M* + *H*]⁺, 515.2658; found, 515.2664.

2-(4-Methoxyphenyl)-7-(piperazin-1-yl)imidazo[1,2-*a*]pyridine (**34**). To a solution of compound **31** (2.0 g, 4.90 mmol) in 1,4-dioxane (20.0 mL), 4(M) HCl in 1,4-dioxane (10.0 mL) was added at 0–5 °C, and the reaction was carried out following general procedure H. Pure compound **34** appeared as a very faint greenish-yellow solid (83%, mp 168 °C). ¹H NMR (400 MHz, CDCl₃): δ 7.85 (d, *J* = 7.4 Hz, 1H), 7.83 (d, *J* = 8.8 Hz, 2H), 7.52 (s, 1H), 6.93 (d, *J* = 8.8 Hz, 2H), 6.79 (d, *J* = 1.9 Hz, 1H), 6.53 (ddd, *J* = 7.5 Hz, 2.4 Hz, 0.9 Hz, 1H), 3.82 (s, 3H), 3.18–3.15 (m, 4H), 3.03–3.00 (m, 4H). ¹³C NMR (100 MHz, CDCl₃): δ 159.3, 149.2, 147.6, 145.3, 127.1, 127.0, 125.4, 114.1, 106.5, 105.4, 97.6, 55.4, 49.8, 45.9. HRMS (ESI) *m/z* (*M* + *H*)⁺ calcd for C₁₈H₂₁N₄O, 309.1715; found, 309.1713. HPLC purity: 99.81%.

2-(2,4-Dimethoxyphenyl)-7-(piperazin-1-yl)imidazo[1,2-*a*]pyridine (**35**). To a solution of compound **32** (2.0 g, 4.56 mmol) in 1,4-dioxane (20.0 mL), 4(M) HCl in 1,4-dioxane (10.0 mL) was added at 0–5 °C, and the reaction was carried out following general procedure H. Pure compound **34** appeared as very faint greenish gummy solid (86%). ¹H NMR (600 MHz, DMSO-*d*₆): δ 8.27 (d, *J* = 7.6 Hz, 1H), 8.14 (d, *J* = 8.5 Hz, 1H), 7.97 (s, 1H), 6.75 (dd, *J* = 7.6, 2.5 Hz, 1H), 6.64 (d, *J* = 2.4 Hz, 1H), 6.63–6.61 (m, 2H), 3.93 (s, 3H), 3.80 (s, 3H), 3.13–3.10 (m, 4H), 2.84–2.82 (m, 4H). ¹³C NMR (150 MHz, DMSO-*d*₆): δ 159.6, 157.3, 148.9, 145.4, 139.5, 128.5, 126.3, 115.6, 109.3, 105.4, 105.1, 98.4, 95.1, 55.4, 55.2, 48.8, 45.4. HRMS (ESI) *m/z* (*M* + *H*)⁺ calcd for C₁₉H₂₃N₄O₂, 339.1821; found, 339.1819. HPLC purity: 98.22%.

2-(2-(Benzyloxy)-4-methoxyphenyl)-7-(piperazin-1-yl)imidazo[1,2-*a*]pyridine (**36**). To a solution of compound **33** (2.0 g, 3.89 mmol) in 1,4-dioxane (20.0 mL), 4(M) HCl in 1,4-dioxane (10.0 mL) was added at 0–5 °C, and the reaction was carried out following general procedure H. Pure compound **36** appeared as a very faint yellowish solid (83%, mp 158 °C). ¹H NMR (400 MHz, CDCl₃): δ

¹H NMR (400 MHz, Chloroform-*d*): δ 8.32 (d, *J* = 8.6 Hz, 1H), 7.78 (s, 1H), 7.73 (d, *J* = 7.5 Hz, 1H), 7.49 (d, *J* = 7.0 Hz, 2H), 7.42–7.35 (m, 3H), 6.79 (d, *J* = 1.7 Hz, 1H), 6.64 (dd, *J* = 8.6, 2.3 Hz, 1H), 6.60 (d, *J* = 2.2 Hz, 1H), 6.47 (dd, *J* = 7.5, 2.3 Hz, 1H), 5.18 (s, 2H), 3.81 (s, 3H), 3.16–3.14 (m, 4H), 3.02–3.00 (m, 4H). ¹³C NMR (100 MHz, CDCl₃): δ 160.1, 156.8, 149.1, 146.2, 140.6, 137.0, 129.4, 128.7, 128.2, 127.9, 125.5, 116.2, 109.9, 106.1, 105.3, 99.9, 97.3, 70.6, 55.5, 49.9, 45.9. HRMS (ESI) *m/z* (*M* + *H*)⁺ calcd for C₂₅H₂₇N₄O₂, 415.2129; found, 415.2135. HPLC purity: 99.92%.

7-(4-Cyclopentylpiperazin-1-yl)-2-(4-methoxyphenyl)imidazo[1,2-*a*]pyridine (**37**). To a mixture of compound **34** (0.3 g, 0.97 mmol) and K₂CO₃ (0.27 g, 1.95 mmol) in dry DMF (3.0 mL), bromocyclopentane (0.128 mL, 1.265 mmol) was added following general procedure I. Pure compound **37** appeared as an off-white solid (82%, mp 232 °C). ¹H NMR (400 MHz, CDCl₃): δ 7.86 (d, *J* = 7.5 Hz, 1H), 7.83 (d, *J* = 8.8 Hz, 2H), 7.53 (s, 1H), 6.94 (d, *J* = 8.8 Hz, 2H), 6.82 (d, *J* = 2.2 Hz, 1H), 6.55 (dd, *J* = 7.5, 2.4 Hz, 1H), 3.83 (s, 3H), 3.29–3.22 (m, 4H), 2.71–2.63 (m, 4H), 2.53 (p, *J* = 7.4 Hz, 1H), 1.94–1.84 (m, 2H), 1.75–1.64 (m, 2H), 1.59–1.54 (m, 2H), 1.49–1.41 (m, 2H). ¹³C NMR (100 MHz, CDCl₃): δ 159.4, 148.8, 147.6, 145.2, 127.1, 126.9, 125.4, 114.1, 106.4, 105.4, 97.6, 67.4, 55.4, 52.0, 48.6, 30.5, 24.2. HRMS (ESI) *m/z* (*M* + *H*)⁺ calcd for C₂₃H₂₉N₄O, 377.2341; found, 377.233. HPLC purity: 96.91%.

7-(4-Cyclopentylpiperazin-1-yl)-2-(2,4-dimethoxyphenyl)imidazo[1,2-*a*]pyridine (**38**). To a mixture of compound **35** (0.3 g, 0.89 mmol) and K₂CO₃ (0.25 g, 1.77 mmol) in dry DMF (3.0 mL), bromocyclopentane (0.117 mL, 1.152 mmol) was added following general procedure I. Pure compound **38** appeared as a faint greenish-white solid (86%, mp 186 °C). ¹H NMR (CDCl₃, 600 MHz): δ 8.25 (d, *J* = 9 Hz, 1H), 7.88 (d, *J* = 7.8 Hz, 1H), 7.84 (s, 1H), 6.86 (d, *J* = 2.4 Hz, 1H), 6.62 (dd, *J* = 8.4 Hz, 2.4 Hz, 1H), 6.55 (dd, *J* = 7.8 Hz, 2.4 Hz, 1H), 6.53 (d, *J* = 2.4 Hz, 1H), 3.94 (s, 3H), 3.84 (s, 3H), 3.26 (t, *J* = 4.8 Hz, 4H), 2.65 (t, *J* = 4.8 Hz, 4H), 2.55–2.49 (m, 1H), 1.92–1.87 (m, 2H), 1.73–1.68 (m, 2H), 1.59–1.55 (m, 2H), 1.46–1.40 (m, 2H). ¹³C NMR (150 MHz, CDCl₃): δ 160.3, 157.6, 148.9, 145.7, 139.6, 129.3, 125.6, 115.0, 109.4, 106.1, 104.7, 98.6, 96.4, 67.4, 55.4, 55.4, 51.9, 48.3, 30.5, 24.2. HRMS (ESI) *m/z* (*M* + *H*)⁺ calcd for C₂₄H₃₁N₄O₂, 407.2447; found, 407.2438. HPLC purity: 99.13%.

2-(2-(Benzyloxy)-4-methoxyphenyl)-7-(4-cyclopentylpiperazin-1-yl)imidazo[1,2-*a*]pyridine (**39**). To a mixture of compound **36** (0.3 g, 0.72 mmol) and K₂CO₃ (0.20 g, 1.45 mmol) in dry DMF (3.0 mL), bromocyclopentane (0.095 mL, 0.941 mmol) was added following general procedure I. Pure compound **39** appeared as a very faint greenish-white solid (80%, mp 210 °C). ¹H NMR (400 MHz, CDCl₃): δ 8.32 (d, *J* = 8.6 Hz, 1H), 7.79 (s, 1H), 7.74 (d, *J* = 7.4 Hz, 1H), 7.50 (d, *J* = 7.1 Hz, 2H), 7.43–7.36 (m, 3H), 6.81 (s, 1H), 6.64 (dd, *J* = 8.6 Hz, 2.0 Hz, 1H), 6.60 (d, *J* = 1.8 Hz, 1H), 6.49 (dd, *J* = 7.4 Hz, 2.0 Hz, 1H), 5.19 (s, 2H), 3.83 (s, 3H), 3.25 (br s, 4H), 2.66 (br s, 4H), 2.53 (p, *J* = 7.6 Hz, 1H), 1.91 (br s, 2H), 1.74–1.68 (m, 2H), 1.61–1.53 (m, 2H), 1.48–1.40 (m, 2H). ¹³C NMR (100 MHz, CDCl₃): δ 160.1, 156.8, 148.7, 146.2, 140.5, 137.0, 129.4, 128.7, 128.2, 127.9, 125.5, 116.2, 109.9, 106.0, 105.2, 99.9, 97.3, 70.6, 67.5, 55.5, 52.0, 48.6, 30.5, 24.2. HRMS (ESI) *m/z* (*M* + *H*)⁺ calcd for C₃₀H₃₅N₄O₂, 483.2760; found, 483.2748. HPLC purity: 98.88%.

2-(7-(4-Cyclopentylpiperazin-1-yl)imidazo[1,2-*a*]pyridin-2-yl)-5-methoxyphenol (**40**). To a suspension of compound **39** (0.1 g, 0.21 mmol) and Pd(OH)₂ (50% in carbon) (0.006 g, 0.041 mmol) in MeOH (2.0 mL), H₂ gas was passed following general procedure K. Pure compound **40** appeared as a brown solid (76%, mp 205 °C). ¹H NMR (600 MHz, CDCl₃): δ 7.88 (d, *J* = 7.8 Hz, 1H), 7.48 (s, 1H), 7.42 (d, *J* = 8.4 Hz, 1H), 6.71 (d, *J* = 1.8 Hz, 1H), 6.60 (dd, *J* = 7.8 Hz, 2.4 Hz, 1H), 6.56 (d, *J* = 2.4 Hz, 1H), 6.44 (dd, *J* = 8.4 Hz, 2.4 Hz, 1H), 3.81 (s, 3H), 3.28 (t, *J* = 4.8 Hz, 4H), 2.67 (t, *J* = 4.8 Hz, 4H), 2.57–2.52 (m, 1H), 1.91–1.90 (m, 2H), 1.75–1.69 (m, 2H), 1.61–1.56 (m, 2H), 1.48–1.42 (m, 2H). ¹³C NMR (150 MHz, CDCl₃): δ 160.6, 158.7, 148.9, 145.3, 144.8, 126.3, 125.2, 109.7, 106.4, 106.3, 103.5, 101.7, 96.4, 67.4, 55.3, 51.9, 48.2, 30.5, 24.2. HRMS (ESI) *m/z* (*M* + *H*)⁺ calcd for C₂₃H₂₉N₄O₂, 393.2291; found, 393.2282. HPLC purity: 99.40%.

7-(4-isopropylpiperazin-1-yl)-2-(4-methoxyphenyl)imidazo[1,2-*a*]pyridine (**41**). To a mixture of compound **34** (0.3 g, 0.97 mmol) and K_2CO_3 (0.27 g, 1.95 mmol) in dry DMF (3.0 mL), 2-iodopropane (0.117 mL, 1.167 mmol) was added following general procedure I. Pure compound **41** appeared as an off-white crystalline solid (78%, mp 209 °C). 1H NMR (400 MHz, $CDCl_3$): δ 7.86–7.82 (m, 3H), 7.52 (s, 1H), 6.94 (d, J = 8.9 Hz, 2H), 6.82 (d, J = 2.4 Hz, 1H), 6.55 (dd, J = 7.5, 2.4 Hz, 1H), 3.83 (s, 3H), 3.26–3.23 (m, 4H), 2.76–2.71 (m, 1H), 2.70–2.67 (m, 4H), 1.09 (d, J = 6.6 Hz, 6H). ^{13}C NMR (100 MHz, $CDCl_3$): δ 158.8, 148.3, 147.0, 144.5, 126.5, 126.2, 124.9, 113.6, 105.9, 104.9, 96.9, 54.8, 54.1, 48.3, 47.9, 18.1. HRMS (ESI) m/z ($M + H$)⁺ calcd for $C_{21}H_{27}N_4O$, 351.2185; found, 351.2192. HPLC purity: 100.0%.

2-(2,4-dimethoxyphenyl)-7-(4-isopropylpiperazin-1-yl)imidazo[1,2-*a*]pyridine (**42**). To a mixture of compound **35** (0.3 g, 0.89 mmol) and K_2CO_3 (0.25 g, 1.77 mmol) in dry DMF (3.0 mL), 2-iodopropane (0.106 mL, 1.1064 mmol) was added following general procedure I. Compound **42** appeared as an off-white solid (82%, mp 156 °C). 1H NMR (400 MHz, $CDCl_3$): δ 8.28 (d, J = 8.6 Hz, 1H), 7.88–7.84 (m, 2H), 6.80 (d, J = 1.8 Hz, 1H), 6.62 (dd, J = 8.6, 2.4 Hz, 1H), 6.54 (d, J = 2.3 Hz, 1H), 6.52 (dd, J = 7.5, 2.4 Hz, 1H), 3.94 (s, 3H), 3.84 (s, 3H), 3.25–3.22 (m, 4H), 2.72 (p, J = 6.5 Hz, 1H), 2.69–2.66 (m, 4H), 1.08 (d, J = 6.5 Hz, 6H). ^{13}C NMR (100 MHz, $CDCl_3$): δ 160.2, 157.7, 148.7, 146.3, 140.8, 129.4, 125.4, 116.1, 109.5, 106.1, 104.8, 98.7, 97.4, 55.5, 55.4, 54.6, 49.0, 48.5, 18.6. HRMS (ESI) m/z ($M + H$)⁺ calcd for $C_{22}H_{29}N_4O_2$, 381.2291; found, 381.2294. HPLC purity: 99.44%.

Cyclopentyl(4-(2-(2,4-dimethoxyphenyl)imidazo[1,2-*a*]pyridin-7-yl)piperazin-1-yl)methanone (**43**). To a mixture of compound **35** (0.2 g, 0.59 mmol) and cyclopentanecarbonyl chloride (0.086 mL, 0.71 mmol) in dry DCM (5.0 mL), DIPEA (0.31 mL, 1.77 mmol) was added following general procedure J. After purification, the pure compound **43** appeared as off-white solid (76%, mp 207 °C). 1H NMR (600 MHz, $CDCl_3$): δ 8.26 (d, J = 8.6 Hz, 1H), 7.91 (d, J = 7.5 Hz, 1H), 7.89 (s, 1H), 6.80 (d, J = 2.4 Hz, 1H), 6.62 (dd, J = 8.6, 2.4 Hz, 1H), 6.54 (d, J = 2.4 Hz, 1H), 6.52 (dd, J = 7.5, 2.4 Hz, 1H), 3.95 (s, 3H), 3.85 (s, 3H), 3.80 (s, 2H), 3.70 (s, 2H), 3.19 (t, J = 5.2 Hz, 4H), 2.92 (p, J = 8.0 Hz, 1H), 1.86 (s, 4H), 1.77 (s, 2H), 1.61 (s, 2H). ^{13}C NMR (150 MHz, $CDCl_3$): δ 174.2, 159.7, 157.2, 147.6, 145.4, 140.5, 128.8, 125.2, 115.3, 109.2, 105.7, 104.3, 98.2, 97.5, 55.0, 54.9, 48.5, 44.5, 41.0, 40.6, 29.7, 25.6. HRMS (ESI) m/z ($M + H$)⁺ calcd for $C_{23}H_{31}N_4O_3$, 435.2396; found, 435.2384. HPLC purity: 96.85%.

(4-(2-(2-(benzyloxy)-4-methoxyphenyl)imidazo[1,2-*a*]pyridin-7-yl)piperazin-1-yl)(cyclopentyl)methanone (**44**). To a mixture of compound **36** (0.2 g, 0.48 mmol) and cyclopentanecarbonyl chloride (0.07 mL, 0.58 mmol) in dry DCM (5.0 mL), DIPEA (0.31 mL, 1.77 mmol) was added following general procedure J. Pure compound **44** appeared as a light-brown solid (78%, mp 138 °C). 1H NMR (300 MHz, $CDCl_3$): δ 8.32 (d, J = 8.7 Hz, 1H), 7.82 (d, J = 7.5 Hz, 1H), 7.69 (s, 1H), 7.50–7.36 (m, 6H), 6.70–6.64 (m, 2H), 6.60 (d, J = 2.4 Hz, 1H), 5.2 (s, 2H), 3.83 (s, 3H), 3.79–3.69 (m, 4H), 3.36 (t, J = 6.0 Hz, 4H), 2.96–2.86 (m, 1H), 1.87–1.81 (m, 4H), 1.77–1.69 (m, 2H), 1.64–1.57 (m, 2H). ^{13}C NMR (75 MHz, $CDCl_3$): δ 174.9, 161.0, 156.9, 149.6, 144.1, 136.5, 129.5, 128.9, 128.4, 128.0, 126.5, 109.6, 106.5, 105.6, 100.0, 94.5, 70.7, 55.6, 48.0, 44.7, 41.1, 30.2, 26.1. HRMS (ESI) m/z ($M + H$)⁺ calcd for $C_{31}H_{35}N_4O_3$, 511.2709; found, 511.2697. HPLC purity: 98.40%.

Cyclopentyl(4-(2-(2-hydroxy-4-methoxyphenyl)imidazo[1,2-*a*]pyridin-7-yl)piperazin-1-yl)methanone (**45**). $Pd(OH)_2$ (50% in carbon) (0.006 g, 0.040 mmol) was added to a solution of compound **44** (0.1 g, 0.20 mmol) in MeOH (2.0 mL) and stirred well under a constant pressure of H_2 gas following general procedure K. Pure compound **45** was isolated as a dark-brown solid (74%, mp 235 °C). 1H NMR (400 MHz, $CDCl_3$): δ 7.89 (d, J = 7.6 Hz, 1H), 7.49 (s, 1H), 7.40 (d, J = 8.8 Hz, 1H), 6.69 (s, 1H), 6.58–6.54 (m, 2H), 6.43 (dd, J = 8.8 Hz, 2.4 Hz, 1H), 3.79 (s, 3H), 3.77–3.76 (m, 2H), 3.67 (m, 2H), 3.20 (t, J = 5.6 Hz, 4H), 2.95–2.87 (m, 1H), 1.86–1.81 (m, 4H), 1.76–1.73 (m, 2H), 1.64–1.57 (m, 2H). ^{13}C NMR ($CDCl_3$, 100 MHz): δ 174.8, 160.8, 158.8, 148.6, 145.0, 126.4, 125.5, 109.7, 106.7,

106.4, 103.9, 101.8, 97.0, 55.3, 48.6, 44.9, 41.4, 41.1, 30.2, 26.1. HRMS (ESI) m/z ($M + H$)⁺ calcd for $C_{24}H_{29}N_4O_3$, 421.2240; found, 421.2252. HPLC purity: 99.57%.

(4-(2-(2-(benzyloxy)-4-methoxyphenyl)imidazo[1,2-*a*]pyridin-7-yl)piperazin-1-yl)(phenyl)methanone (**46**). To a mixture of compound **36** (0.2 g, 0.48 mmol) and benzoyl chloride (0.067 mL, 0.58 mmol) in dry DCM (5.0 mL), DIPEA (0.31 mL, 1.77 mmol) was added following general procedure J. Pure compound **46** appeared as a white solid (81%, mp 168 °C). 1H NMR (400 MHz, $CDCl_3$): δ 8.31 (d, J = 8.4 Hz, 1H), 7.80 (s, 1H), 7.77 (d, J = 7.0 Hz, 1H), 7.49 (d, J = 6.0 Hz, 2H), 7.43 (br s, 8H), 6.81 (s, 1H), 6.64 (d, J = 8.6 Hz, 1H), 6.60 (s, 1H), 6.48 (d, J = 6.9 Hz, 1H), 5.18 (s, 2H), 3.82 (s, 3H), 3.60 (br s, 2H), 3.33–3.09 (m, 4H), 2.34–2.14 (m, 2H). ^{13}C NMR (150 MHz, $CDCl_3$): δ 170.5, 160.2, 156.8, 148.3, 145.4, 140.1, 136.7, 135.3, 130.1, 129.4, 128.7, 128.2, 127.9, 127.1, 125.8, 115.3, 119.9, 106.2, 105.2, 99.8, 97.6, 70.5, 69.8, 55.5, 54.9, 48.8. HRMS (ESI) m/z ($M + H$)⁺ calcd for $C_{32}H_{31}N_4O_3$, 519.2396; found, 519.2396. HPLC purity: 99.97%.

(4-(2-(2-(benzyloxy)-4-methoxyphenyl)imidazo[1,2-*a*]pyridin-7-yl)piperazin-1-yl)(4-fluorophenyl)methanone (**47**). DIPEA (0.31 mL, 1.77 mmol) was added to a mixture of compound **36** (0.2 g, 0.48 mmol) and 4-fluorobenzoyl chloride (0.069 mL, 0.58 mmol) in dry DCM (5.0 mL) following general procedure J. Pure compound **47** appeared as an off-white solid (76%, mp 179 °C). 1H NMR (600 MHz, $CDCl_3$): δ 8.32 (d, J = 8.0 Hz, 1H), 7.82 (s, 1H), 7.79 (d, J = 7.4 Hz, 1H), 7.50 (d, J = 7.1 Hz, 2H), 7.48–7.45 (m, 2H), 7.42 (t, J = 7.1 Hz, 2H), 7.38 (d, J = 7.3 Hz, 1H), 7.13 (t, J = 8.6 Hz, 2H), 6.83 (s, 1H), 6.65 (dd, J = 8.6 Hz, 2.3 Hz, 1H), 6.61 (d, J = 2.4 Hz, 1H), 6.49 (dd, J = 7.4 Hz, 2.5 Hz, 1H), 5.20 (s, 2H), 3.93 (s, 2H), 3.83 (s, 3H), 3.65 (br s, 2H), 3.24 (br s, 4H). ^{13}C NMR ($CDCl_3$, 150 MHz): δ 169.6, 164.4, 162.8, 160.1, 156.8, 148.0, 145.6, 136.8, 131.3, 129.6, 129.5, 129.4, 128.7, 128.2, 127.9, 125.8, 115.8, 115.7, 110.0, 106.2, 105.1, 99.8, 98.1, 70.5, 55.5, 48.8, 31.0. HRMS (ESI) m/z ($M + H$)⁺ calcd for $C_{32}H_{30}FN_4O_3$, 537.2302; found, 537.2302. HPLC purity: 95.86%.

tert-Butyl 4-(2-(2-hydroxy-4-methoxyphenyl)imidazo[1,2-*a*]pyridin-7-yl)piperazine-1-carboxylate (**48**). $Pd(OH)_2$ (50% in carbon) (0.055 g, 0.39 mmol) was added to a solution of compound **33** (1.0 g, 1.94 mmol) in MeOH (20.0 mL) and stirred well under a constant pressure of H_2 gas following general procedure K. Pure compound **48** was isolated as a brown solid (78%, mp 220 °C). 1H NMR (300 MHz, $CDCl_3$): δ 7.93 (d, J = 7.5 Hz, 1H), 7.53 (s, 1H), 7.43 (d, J = 8.3 Hz, 1H), 6.75 (br s, 1H), 6.61 (dd, J = 7.5 Hz, 2.4 Hz, 1H), 6.56 (d, J = 2.6 Hz, 1H), 6.45 (dd, J = 8.6 Hz, 2.5 Hz, 1H), 3.81 (s, 3H), 3.63–3.58 (m, 4H), 3.25–3.19 (m, 4H), 1.50 (s, 9H). ^{13}C NMR ($CDCl_3$, 150 MHz): δ 160.7, 158.6, 154.6, 148.7, 145.0, 126.3, 125.3, 109.5, 106.8, 106.3, 103.7, 101.7, 97.1, 80.2, 55.2, 48.4, 28.4. HRMS (ESI) m/z ($M + H$)⁺ calcd for $C_{23}H_{29}N_4O_4$, 425.2189; found, 425.2186.

tert-Butyl 4-(2-(4-methoxy-2-(3-morpholinopropoxy)phenyl)imidazo[1,2-*a*]pyridin-7-yl)piperazine-1-carboxylate (**49**). To a mixture of compound **48** (0.3 g, 0.71 mmol) and K_2CO_3 (0.2 g, 1.41 mmol) in dry DMF (3.0 mL), 4-(3-chloropropyl)morpholine (0.15 g, 0.919 mmol) was added following general procedure I. Pure compound **49** appeared as a white solid (67%, mp 98 °C). 1H NMR (600 MHz, $CDCl_3$): δ 8.28 (d, J = 9.0 Hz, 1H), 7.92 (d, J = 7.2 Hz, 1H), 7.88 (s, 1H), 6.86 (s, 1H), 6.63 (dd, J = 8.4 Hz, 1.8 Hz, 1H), 6.56–6.54 (m, 2H), 4.16 (t, J = 6 Hz, 2H), 3.84 (s, 3H), 3.74 (m, 4H), 3.59 (m, 4H), 3.19 (m, 4H), 2.59 (t, J = 7.2 Hz, 2H), 2.49–2.48 (m, 4H), 2.16–2.11 (m, 2H), 1.49 (s, 9H). ^{13}C NMR (150 MHz, $CDCl_3$): δ 160.2, 156.9, 154.6, 148.6, 145.7, 140.4, 129.4, 125.6, 115.3, 109.5, 106.5, 104.7, 99.4, 97.5, 80.2, 67.0, 66.5, 55.8, 55.5, 53.9, 48.6, 28.4, 26.6. HRMS (ESI) m/z ($M + H$)⁺ calcd for $C_{30}H_{42}N_5O_5$, 552.3186; found, 552.3203. HPLC purity: 98.17%.

tert-Butyl 4-(2-(4-methoxy-2-(3-pyrrolidin-1-yl)propoxy)phenyl)imidazo[1,2-*a*]pyridin-7-yl)piperazine-1-carboxylate (**50**). To a mixture of compound **48** (0.3 g, 0.71 mmol) and K_2CO_3 (0.2 g, 1.41 mmol) in dry DMF (3.0 mL), 1-(3-chloropropyl)pyrrolidine (0.135 g, 0.919 mmol) was added following general procedure I. Pure compound **49** appeared as an off-white solid (62%, mp 100 °C). 1H

NMR (CDCl₃, 600 MHz): δ 8.98 (d, J = 7.2 Hz, 1H), 8.19 (s, 1H), 8.15 (d, J = 9 Hz, 1H), 7.12 (s, 1H), 6.69 (dd, J = 7.2 Hz, 1.8 Hz, 1H), 6.55 (dd, J = 8.4 Hz, 1.8 Hz, 1H), 6.36 (s, 1H), 4.12 (t, J = 4.8 Hz, 2H), 3.76 (s, 3H), 3.59 (t, J = 4.8 Hz, 4H), 3.39–3.36 (m, 7H), 3.31 (br s, 3H), 2.57–2.53 (m, 2H), 2.14 (s, 4H), 1.49 (s, 9H). ¹³C NMR (CDCl₃, 150 MHz): δ 161.0, 156.4, 154.5, 150.8, 143.2, 129.4, 128.8, 109.8, 106.4, 105.2, 100.0, 99.2, 80.4, 64.9, 55.5, 53.4, 52.5, 47.2, 28.4, 26.2, 23.3. HRMS (ESI) m/z ($M + H$)⁺ calcd for C₃₀H₄₂N₅O₄, 536.3237; found, 536.3239. HPLC purity: 94.17%.

4-(3-(5-Methoxy-2-(7-(piperazin-1-yl)imidazo[1,2-*a*]pyridin-2-yl)phenoxy)propyl)morpholine (51). To a solution of compound 49 (0.25 g, 0.45 mmol) in 1,4-dioxane (2.0 mL), 4(M) HCl in 1,4-dioxane (1.0 mL) was added at 0–5 °C, and the reaction was carried out following general procedure H. Pure compound 51 appeared as a light-yellowish-brown solid (76%, mp 74 °C). ¹H NMR (400 MHz, Chloroform-*d*): δ 8.28 (d, J = 8.6 Hz, 1H), 7.88 (d, J = 7.6 Hz, 1H), 7.86 (s, 1H), 6.82 (s, 1H), 6.61 (d, J = 8.5 Hz, 1H), 6.53 (br s, 2H), 4.15 (t, J = 6.1 Hz, 2H), 3.84 (s, 3H), 3.74–3.71 (m, 4H), 3.20–3.17 (m, 4H), 3.05–3.02 (m, 4H), 2.58 (t, J = 7.1 Hz, 2H), 2.48 (br s, 4H), 2.21 (s, 4H), 2.15–2.09 (m, 2H). ¹³C NMR (100 MHz, CDCl₃): δ 160.2, 157.0, 149.1, 146.2, 140.7, 129.4, 125.5, 115.8, 109.4, 106.2, 104.8, 99.5, 97.3, 67.0, 66.6, 55.9, 55.5, 53.9, 49.8, 45.8, 26.6. HRMS (ESI) m/z ($M + H$)⁺ calcd for C₂₅H₃₄N₅O₃, 452.2662; found, 452.2655. HPLC purity: 97.90%.

2-(4-Methoxy-2-(3-(pyrrolidin-1-yl)propoxy)phenyl)-7-(piperazin-1-yl)imidazo[1,2-*a*]pyridine (52). 4(M) HCl in 1,4-dioxane (1.0 mL) was added to a solution of compound 50 (0.25 g, 0.47 mmol) in 1,4-dioxane (2.0 mL) at 0–5 °C, and the reaction was carried out following general procedure H. Pure compound 52 appeared as a greenish solid (67%, mp 72 °C). ¹H NMR (400 MHz, CDCl₃): δ 8.26 (d, J = 8.2 Hz, 1H), 7.96 (d, J = 6.7 Hz, 1H), 7.90 (s, 1H), 6.78 (s, 1H), 6.59 (d, J = 8.3 Hz, 1H), 6.50 (br s, 2H), 4.11 (br s, 2H), 3.81 (br s, 3H), 3.51 (br s, 4H), 3.01 (br s, 4H), 2.73 (t, J = 7.6 Hz, 2H), 2.61 (br s, 4H), 2.18 (br s, 2H), 1.81 (br s, 4H). ¹³C NMR (100 MHz, CDCl₃): δ 160.1, 156.9, 149.1, 146.2, 140.7, 129.3, 125.7, 115.9, 109.6, 106.1, 104.9, 99.3, 97.2, 66.6, 55.5, 54.2, 53.4, 49.8, 45.8, 28.7, 23.5. HRMS (ESI) m/z ($M + H$)⁺ calcd for C₂₅H₃₄N₅O₂, 436.2713; found, 436.2731. HPLC purity: 97.47%.

4-(3-(2-(7-(4-Cyclopentylpiperazin-1-yl)imidazo[1,2-*a*]pyridin-2-yl)-5-methoxyphenoxy)propyl)morpholine (53). To a mixture of compound 51 (0.12 g, 0.27 mmol) and K₂CO₃ (0.074 g, 0.53 mmol) in dry DMF (1.5 mL), bromocyclopentane (0.035 mL, 0.35 mmol) was added following the general procedure I. Pure compound 53 appeared as a light-brown solid (71%, mp 147 °C). ¹H NMR (600 MHz, CDCl₃): δ 8.30 (d, J = 8.6 Hz, 1H), 7.88 (d, J = 7.5 Hz, 1H), 7.86 (s, 1H), 6.84 (s, 1H), 6.62 (dd, J = 8.6, 2.4 Hz, 1H), 6.56 (dd, J = 7.5, 2.5 Hz, 1H), 6.54 (d, J = 2.4 Hz, 1H), 4.16 (t, J = 6.4 Hz, 2H), 3.84 (s, 3H), 3.75–3.72 (m, 4H), 3.27–3.25 (m, 4H), 2.69–2.66 (m, 4H), 2.58 (t, J = 7.3 Hz, 2H), 2.56–2.53 (m, 1H), 2.48 (br s, 4H), 2.13 (p, J = 7.0 Hz, 2H), 1.93–1.88 (m, 2H), 1.75–1.70 (m, 2H), 1.60–1.54 (m, 2H), 1.48–1.42 (m, 2H). ¹³C NMR (150 MHz, CDCl₃): δ 159.6, 156.4, 128.9, 124.9, 108.8, 105.6, 104.2, 99.0, 96.7, 66.9, 66.5, 66.0, 55.4, 55.0, 53.4, 21.5, 48.1, 30.1, 26.1, 23.7. HRMS (ESI) m/z ($M + H$)⁺ calcd for C₃₀H₄₂N₅O₃, 520.3288; found, 520.3289. HPLC purity: 100.00%.

7-(4-Cyclopentylpiperazin-1-yl)-2-(4-methoxy-2-(3-(pyrrolidin-1-yl)propoxy)phenyl)imidazo[1,2-*a*]pyridine (54). To a mixture of compound 52 (0.12 g, 0.28 mmol) and K₂CO₃ (0.076 g, 0.55 mmol) in dry DMF (1.5 mL), bromocyclopentane (0.036 mL, 0.36 mmol) was added following general procedure I. Pure compound 53 appeared as a white solid (66%, mp 171 °C). ¹H NMR (400 MHz, CHCl₃): δ 8.29 (d, J = 8.6 Hz, 1H), 7.91 (s, 1H), 7.89 (d, J = 7.4 Hz, 1H), 6.81 (d, J = 2.4 Hz, 1H), 6.61 (dd, J = 8.7, 2.4 Hz, 1H), 6.55–6.52 (m, 2H), 4.15 (t, J = 6.3 Hz, 2H), 3.83 (s, 3H), 3.26–3.23 (m, 4H), 2.71 (t, J = 7.5 Hz, 2H), 2.68–2.65 (m, 4H), 2.58–2.50 (m, 5H), 2.17 (p, J = 7.9 Hz, 2H), 1.95–1.87 (m, 2H), 1.83–1.80 (m, 4H), 1.74–1.68 (m, 2H), 1.61–1.53 (m, 2H), 1.49–1.40 (m, 2H). ¹³C NMR (100 MHz, CDCl₃): δ 160.1, 157.0, 148.6, 146.2, 140.9, 129.3, 125.5, 116.0, 109.5, 106.1, 104.8, 99.4, 97.5, 67.5, 66.8, 55.5, 54.5, 53.6, 52.1, 48.7, 30.6, 29.1, 24.2, 23.6. HRMS (ESI) m/z ($M +$

H)⁺ calcd for C₃₀H₄₂N₅O₂, 504.3339; found, 504.3332. HPLC purity: 100.00%.

4-(4-Cyclopentylpiperazin-1-yl)pyridin-2-amine (56). To a mixture of compound 4 (5.0 g, 28.9 mmol) and DIPEA (10.06 mL, 57.8 mmol) in ^{*n*}BuOH, 1-cyclopentylpiperazine (4.90 g, 31.79 mmol) was added following general procedure B. Compound 56 appeared as an off-white solid (88%, mp 243 °C). ¹H NMR (CD₃OD, 300 MHz): δ 7.55 (d, J = 6.3 Hz, 1H), 6.28 (dd, J = 6.6 Hz, 2.1 Hz, 1H), 5.95 (d, J = 1.8 Hz, 1H), 3.33 (t, J = 4.8 Hz, 4H), 2.61 (t, J = 5.1 Hz, 4H), 2.55–2.52 (m, 1H), 1.97–1.87 (m, 2H), 1.74–1.72 (m, 2H), 1.69–1.59 (m, 2H), 1.48–1.36 (m, 2H). ¹³C NMR (CD₃OD, 75 MHz): δ 159.6, 157.1, 148.2, 101.7, 91.5, 67.5, 51.9, 46.4, 30.6, 24.3. HRMS (ESI) m/z ($M + H$)⁺ calcd for C₁₄H₂₃N₄, 247.1917; found, 247.1931.

N-Cyclohexyl-7-(4-cyclopentylpiperazin-1-yl)-2-(2,4-dimethoxyphenyl)imidazo[1,2-*a*]pyridin-3-amine (57). A mixture of compound 56 (0.2 g, 0.81 mmol), compound 18 (0.135 g, 0.81 mmol), and isocyanocyclohexane (0.106 mL, 0.85 mmol) taken in a microwave tube was heated at 130 °C according to general procedure L. Pure compound 57 was isolated as a faint yellowish-brown solid (62%, mp 116 °C). ¹H NMR (400 MHz, CDCl₃): δ 7.89 (d, J = 7.6 Hz, 1H), 7.73 (d, J = 8.5 Hz, 1H), 6.74 (s, 1H), 6.64 (dd, J = 8.5, 2.3 Hz, 1H), 6.59–6.53 (m, 2H), 3.85 (s, 6H), 3.80–3.78 (m, 1H), 3.25–3.22 (m, 4H), 2.68–2.65 (m, 4H), 2.58–2.52 (m, 3H), 1.93–1.85 (m, 2H), 1.74–1.65 (m, 4H), 1.60–1.53 (m, 4H), 1.49–1.42 (m, 2H), 1.09–1.00 (m, 4H). ¹³C NMR (100 MHz, CDCl₃): δ 160.3, 156.8, 148.0, 143.4, 132.1, 125.4, 122.7, 117.4, 105.7, 105.6, 99.3, 97.8, 67.5, 56.9, 56.1, 55.5, 52.1, 48.9, 34.1, 30.5, 25.8, 24.9, 24.2. HRMS (ESI) m/z ($M + H$)⁺ calcd for C₃₀H₄₂N₅O₂, 504.3339; found, 504.3352. HPLC purity: 98.94%.

N-Benzyl-7-(4-cyclopentylpiperazin-1-yl)-2-(2,4-dimethoxyphenyl)imidazo[1,2-*a*]pyridin-3-amine (58). Compound 58 was synthesized by following general procedure L where a mixture of compound 56 (0.2 g, 0.81 mmol), compound 18 (0.135 g, 0.81 mmol), and (isocyanomethyl)benzene (0.104 mL, 0.85 mmol) taken in a microwave tube was heated at 130 °C. Pure compound 58 was isolated as a yellow solid (60%, mp 140 °C). ¹H NMR (400 MHz, CDCl₃): δ 7.87 (d, J = 7.5 Hz, 1H), 7.66 (d, J = 8.5 Hz, 1H), 7.20–7.18 (m, 5H), 6.76 (s, 1H), 6.62 (d, J = 8.4 Hz, 1H), 6.57 (d, J = 7.4 Hz, 1H), 6.51 (s, 1H), 4.10 (t, J = 6.4 Hz, 1H), 6.57 (d, J = 6.4 Hz, 2H), 3.85 (s, 3H), 3.79 (s, 3H), 3.24 (br s, 4H), 2.67 (br s, 4H), 2.54 (p, J = 8.2 Hz, 1H), 1.92–1.87 (m, 2H), 1.74–1.68 (m, 2H), 1.60–1.54 (m, 2H), 1.47–1.41 (m, 2H). ¹³C NMR (100 MHz, CDCl₃): δ 160.5, 156.9, 148.2, 143.3, 139.7, 132.1, 128.4, 128.1, 127.3, 126.0, 122.5, 116.7, 105.9, 105.6, 99.2, 97.6, 67.5, 56.1, 55.5, 53.0, 52.0, 48.8, 30.5, 24.2. HRMS (ESI) m/z ($M + H$)⁺ calcd for C₃₁H₃₈N₅O₂, 512.3026; found, 512.3021. HPLC purity: 100.00%.

4-(7-(4-Cyclopentylpiperazin-1-yl)-2-(2,4-dimethoxyphenyl)imidazo[1,2-*a*]pyridin-3-yl)methyl)morpholine (59). Compound 38 (0.12 g, 0.30 mmol) was added to a mixture of HCHO (0.028 mL, 0.34 mmol) and morpholine (0.031 mL, 0.354 mmol) in glacial AcOH (1.5 mL) following general procedure M. Pure compound 59 was isolated as a white crystalline solid (56%, 100 °C). ¹H NMR (CDCl₃, 300 MHz): δ 8.24 (d, J = 7.5 Hz, 1H), 7.33 (d, J = 8.1 Hz, 1H), 6.78 (s, 1H), 6.59–6.55 (m, 2H), 6.51 (s, 1H), 3.82 (s, 3H), 3.73 (s, 3H), 3.65 (s, 2H), 3.59 (m, 4H), 3.23 (m, 4H), 2.65 (m, 4H), 2.54–2.49 (m, 1H), 2.30 (m, 4H), 1.87 (m, 2H), 1.69–1.67 (m, 2H), 1.60–1.53 (m, 2H), 1.47–1.38 (m, 2H). ¹³C NMR (150 MHz, CDCl₃): δ 160.7, 158.0, 148.3, 146.7, 141.2, 132.5, 125.3, 116.5, 115.2, 105.5, 104.3, 98.6, 97.5, 67.3, 67.0, 55.4, 55.3, 53.0, 52.3, 51.9, 48.5, 30.4, 24.1. HRMS (ESI) m/z ($M + H$)⁺ calcd for C₂₉H₄₀N₅O₃, 506.3131; found, 506.3126. HPLC purity: 100.00%.

7-(4-Cyclopentylpiperazin-1-yl)-2-(2,4-dimethoxyphenyl)-3-(pyrrolidin-1-yl)methyl)imidazo[1,2-*a*]pyridine (60). Compound 38 (0.12 g, 0.30 mmol) was added to a mixture of HCHO (0.028 mL, 0.34 mmol) and pyrrolidine (0.029 mL, 0.354 mmol) in glacial AcOH (1.5 mL) following general procedure M. Pure compound 60 was obtained as an off-white solid (51%, mp 71 °C). ¹H NMR (400 MHz, CDCl₃): δ 8.27 (d, J = 7.6 Hz, 1H), 7.37 (d, J = 8.3 Hz, 1H), 6.82 (d, J = 2.2 Hz, 1H), 6.59–6.52 (m, 3H), 3.85 (s, 3H), 3.80 (s, 2H), 3.76 (s, 3H), 3.27–3.24 (m, 4H), 2.69–2.66 (m, 4H), 2.55 (p, J = 7.5 Hz,

1H), 2.37 (br s, 4H), 1.94–1.86 (m, 4H), 1.67 (br s, 4H), 1.60–1.55 (m, 2H), 1.49–1.42 (m, 2H). ¹³C NMR (100 MHz, CDCl₃): δ 160.8, 158.2, 148.4, 146.5, 132.8, 125.4, 117.5, 105.7, 104.4, 100.0, 98.8, 97.7, 67.5, 55.6, 55.4, 53.7, 52.1, 49.2, 48.7, 30.6, 24.2, 23.7. HRMS (ESI) *m/z* (M + H)⁺ calcd for C₂₉H₄₀N₃O₂, 490.3182; found, 490.3177. HPLC purity: 98.59%.

2-(2-(Benzyloxy)-4-methoxyphenyl)-7-(4-cyclopentylpiperazin-1-yl)-3-(pyrrolidin-1-ylmethyl)imidazo[1,2-*a*]pyridine (61). Compound **39** (0.25 g, 0.52 mmol) was added to a mixture of HCHO (0.048 mL, 0.60 mmol) and pyrrolidine (0.051 mL, 0.622 mmol) in glacial AcOH (3.0 mL) following general procedure **M**. Pure compound **59** was isolated as an off-white sticky solid (56%). ¹H NMR (300 MHz, CDCl₃): δ 8.28 (d, *J* = 7.6 Hz, 1H), 7.45 (d, *J* = 8.2 Hz, 1H), 7.27 (br s, 5H), 6.93 (d, *J* = 2.4 Hz, 1H), 6.63–6.57 (m, 3H), 5.02 (s, 2H), 3.85 (s, 2H), 3.80 (s, 3H), 3.29 (br s, 4H), 2.67 (br s, 4H), 2.54 (p, *J* = 7.9 Hz, 1H), 2.37 (br s, 4H), 1.89 (br s, 2H), 1.71 (br s, 2H), 1.64 (br s, 4H), 1.53–1.49 (m, 2H), 1.49–1.40 (m, 4H). ¹³C NMR (75 MHz, CDCl₃): δ 160.4, 157.1, 148.1, 146.4, 137.1, 132.8, 128.3, 127.6, 127.3, 125.3, 117.8, 117.5, 105.5, 105.3, 100.7, 97.5, 70.8, 67.4, 55.3, 53.6, 52.0, 49.6, 48.6, 30.5, 24.1, 23.5. HRMS (ESI) *m/z* (M + H)⁺ calcd for C₃₅H₄₄N₅O₂, 566.3495; found, 566.3490. HPLC purity: 100.00%.

2-(7-(4-Cyclopentylpiperazin-1-yl)-3-(pyrrolidin-1-ylmethyl)imidazo[1,2-*a*]pyridin-2-yl)-5-methoxyphenol (62). Pd(OH)₂ (50% in carbon) (0.005 g, 0.035 mmol) was added to a solution of compound **61** (0.1 g, 0.18 mmol) in MeOH (2.0 mL) and stirred well under a constant pressure of H₂ gas following general procedure **K**. Pure compound **62** was isolated as a brown gummy solid (53%). ¹H NMR (600 MHz, CDCl₃): δ 7.66 (d, *J* = 8.6 Hz, 1H), 7.26 (d, *J* = 7.6 Hz, 1H), 6.70 (d, *J* = 2.6 Hz, 1H), 6.59 (d, *J* = 2.5 Hz, 1H), 6.54 (dd, *J* = 8.6 Hz, 2.6 Hz, 1H), 6.28 (dd, *J* = 7.8 Hz, 2.5 Hz, 1H), 5.03 (s, 1H), 3.86 (s, 3H), 3.81 (s, 1H), 3.30–3.28 (m, 2H), 3.18–3.16 (m, 4H), 2.68–2.67 (m, 2H), 2.58–2.56 (m, 4H), 2.49 (q, *J* = 7.6 Hz, 1H), 1.95–1.85 (m, 4H), 1.76–1.67 (m, 4H), 1.56–1.53 (m, 2H), 1.42–1.38 (m, 2H). ¹³C NMR (150 MHz, CDCl₃): δ 160.8, 159.2, 148.6, 145.4, 140.5, 127.8, 123.7, 110.9, 110.6, 106.2, 105.9, 102.5, 95.6, 67.3, 55.3, 53.6, 51.9, 51.7, 48.1, 47.7, 30.4, 24.1. HRMS (ESI) *m/z* (M + H)⁺ calcd for C₂₈H₃₈N₅O₂, 476.3026; found, 476.3036. HPLC purity: 100.00%.

4-((2-(2,4-Dimethoxyphenyl)-7-(4-isopropylpiperazin-1-yl)imidazo[1,2-*a*]pyridin-3-yl)methyl)morpholine (63). Compound **42** (0.12 g, 0.315 mmol) was added to a mixture of HCHO (0.03 mL, 0.36 mmol) and morpholine (0.033 mL, 0.378 mmol) in glacial AcOH (1.5 mL) following general procedure **M**. Pure compound **63** was isolated as an off-white solid (53%, mp 73 °C). ¹H NMR (400 MHz, CDCl₃): δ 8.26 (d, *J* = 7.6 Hz, 1H), 7.35 (d, *J* = 8.3 Hz, 1H), 6.83 (d, *J* = 2.1 Hz, 1H), 6.62–6.53 (m, 3H), 3.85 (s, 3H), 3.76 (s, 3H), 3.68 (s, 2H), 3.64–3.60 (m, 4H), 3.28–3.24 (m, 4H), 2.77–2.71 (m, 1H), 2.71–2.68 (m, 4H), 2.34 (br s, 4H), 1.09 (d, *J* = 6.5 Hz, 6H). ¹³C NMR (100 MHz, CDCl₃): δ 160.9, 158.1, 148.6, 146.8, 141.1, 132.7, 125.4, 116.4, 115.4, 105.7, 104.5, 98.8, 97.5, 67.1, 55.6, 55.5, 54.6, 53.2, 52.5, 49.0, 48.5, 18.6. HRMS (ESI) *m/z* (M + H)⁺ calcd for C₂₇H₃₈N₅O₃, 480.2975; found, 480.2976. HPLC purity: 100.00%.

2-(2,4-Dimethoxyphenyl)-7-(4-isopropylpiperazin-1-yl)-3-(pyrrolidin-1-ylmethyl)imidazo[1,2-*a*]pyridine (64). Compound **42** (0.12 g, 0.315 mmol) was added to a mixture of HCHO (0.03 mL, 0.36 mmol) and pyrrolidine (0.031 mL, 0.378 mmol) in glacial AcOH (1.5 mL) following general procedure **M**. Pure compound **64** was isolated as a brownish sticky solid (56%). ¹H NMR (400 MHz, CDCl₃): δ 8.27 (d, *J* = 7.6 Hz, 1H), 7.37 (d, *J* = 8.2 Hz, 1H), 6.81 (d, *J* = 2.2 Hz, 1H), 6.59–6.53 (m, 3H), 3.85 (s, 3H), 3.79 (s, 2H), 3.76 (s, 3H), 3.26–3.23 (m, 4H), 2.76–2.71 (m, 1H), 2.71–2.67 (m, 4H), 2.36 (br s, 4H), 1.69–1.65 (m, 4H), 1.09 (d, *J* = 6.5 Hz, 6H). ¹³C NMR (100 MHz, CDCl₃): δ 160.8, 158.2, 148.5, 146.5, 139.9, 132.8, 125.4, 117.5, 116.9, 105.7, 104.4, 98.8, 97.6, 55.6, 55.4, 54.6, 53.7, 49.2, 49.1, 48.5, 23.7, 18.7. HRMS (ESI) *m/z* (M + H)⁺ calcd for C₂₇H₃₈N₅O₂, 464.3026; found, 464.3024. HPLC purity: 100.00%.

Cyclopentyl(4-(2-(2,4-dimethoxyphenyl)-3-(pyrrolidin-1-ylmethyl)imidazo[1,2-*a*]pyridin-7-yl)piperazin-1-yl)methanone

(65). Compound **43** (0.12 g, 0.276 mmol) was added to a mixture of HCHO (0.026 mL, 0.318 mmol) and pyrrolidine (0.027 mL, 0.331 mmol) in glacial AcOH (1.5 mL) following general procedure **M**. Pure compound **64** was obtained as a brown solid (54%, mp 126 °C). ¹H NMR (600 MHz, CDCl₃): δ 8.32 (s, 1H), 7.37 (s, 1H), 6.84 (s, 1H), 6.57 (s, 2H), 6.53 (s, 1H), 3.85 (s, 3H), 3.82 (br s, 4H), 3.76 (s, 3H), 3.70 (s, 2H), 3.20 (s, 4H), 2.93 (s, 1H), 2.38 (s, 4H), 1.84 (s, 4H), 1.74 (s, 2H), 1.68 (s, 4H), 1.59 (s, 2H). ¹³C NMR (150 MHz, CDCl₃): δ 174.2, 160.3, 157.6, 147.4, 145.6, 132.2, 125.2, 117.1, 116.0, 105.4, 103.9, 98.2, 97.8, 55.1, 54.9, 53.1, 48.6, 48.5, 44.6, 41.0, 40.6, 29.7, 25.6, 23.1. HRMS (ESI) *m/z* (M + H)⁺ calcd for C₃₀H₄₀N₅O₃, 518.3131; found, 518.3113. HPLC purity: 99.95%.

■ ASSOCIATED CONTENT

Supporting Information

The Supporting Information is available free of charge at <https://pubs.acs.org/doi/10.1021/acs.jmedchem.2c00386>.

Reporter assay for evaluating TLR9 antagonist activity, reporter assay for evaluating TLR7 antagonist activity, reporter assay for evaluating TLR8 antagonist activity, molecular docking score table, selectivity against TLR8 through computational study, aqueous solubility assay data, plasma stability assay data, Caco-2 permeability assay data, microsomal stability assay data, ¹H NMR and ¹³C NMR spectra of compounds **7–65**, and HPLC purity profile for lead molecules (PDF)

Molecular formula strings (CSV)

TLR7 Homology Model (PDB)

Figure 2A_TLR7-Compound **12** complex (PDB)

Figure 2B_TLR7-Compound **26** complex (PDB)

Figure 2C_TLR7-Compound **41** complex (PDB)

Figure 2D_TLR7-Compound **42** complex (PDB)

Figure 3_TLR7-Compound **43** complex (PDB)

■ AUTHOR INFORMATION

Corresponding Authors

Dipayan Ganguly – IICB-Translational Research Unit of Excellence, Department of Cancer Biology and Inflammatory Disorders, CSIR-Indian Institute of Chemical Biology, Kolkata 700091 West Bengal, India; Academy of Scientific and Innovative Research, Ghaziabad 201002, India; Email: dipayan@iicb.res.in

Arindam Talukdar – Department of Organic and Medicinal Chemistry, CSIR-Indian Institute of Chemical Biology, Kolkata 700032 West Bengal, India; Academy of Scientific and Innovative Research, Ghaziabad 201002, India; orcid.org/0000-0002-7831-1795; Email: atalukdar@iicb.res.in

Authors

Nirmal Das – Department of Organic and Medicinal Chemistry, CSIR-Indian Institute of Chemical Biology, Kolkata 700032 West Bengal, India; Academy of Scientific and Innovative Research, Ghaziabad 201002, India

Purbita Bandopadhyay – IICB-Translational Research Unit of Excellence, Department of Cancer Biology and Inflammatory Disorders, CSIR-Indian Institute of Chemical Biology, Kolkata 700091 West Bengal, India; Academy of Scientific and Innovative Research, Ghaziabad 201002, India

Swarnali Roy – Department of Organic and Medicinal Chemistry, CSIR-Indian Institute of Chemical Biology, Kolkata 700032 West Bengal, India

Bishnu Prasad Sinha – IICB-Translational Research Unit of Excellence, Department of Cancer Biology and Inflammatory Disorders, CSIR-Indian Institute of Chemical Biology, Kolkata 700091 West Bengal, India; Academy of Scientific and Innovative Research, Ghaziabad 201002, India

Uddipta Ghosh Dastidar – Department of Organic and Medicinal Chemistry, CSIR-Indian Institute of Chemical Biology, Kolkata 700032 West Bengal, India; Academy of Scientific and Innovative Research, Ghaziabad 201002, India

Oindrila Rahaman – IICB-Translational Research Unit of Excellence, Department of Cancer Biology and Inflammatory Disorders, CSIR-Indian Institute of Chemical Biology, Kolkata 700091 West Bengal, India

Sourav Pal – Department of Organic and Medicinal Chemistry, CSIR-Indian Institute of Chemical Biology, Kolkata 700032 West Bengal, India; Academy of Scientific and Innovative Research, Ghaziabad 201002, India

Complete contact information is available at:

<https://pubs.acs.org/10.1021/acs.jmedchem.2c00386>

Author Contributions

[†]N.D., P.B., and S.R. contributed equally to the study.

Notes

The authors declare no competing financial interest.

ACKNOWLEDGMENTS

The project was supported by the Council of Scientific and Industrial Research (CSIR) Mission mode Project MLP-135 to D.G. and A.T., as well as by the Swarnajayanti Fellowship from the DST to D.G. The authors N.D. and P.B. would like to thank the CSIR for the fellowship. S.R. and O.R. thank the University Grant Commission (UGC), Govt. of India, for the fellowship. U.G.D. would like to acknowledge the CSIR for funding. B.P.S. and S.P. would like to thank the Senior Research Fellowship from the Indian Council of Medical Research. The authors would like to acknowledge Dr. Ramdhan Majhi for helping with HPLC and the Central Instrument Facility of CSIR-IICB.

ABBREVIATIONS

ACN, acetonitrile; AcOH, acetic acid; (\pm)BINAP, ([1,1'-binaphthalene]-2,2'-diyl)bis(diphenylphosphane); CHCl₃, chloroform; Cu₂O, cuprous oxide; DCE, 1,2-dichloroethane; DCM, dichloromethane; DIPEA, *N,N*-diisopropylethylamine; DMEM, Dulbecco's modified Eagle's medium; DMF, *N,N*-dimethylformamide; Et₂O, diethyl ether; EtOAc, ethyl acetate; g, gram; HBSS, Hank's balanced salt solution; HCHO, formaldehyde; hPBMC, human peripheral blood mononuclear cell; IFN, interferon; ISG15, interferon-stimulated gene 15; K₂CO₃, potassium carbonate; LC-MS, liquid chromatography-mass spectrometry; MeOH, methanol; Na₂SO₄, sodium sulfate; NaHCO₃, sodium bicarbonate; Na^tOBu, sodium *tert*-butoxide; ⁿBuOH, *n*-butanol; NH₃, ammonia; NH₄Cl, ammonium chloride; NMP, *N*-methyl-2-pyrrolidone; NMR, nuclear magnetic resonance; Pd(OH)₂, palladium hydroxide; Pd₂(dba)₃, tris(dibenzylideneacetone)dipalladium; PTSA, *p*-toluenesulfonic acid; SEAP, secreted alkaline phosphatase; SLE, systemic lupus erythematosus; TBAB, tetrabutylammonium bromide; TBATB, tetrabutylammonium tribromide; THF, tetrahydrofuran; TLC, thin-layer chromatography; TLR, toll-like receptor

REFERENCES

- (1) Takeda, K.; Kaisho, T.; Akira, S. Toll-Like Receptors. *Annu. Rev. Immunol.* **2003**, *21*, 335–376.
- (2) Akira, S.; Uematsu, S.; Takeuchi, O. Pathogen Recognition and Innate Immunity. *Cell* **2006**, *124*, 783–801.
- (3) Akira, S.; Takeda, K. Toll-like Receptor Signalling. *Nat. Rev. Immunol.* **2004**, *4*, 499–511.
- (4) Akira, S.; Takeda, K.; Kaisho, T. Toll-like Receptors: Critical Proteins Linking Innate and Acquired Immunity. *Nat. Immunol.* **2001**, *2*, 675–680.
- (5) Gay, N. J.; Symmons, M. F.; Gangloff, M.; Bryant, C. E. Assembly and Localization of Toll-like Receptor Signalling Complexes. *Nat. Rev. Immunol.* **2014**, *14*, 546–558.
- (6) Gay, N. J.; Gangloff, M. Structure and Function of Toll Receptors and Their Ligands. *Annu. Rev. Biochem.* **2007**, *76*, 141–165.
- (7) O'Neill, L. A. J.; Golenbock, D.; Bowie, A. G. The History of Toll-like Receptors — Redefining Innate Immunity. *Nat. Rev. Immunol.* **2013**, *13*, 453–460.
- (8) Takeuchi, O.; Akira, S. Signaling Pathways Activated by Microorganisms. *Curr. Opin. Cell Biol.* **2007**, *19*, 185–191.
- (9) Junt, T.; Barchet, W. Translating Nucleic Acid-Sensing Pathways into Therapies. *Nat. Rev. Immunol.* **2015**, *15*, 529–544.
- (10) He, S.; Mao, X.; Sun, H.; Shirakawa, T.; Zhang, H.; Wang, X. Potential Therapeutic Targets in the Process of Nucleic Acid Recognition: Opportunities and Challenges. *Trends Pharmacol. Sci.* **2015**, *36*, 51–64.
- (11) Lee, B. L.; Barton, G. M. Trafficking of Endosomal Toll-like Receptors. *Trends Cell Biol.* **2014**, *24*, 360–369.
- (12) Hu, Y.-B.; Dammer, E. B.; Ren, R.-J.; Wang, G. The Endosomal-Lysosomal System: From Acidification and Cargo Sorting to Neurodegeneration. *Transl. Neurodegener.* **2015**, *4*, 18.
- (13) Heil, F.; Hemmi, H.; Hochrein, H.; Ampenberger, F.; Kirschning, C.; Akira, S.; Lipford, G.; Wagner, H.; Bauer, S. Species-Specific Recognition of Single-Stranded RNA via Toll-like Receptor 7 and 8. *Science* **2004**, *303*, 1526.
- (14) Diebold, S. S.; Kaisho, T.; Hemmi, H.; Akira, S.; Reis e Sousa, C. Innate Antiviral Responses by Means of TLR7-Mediated Recognition of Single-Stranded RNA. *Science* **2004**, *303*, 1529.
- (15) Hemmi, H.; Takeuchi, O.; Kawai, T.; Kaisho, T.; Sato, S.; Sanjo, H.; Matsumoto, M.; Hoshino, K.; Wagner, H.; Takeda, K.; Akira, S. A Toll-like Receptor Recognizes Bacterial DNA. *Nature* **2000**, *408*, 740–745.
- (16) Ohto, U.; Shibata, T.; Tanji, H.; Ishida, H.; Krayukhina, E.; Uchiyama, S.; Miyake, K.; Shimizu, T. Structural Basis of CpG and Inhibitory DNA Recognition by Toll-like Receptor 9. *Nature* **2015**, *520*, 702–705.
- (17) Miyake, K.; Shibata, T.; Ohto, U.; Shimizu, T.; Saitoh, S.-I.; Fukui, R.; Murakami, Y. Mechanisms Controlling Nucleic Acid-Sensing Toll-like Receptors. *Int. Immunol.* **2018**, *30*, 43–51.
- (18) Hornung, V.; Rothenfusser, S.; Britsch, S.; Krug, A.; Jahrsdörfer, B.; Giese, T.; Endres, S.; Hartmann, G. Quantitative Expression of Toll-Like Receptor 1-10 mRNA in Cellular Subsets of Human Peripheral Blood Mononuclear Cells and Sensitivity to CpG Oligodeoxynucleotides. *J. Immunol.* **2002**, *168*, 4531.
- (19) Gilliet, M.; Cao, W.; Liu, Y.-J. Plasmacytoid Dendritic Cells: Sensing Nucleic Acids in Viral Infection and Autoimmune Diseases. *Nat. Rev. Immunol.* **2008**, *8*, 594–606.
- (20) Patinote, C.; Karroum, N. B.; Moarbes, G.; Cirnat, N.; Kassab, I.; Bonnet, P.-A.; Deleuze-Masquéfa, C. Agonist and Antagonist Ligands of Toll-like Receptors 7 and 8: Ingenious Tools for Therapeutic Purposes. *Eur. J. Med. Chem.* **2020**, *193*, 112238.
- (21) Federico, S.; Pozzetti, L.; Papa, A.; Carullo, G.; Gemma, S.; Butini, S.; Campiani, G.; Relitti, N. Modulation of the Innate Immune Response by Targeting Toll-like Receptors: A Perspective on Their Agonists and Antagonists. *J. Med. Chem.* **2020**, *63*, 13466–13513.
- (22) Hennessy, E. J.; Parker, A. E.; O'Neill, L. A. J. Targeting Toll-like Receptors: Emerging Therapeutics? *Nat. Rev. Drug Discovery* **2010**, *9*, 293–307.

- (23) Marshak-Rothstein, A. Toll-like Receptors in Systemic Autoimmune Disease. *Nat. Rev. Immunol.* **2006**, *6*, 823–835.
- (24) El-Zayat, S. R.; Sibaii, H.; Mannaa, F. A. Toll-like Receptors Activation, Signaling, and Targeting: An Overview. *Bull. Natl. Res. Cent.* **2019**, *43*, 187.
- (25) Anwar, M. A.; Shah, M.; Kim, J.; Choi, S. Recent clinical trends in Toll-like receptor targeting therapeutics. *Med. Res. Rev.* **2019**, *39*, 1053–1090.
- (26) Hemmi, H.; Kaisho, T.; Takeda, K.; Akira, S. The Roles of Toll-Like Receptor 9, MyD88, and DNA-Dependent Protein Kinase Catalytic Subunit in the Effects of Two Distinct CpG DNAs on Dendritic Cell Subsets. *J. Immunol.* **2003**, *170*, 3059.
- (27) Uematsu, S.; Akira, S. Toll-like Receptors and Type I Interferons. *J. Biol. Chem.* **2007**, *282*, 15319–15323.
- (28) Van Beek, M. J.; Piette, W. W. Antimalarials. *Dermatol. Clin.* **2001**, *19*, 147–160.
- (29) Karlsson, L.; Sun, S.; Rao, L. N.; Venable, J.; Thurmond, R. TLR7/9 Antagonists as Therapeutics for Immune-Mediated Inflammatory Disorders. *Inflammation Allergy: Drug Targets* **2007**, *6*, 223–235.
- (30) Curtis, J. R.; Xi, J.; Patkar, N.; Xie, A.; Saag, K. G.; Martin, C. Drug-specific and time-dependent risks of bacterial infection among patients with rheumatoid arthritis who were exposed to tumor necrosis factor α antagonists. *Arthritis Rheum.* **2007**, *56*, 4226–4227.
- (31) Jiang, W.; Zhu, F.; Tang, J.; Kandimalla, E.; La Monica, N.; Agrawal, S. IMO-8400, a Novel TLR7, TLR8 and TLR9 Antagonist, Inhibits Disease Development in Mouse Models of Psoriasis. *J. Immunol.* **2012**, *188*, 119.8.
- (32) Wu, Y.; Tang, W.; Zuo, J. Toll-like Receptors: Potential Targets for Lupus Treatment. *Acta Pharmacol. Sin.* **2015**, *36*, 1395–1407.
- (33) Zhu, F.-G.; Jiang, W.; Dong, Y.; Kandimalla, E.; La Monica, N.; Agrawal, S. IMO-8400, a Novel TLR7, TLR8 and TLR9 Antagonist, Inhibits Disease Development in Lupus-Prone NZBW/F1 Mice. *J. Immunol.* **2012**, *188*, 119.12.
- (34) Gao, W.; Xiong, Y.; Li, Q.; Yang, H. Inhibition of Toll-Like Receptor Signaling as a Promising Therapy for Inflammatory Diseases: A Journey from Molecular to Nano Therapeutics. *Front. Physiol.* **2017**, *8*, 508.
- (35) Suárez-Fariñas, M.; Arbeit, R.; Jiang, W.; Ortenzio, F. S.; Sullivan, T.; Krueger, J. G. Suppression of Molecular Inflammatory Pathways by Toll-Like Receptor 7, 8, and 9 Antagonists in a Model of IL-23-Induced Skin Inflammation. *PLoS One* **2013**, *8*, No. e84634.
- (36) Kim, Y. J.; Schiopu, E.; Dankó, K.; Mozaffar, T.; Chunduru, S.; Lees, K.; Goyal, N.; Sarazin, J.; Fiorentino, D. F.; Sarin, K. Y. AB016. A Double-Blind, Placebo-Controlled, Phase 2 Trial of a Novel Toll-like Receptor 7/8/9 Antagonist (IMO-8400) in Dermatomyositis. *Ann. Transl. Med.* **2021**, *9*, AB016.
- (37) Kim, Y. J.; Schiopu, E.; Dankó, K.; Mozaffar, T.; Chunduru, S.; Lees, K.; Goyal, N. A.; Sarazin, J.; Fiorentino, D. F.; Sarin, K. Y. A Phase 2, Double-Blinded, Placebo-Controlled Trial of Toll-like Receptor 7/8/9 Antagonist, IMO-8400, in Dermatomyositis. *J. Am. Acad. Dermatol.* **2021**, *84*, 1160–1162.
- (38) Balak, D. M. W.; van Doorn, M. B. A.; Arbeit, R. D.; Rijneveld, R.; Klaassen, E.; Sullivan, T.; Brevard, J.; Thio, H. B.; Prens, E. P.; Burggraaf, J.; Rissmann, R. IMO-8400, a Toll-like Receptor 7, 8, and 9 Antagonist, Demonstrates Clinical Activity in a Phase 2a, Randomized, Placebo-Controlled Trial in Patients with Moderate-to-Severe Plaque Psoriasis. *Clin. Immunol.* **2017**, *174*, 63–72.
- (39) Czarniecki, M. Small Molecule Modulators of Toll-like Receptors. *J. Med. Chem.* **2008**, *51*, 6621–6626.
- (40) Lamphier, M.; Zheng, W.; Latz, E.; Spyvee, M.; Hansen, H.; Rose, J.; Genest, M.; Yang, H.; Shaffer, C.; Zhao, Y.; Shen, Y.; Liu, C.; Liu, D.; Mempel, T. R.; Rowbottom, C.; Chow, J.; Twine, N. C.; Yu, M.; Gusovsky, F.; Ishizaka, S. T. Novel Small Molecule Inhibitors of TLR7 and TLR9: Mechanism of Action and Efficacy In Vivo. *Mol. Pharmacol.* **2014**, *85*, 429.
- (41) Roy, S.; Mukherjee, A.; Paul, B.; Rahaman, O.; Roy, S.; Maithri, G.; Ramya, B.; Pal, S.; Ganguly, D.; Talukdar, A. Design and Development of Benzoxazole Derivatives with Toll-like Receptor 9 Antagonism. *Eur. J. Med. Chem.* **2017**, *134*, 334–347.
- (42) Paul, B.; Rahaman, O.; Roy, S.; Pal, S.; Satish, S.; Mukherjee, A.; Ghosh, A. R.; Raychaudhuri, D.; Bhattacharya, R.; Goon, S.; Ganguly, D.; Talukdar, A. Activity-Guided Development of Potent and Selective Toll-like Receptor 9 Antagonists. *Eur. J. Med. Chem.* **2018**, *159*, 187–205.
- (43) Pal, S.; Paul, B.; Bandopadhyay, P.; Preethy, N.; Sarkar, D.; Rahaman, O.; Goon, S.; Roy, S.; Ganguly, D.; Talukdar, A. Synthesis and Characterization of New Potent TLR7 Antagonists Based on Analysis of the Binding Mode Using Biomolecular Simulations. *Eur. J. Med. Chem.* **2021**, *210*, 112978.
- (44) Talukdar, A.; Ganguly, D.; Paul, B.; Mukherjee, A.; Roy, S.; Roy, S.; Ghosh, A. R.; Bhattacharya, R.; Rahaman, O.; Kundu, B. Blocking Toll-like Receptor 9 Signaling with Small Molecule Antagonist. U.S. Patent 20,190,092,758 A1, 2019.
- (45) Yang, M.; Larson, P. G.; Brown, L.; Schultz, J. R.; Kucaba, T. A.; Griffith, T. S.; Ferguson, D. M. Toll-like Receptor 7 and 8 Imidazoquinoline-Based Agonist/Antagonist Pairs. *Bioorg. Med. Chem. Lett.* **2022**, *59*, 128548.
- (46) Mukherjee, A.; Raychaudhuri, D.; Sinha, B. P.; Kundu, B.; Mitra, M.; Paul, B.; Bandopadhyay, P.; Ganguly, D.; Talukdar, A. A Chemical Switch for Transforming a Purine Agonist for Toll-like Receptor 7 to a Clinically Relevant Antagonist. *J. Med. Chem.* **2020**, *63*, 4776–4789.
- (47) Kundu, B.; Raychaudhuri, D.; Mukherjee, A.; Sinha, B. P.; Sarkar, D.; Bandopadhyay, P.; Pal, S.; Das, N.; Dey, D.; Ramarao, K.; Nagireddy, K.; Ganguly, D.; Talukdar, A. Systematic Optimization of Potent and Orally Bioavailable Purine Scaffold as a Dual Inhibitor of Toll-Like Receptors 7 and 9. *J. Med. Chem.* **2021**, *64*, 9279–9301.
- (48) Talukdar, A.; Ganguly, D.; Mukherjee, A.; Paul, B.; Rahaman, O.; Kundu, B.; Roy, S.; Raychaudhuri, D. Purine Based Compounds as Toll-Like Receptor 9 Antagonist. U.S. Patent 20200347062, 2020.
- (49) Talukdar, A.; Ganguly, D.; Roy, S.; Das, N.; Sarkar, D. Structural Evolution and Translational Potential for Agonists and Antagonists of Endosomal Toll-like Receptors. *J. Med. Chem.* **2021**, *64*, 8010–8041.
- (50) Bou Karroum, N.; Moarbess, G.; Guichou, J.-F.; Bonnet, P.-A.; Patinote, C.; Bouharoun-Tayoun, H.; Chamat, S.; Cuq, P.; Diab-Assaf, M.; Kassab, I.; Deleuze-Masquefa, C. Novel and Selective TLR7 Antagonists among the Imidazo[1,2-a]Pyrazines, Imidazo[1,5-a]-Quinoxalines, and Pyrazolo[1,5-a]Quinoxalines Series. *J. Med. Chem.* **2019**, *62*, 7015–7031.
- (51) Mussari, C. P.; Dodd, D. S.; Sreekantha, R. K.; Pasunoori, L.; Wan, H.; Posy, S. L.; Critton, D.; Ruepp, S.; Subramanian, M.; Watson, A.; Davies, P.; Schieven, G. L.; Salter-Cid, L. M.; Srivastava, R.; Tagore, D. M.; Dudhgaonkar, S.; Poss, M. A.; Carter, P. H.; Dyckman, A. J. Discovery of Potent and Orally Bioavailable Small Molecule Antagonists of Toll-like Receptors 7/8/9 (TLR7/8/9). *ACS Med. Chem. Lett.* **2020**, *11*, 1751–1758.
- (52) Talukdar, A.; Mukherjee, A.; Ganguly, D. Small Molecule Modulators of Endo-Lysosomal Toll-like Receptors. In *Protein-Protein Interaction Regulators*; Roy, S., Fu, H., Eds.; The Royal Society of Chemistry: London, U.K., 2021; pp 339–372.
- (53) Pal, S.; Ghosh Dastidar, U.; Ghosh, T.; Ganguly, D.; Talukdar, A. Integration of Ligand-Based and Structure-Based Methods for the Design of Small-Molecule TLR7 Antagonists. *Molecules* **2022**, *27*, 4026.
- (54) Gobbi, L.; Knust, H.; Koerner, M.; Muri, D. Preparation of Imidazo[1,2-a]Pyridine-7-Amines as Imaging Tools. WO 2015044095, 2015.
- (55) Tyagi, V.; Khan, S.; Bajpai, V.; Gauniyal, H. M.; Kumar, B.; Chauhan, P. M. S. Skeletal Diverse Synthesis of N-Fused Polycyclic Heterocycles via the Sequence of Ugi-Type MCR and CuI-Catalyzed Coupling/Tandem Pictet-Spengler Reaction. *J. Org. Chem.* **2012**, *77*, 1414–1421.
- (56) Ansari, A. J.; Sharma, S.; Pathare, R. S.; Gopal, K.; Sawant, D. M.; Pardasani, R. T. Solvent-free Multicomponent Synthesis of Biologically-active Fused-imidazo Heterocycles Catalyzed by Reusable

Yb(OTf)₃ Under Microwave Irradiation. *ChemistrySelect* **2016**, *1*, 1016–1021.

(57) Watanabe, M.; Kasai, M.; Tomizawa, H.; Aoki, M.; Eiho, K.; Isobe, Y.; Asano, S. Dihydropyrrrolo[2,3-d]Pyrimidines: Selective Toll-Like Receptor 9 Antagonists from Scaffold Morphing Efforts. *ACS Med. Chem. Lett.* **2014**, *5*, 1235–1239.

(58) Zatzepin, M.; Mattes, A.; Rupp, S.; Finkelmeier, D.; Basu, A.; Burger-Kentscher, A.; Goldblum, A. Computational Discovery and Experimental Confirmation of TLR9 Receptor Antagonist Leads. *J. Chem. Inf. Model.* **2016**, *56*, 1835–1846.

(59) Huang, L.-Y.; DuMontelle, J. L.; Zolod, M.; Deora, A.; Mozier, N. M.; Golding, B. Use of Toll-Like Receptor Assays To Detect and Identify Microbial Contaminants in Biological Products. *J. Clin. Microbiol.* **2009**, *47*, 3427.

(60) Tojo, S.; Zhang, Z.; Matsui, H.; Tahara, M.; Ikeguchi, M.; Kochi, M.; Kamada, M.; Shigematsu, H.; Tsutsumi, A.; Adachi, N.; Shibata, T.; Yamamoto, M.; Kikkawa, M.; Senda, T.; Isobe, Y.; Ohto, U.; Shimizu, T. Structural Analysis Reveals TLR7 Dynamics Underlying Antagonism. *Nat. Commun.* **2020**, *11*, 5204.

(61) Zhang, Z.; Ohto, U.; Shibata, T.; Krayukhina, E.; Taoka, M.; Yamauchi, Y.; Tanji, H.; Isobe, T.; Uchiyama, S.; Miyake, K.; Shimizu, T. Structural Analysis Reveals That Toll-like Receptor 7 Is a Dual Receptor for Guanosine and Single-Stranded RNA. *Immunity* **2016**, *45*, 737–748.

(62) Ishida, H.; Asami, J.; Zhang, Z.; Nishizawa, T.; Shigematsu, H.; Ohto, U.; Shimizu, T. Cryo-EM Structures of Toll-like Receptors in Complex with UNC93B1. *Nat. Struct. Mol. Biol.* **2021**, *28*, 173–180.

(63) Leeson, P. D.; Springthorpe, B. The Influence of Drug-like Concepts on Decision-Making in Medicinal Chemistry. *Nat. Rev. Drug Discovery* **2007**, *6*, 881–890.

(64) Veber, D. F.; Johnson, S. R.; Cheng, H.-Y.; Smith, B. R.; Ward, K. W.; Kopple, K. D. Molecular Properties That Influence the Oral Bioavailability of Drug Candidates. *J. Med. Chem.* **2002**, *45*, 2615–2623.

(65) Hiromi, T.; Umeharu, O.; Takuma, S.; Kensuke, M.; Toshiyuki, S. Structural Reorganization of the Toll-Like Receptor 8 Dimer Induced by Agonistic Ligands. *Science* **2013**, *339*, 1426–1429.

(66) Asami, J.; Shimizu, T. Structural and functional understanding of the toll-like receptors. *Protein Sci.* **2021**, *30*, 761–772.

(67) Zhang, S.; Hu, Z.; Tanji, H.; Jiang, S.; Das, N.; Li, J.; Sakaniwa, K.; Jin, J.; Bian, Y.; Ohto, U.; Shimizu, T.; Yin, H. Small-Molecule Inhibition of TLR8 through Stabilization of Its Resting State. *Nat. Chem. Biol.* **2018**, *14*, 58–64.

(68) Kundu, B.; Sarkar, D.; Chowdhuri, S. P.; Pal, S.; Das, S. K.; Das, B. B.; Talukdar, A. Development of a Metabolically Stable Topoisomerase I Poison as Anticancer Agent. *Eur. J. Med. Chem.* **2020**, *202*, 112551.

(69) Gunaydin, H.; Altman, M. D.; Ellis, J. M.; Fuller, P.; Johnson, S. A.; Lahue, B.; Lapointe, B. Strategy for Extending Half-Life in Drug Design and Its Significance. *ACS Med. Chem. Lett.* **2018**, *9*, 528–533.

(70) Engel, A. L.; Holt, G. E.; Lu, H. The Pharmacokinetics of Toll-like Receptor Agonists and the Impact on the Immune System. *Expert Rev. Clin. Pharmacol.* **2011**, *4*, 275–289.

(71) Benson, N.; de Jongh, J.; Duckworth, J. D.; Jones, H. M.; Pertinez, H. E.; Rawal, J. K.; van Steeg, T. J.; Van der Graaf, P. H. Pharmacokinetic-Pharmacodynamic Modeling of Alpha Interferon Response Induced by a Toll-Like 7 Receptor Agonist in Mice. *Antimicrob. Agents Chemother.* **2010**, *54*, 1179.

(72) Gentile, F.; Deriu, M. A.; Licandro, G.; Prunotto, A.; Danani, A.; Tuszyński, J. A. Structure Based Modeling of Small Molecules Binding to the TLR7 by Atomistic Level Simulations. *Molecules* **2015**, *5*, 8316.

(73) Pal, S.; Kumar, V.; Kundu, B.; Bhattacharya, D.; Preethy, N.; Reddy, M. P.; Talukdar, A. Ligand-Based Pharmacophore Modeling, Virtual Screening and Molecular Docking Studies for Discovery of Potential Topoisomerase I Inhibitors. *Comput. Struct. Biotechnol. J.* **2019**, *17*, 291–310.

(74) Jones, G.; Willett, P.; Glen, R. C.; Leach, A. R.; Taylor, R. Development and validation of a genetic algorithm for flexible docking 1 Edited by F. E. Cohen. *J. Mol. Biol.* **1997**, *267*, 727–748.

(75) Azam, S. S.; Abbasi, S. W. Molecular Docking Studies for the Identification of Novel Melatoninergic Inhibitors for Acetylserotonin-O-Methyltransferase Using Different Docking Routines. *Theor. Biol. Med. Model.* **2013**, *10*, 63.

(76) Hu, Z.; Zhang, T.; Jiang, S.; Yin, H. Protocol for Evaluation and Validation of TLR8 Antagonists in HEK-Blue Cells via Secreted Embryonic Alkaline Phosphatase Assay. *STAR Protoc.* **2022**, *3*, 101061.

NOTE ADDED AFTER ASAP PUBLICATION

This paper was published ASAP on August 12, 2022, with an error in the graph for compound **42** in the Table of Contents/Abstract graphic. The graphic was replaced, and the corrected version was reposted on August 15, 2022. PDB files were added to the paper, and the corrected version was reposted on August 22, 2022.

Recommended by ACS

Discovery of 5-Aryl-2,4-diaminopyrimidine Compounds as Potent and Selective IRAK4 Inhibitors

Yan Chen, Donald G. Payan, *et al.*

APRIL 04, 2022
ACS MEDICINAL CHEMISTRY LETTERS

READ 

Discovery and Optimization of Novel Pyrazolopyrimidines as Potent and Orally Bioavailable Allosteric HIV-1 Integrase Inhibitors

Guo Li, Annapurna Pendri, *et al.*

FEBRUARY 21, 2020
JOURNAL OF MEDICINAL CHEMISTRY

READ 

Target-Based Identification and Optimization of 5-Indazol-5-yl Pyridones as Toll-like Receptor 7 and 8 Antagonists Using a Biochemical TLR8 Antagonist Competition Assay

Thomas Knoepfel, Claudia Betschart, *et al.*

JULY 30, 2020
JOURNAL OF MEDICINAL CHEMISTRY

READ 

Targeting Acute Myelogenous Leukemia Using Potent Human Dihydroorotate Dehydrogenase Inhibitors Based on the 2-Hydroxypyrazolo[1,5-a]pyridine Scaffold: SAR of t...

Stefano Sainas, Marco L. Lolli, *et al.*

SEPTEMBER 26, 2022
JOURNAL OF MEDICINAL CHEMISTRY

READ 

Get More Suggestions >